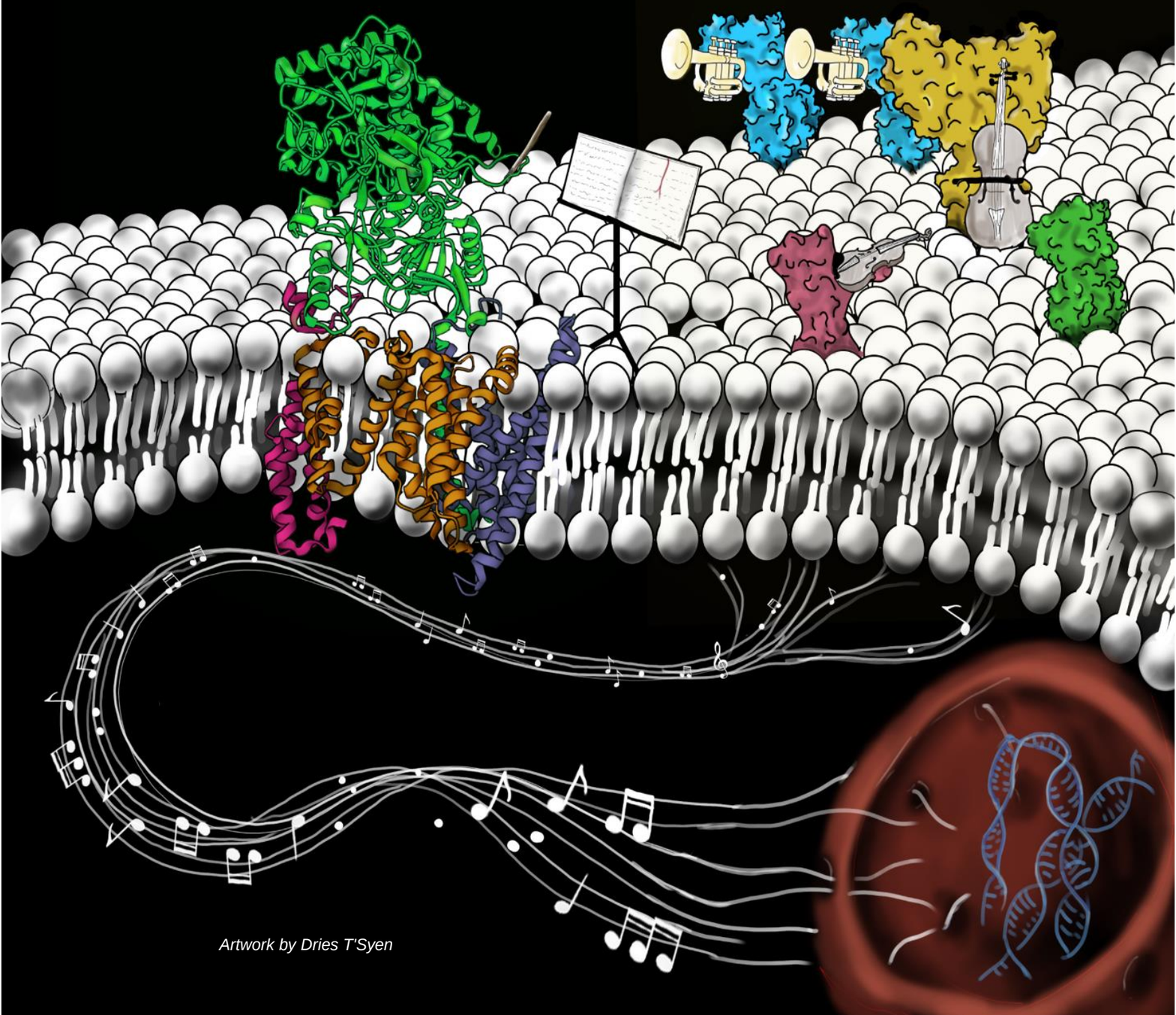
γ-Secretase acts as the conductor of the silent notes generated by the many protein receptors in the cell membrane. γ-Secretase's subtle baton guides activation in vitro, homeostasis in vivo, and the elusive DAM tune in Alzheimer's Disease context.

THE γ-SECRETASE SUBSTRATE PROTEOME AND ITS ROLE IN CELL SIGNALING REGULATION

Pengfei Hou



Artwork by Dries T'Syen

Table of Contents

Key Abbreviations 7
Summary 9
Chapter 1: Introduction 11
1.1 γ-Secretase 11
1.1.1 Discovery of the enzyme associated to γ-secretase activity 11
1.1.2 Heterogeneity of γ-secretase complexes 12
1.1.3 The controversy of γ-secretase function in cell biology 14
1.1.4 The obstacles in γ-secretase research methodology 15
1.2 Microglia 18
1.2.1 The guardians of central nervous system? 18
1.2.2 Dynamic players in the cellular phase of Alzheimer's disease 20
1.2.3 γ-Secretase substrates participate in microglia biology 23
Chapter 2: Research objectives 35
Chapter 3: Materials and Methods 37
3.1 Key Resources Table 37
3.2 Experimental Model And Study Participant Details 43
3.2.1 Mice 43
3.2.2 Primary human microglia 43
3.2.3 H9MG 44
3.2.4 HEK293T cell line 45
3.3 Method Details 45
3.3.1 Mice 45
3.3.2 Isolation of human and mouse primary microglia 45
3.3.3 RNA isolation, reverse transcription and real-time qPCR 46
3.3.4 Expression and validation of novel γ-secretase substrates 47
3.3.5 Immunoblotting 47
3.3.6 Immunofluorescence staining of brain sections 48
3.3.7 Gamma-secretase Substrate Identification (G-SECSI) workflow 48
3.3.8 Preparation of H9MG single-cell samples 53
3.3.9 Single-cell mRNA libraries preparation and sequencing 53
3.4 Quantification And Statistical Analysis 54
3.4.1 Quantitative analysis of the abundance of the CTFs 54
3.4.2 Functional and Pathway Enrichment Analysis of Candidate Substrates 55
3.4.3 Single-cell sequencing data analysis 55
3.4.4 Imaging and quantitative analysis of the Immunofluorescent images 58
3.5 Resource Availability 59

Chapter 4: Results 61
4.1 Identification and characterization of γ-secretase substrate proteome in H9MG cells 61
4.1.1 G-SECSI to identify substrates of γ-secretase 61
4.1.2 Identification of novel γ-secretase substrates in H9MG 64
4.1.3 Validation of the identified novel γ-secretase substrates 66
4.1.4 γ-Secretase substrates are central in intracellular microglial signaling 66
4.2 Effects of γ-secretase deficiency on microglia transcriptional cell states 71
4.2.1 γ-Secretase inhibition causes substantial changes of microglia transcriptomes but does not affect the strong cell state response to LPS *in vitro* 71
4.2.2 γ-Secretase deficiency alters cell signaling in microglia *in vivo* 74
4.2.3 γ-Secretase deficiency impedes the formation of activated microglial cell states in $App^{NL\text{-}G\text{-}F}$ mice 76
4.2.4 γ-Secretase deficiency blocks *in vivo* microglia in a pre-DAM state in response to amyloid pathology 79
Chapter 5: General Discussion and Conclusions 89
Scientific Acknowledgments, Personal Contributions and Conflict of Interests 97
Supplemental table titles and legends 99
References 101
Curriculum Vitae 125
Personal Acknowledgement 129

Key Abbreviations

αSyn	α-synuclein
aa	Amino acid
Aβ	β-amyloid
AD	Alzheimer’s disease
APH1	Anterior pharynx defective-1
APOE	Apolipoprotein E
APP	Amyloid precursor protein
BACE1	Beta-site amyloid precursor protein cleaving enzyme 1
CAA	Cerebral amyloid angiopathy
CNS	Central nervous system
CRM	Cytokine response microglia
CTF	C-terminal fragments
DAM	Disease associated microglia
DEG	Differentially expressed gene
FAD	Familial Alzheimer's disease
FACS	Fluorescence-activated cell sorting
FIRE	Fms intronic regulatory element
FL	Full-length protein
GAM	γ-Secretase allosteric modulator
GPNMB	Glycoprotein non-metastatic melanoma protein B
GS	γ-Secretase
GSI	γ-Secretase inhibitor
$GS^{i\Delta MG}$	Microglia-specific γ-secretase conditional knock-out
G-SECSI	γ-Secretase substrate identification
GWAS	Genome-wide association studies
HM	Homeostatic microglia
H9MG	H9 embryonic stem cells into microglia-like cells
ICD	Intracellular domain
IF	Immunofluorescence
IRM	Interferon response microglia
ITAM	Immunoreceptor tyrosine-based activation motif
ITIM	Immunoreceptor tyrosine-based inhibition motif

KO	Knock-out
LOAD	Late-Onset Alzheimer's disease
LPS	Lipopolysaccharide
MAPK	Mitogen-activated protein kinase
MS	Mass spectrometry
MW	Molecular weight
NCT	Nicastrin
NFTs	Neurofibrillary tau tangles
NHD	Nasu-Hakola disease
OLIGs	Oligodendrocyte genes
PCA	Principal Component Analysis
PEN2	Presenilin enhancer-2
PIGs	Plaque-induced genes
PLCγ	Phospholipase Cγ
PMEL	Premelanosome protein
PSEN	Presenilin
PtdSer	Phosphatidylserine
RIP	Regulated intramembrane proteolysis
S2P	Site-2 protease
scRNA-seq	Single-cell RNA sequencing
SDS-PAGE	Sodium Dodecyl Sulfate Polyacrylamide Gel Electrophoresis
SPC	Signal peptidases complex
SPECS	Secretome protein enrichment with click sugars
SREBP	Sterol regulatory element-binding protein
tCRM	Transitioning cytokine response
TGN	Trans-Golgi network
TMD	Transmembrane domain
TRM	Transiting response microglia
TREM2	Triggering receptor expressed on myeloid cells 2
T-ALL	T-cell Acute lymphoblastic leukemia
UMAP	Uniform Manifold Approximation and Projection
WT	Wild type

Summary

γ-Secretases mediate the regulated intramembrane proteolysis (RIP) of more than 150 integral membrane proteins. In some cases, a clear function can be assigned to this cleavage: for instance, it is the rate limiting step in Notch signaling. For most proteins, however, it is unclear what this cleavage exactly means. The “proteasome of the membrane” hypothesis raised by Kopan et al. in 2004, suggesting mainly a clearance function, has been implicitly accepted in the field. However, so far it has been reported for at least 61 substrates that this cleavage leads to signaling events. Therefore, an alternative interpretation is that γ-secretase is a checkpoint for a whole series of signaling pathways and that the function of γ-secretase should not be investigated substrate per substrate but as the integrated result of the multiple signaling pathways. This also implies that to understand the function of γ-secretase one needs to take into account the cell type (e.g. microglia) and the condition to which the cell is exposed (i.e. the summation of all ligands and other stimuli in the milieu of the cell *in vitro* or *in vivo*).

In this study, we developed an unbiased γ-Secretase Substrate Identification (G-SECSI) method to study to what extent the multiple substrates are processed in parallel. We differentiated human H9 embryonic stem cells into microglia-like cells (H9MG) and demonstrated here parallel processing of at least 85 membrane proteins in these steady state microglial cell cultures. These substrates are important signaling receptors, including tyrosine receptor kinases, interleukin receptors, tumor necrosis factor receptors, ITAM- or ITIM-receptors, etc., and are involved in distinct microglia biological processes, including proliferation, phagocytosis, cytokines production, axon guidance, migration, etc. γ-Secretase activity thus appears in the center of a variety of crucial signaling pathways in microglia.

To address the question of whether γ-secretase deficiency affects the microglia transcriptome, we analyzed the single-cell transcriptomes of H9MG before and after γ-secretase inhibitor (Semagacestat) treatment. Pharmacological inhibition of γ-secretase caused substantial changes of microglia transcriptomes, including the down-expression of genes related to the disease-associated microglia (DAM) response described in Alzheimer’s disease (AD), while limited effects on the general transcriptomic cell states were observed. Similar to the observations *in vitro*, the overall effects of γ-secretase blockage on transcriptomic cell states remained limited in control conditions *in vivo*, while the strong upregulation of genes related to DAM response was

observed. Thus, our results suggest that normal γ-secretase activity promotes activating gene expression *in vitro* and homeostatic gene expression *in vivo*—the natural states of microglia in these two conditions. Next, we asked whether γ-secretases deficiency affects microglia in an amyloid context. Surprisingly, we found that γ-secretase deficient microglia failed to mount the putatively protective DAM cell state and were blunted in their response to amyloid plaques in $App^{NL\text{-}G\text{-}F}$ -$GS^{i\Delta MG}$ mice. Therefore, γ-secretases are highly involved in cell signaling regulation in microglial responses under the diverse conditions.

Taken together, we systemically investigated the role of γ-secretase in microglia by identifying the microglia-specific γ-secretase substrate proteome and evaluating the effects of γ-secretase deficiency on microglia transcriptomes under different conditions. We conclude that γ-secretase serves as a critical signaling hub integrating the effect of multiple extracellular stimuli into the overall transcriptome of the cell.

Chapter 1: Introduction

1.1 γ-Secretase

1.1.1 Discovery of the enzyme associated to γ-secretase activity

The history of γ-secretase research is closely intertwined with the history of the molecular understanding of Alzheimer's Disease (AD). One of the pivotal landmarks in the evolution of Alzheimer's research has been the identification of Aβ peptide as the main component of senile plaques in human brains in 1984.[1–3] This finding initiated the vast modern research focusing on this unique peptide. In 1987, researchers mapped the cDNA of Aβ peptide to the locus of chromosome 21 encoding a much larger single-pass type I transmembrane protein, which is the so-called amyloid precursor protein (APP).[4–7] Four years later, the first batch of mutations in *APP* genes were uncovered in familial AD (FAD) patients which cause the disease in an autosomal dominant way.[8–10] Sporadic AD and FAD are pathologically indistinguishable, e.g. both are featured with extracellular amyloid (Aβ) plaques, intracellular neurofibrillary tau tangles (NFTs), neuroinflammation and neuronal loss. Therefore, the genetic studies and the clinical observations firmly linked Aβ/APP to the etiology of AD. The following question is therefore how the putative AD-causing Aβ peptides are generated from its large precursor. With the identification of the various APP proteolytic fragments, at least 4 secretory activities mediating cleavage on APP were proposed and termed sequentially, i.e. α-, β-, γ- and δ-secretase, even though the underlying entities were unidentified when they were proposed (Figure 1).[11–13]

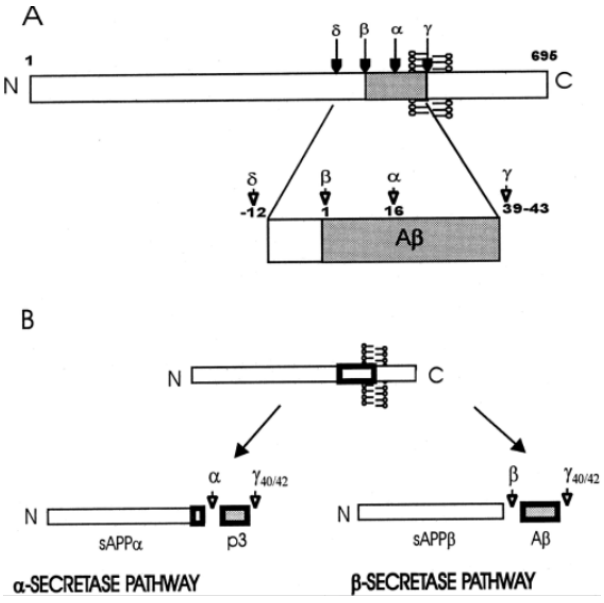


Figure 1. Cleavage sites of APP proposed in 1999.

A. APP is cleaved inside the Aβ sequence by α-secretase at Lys16 (amino acide number within Aβ). β- and γ-secretase cleave APP on Aβ sequence at Met1 or in the region of Val39-Thr43, respectively. δ-Secretase cleaves APP 12 residues from the N-terminus of the Aβ domain (Thr-12).

B. APP is processed via two alternative pathways, resulting in cleavage by α- or β-secretase yielding sAPPα or sAPPβ, respectively.

Adapted from *Mills, et al. 1999*.[14]

Different to the others, γ-secretase activity was initially considered “unlikely” to be a physiological process, since it has to occur within the membrane.[4] It was thought that hydrolysis in the membrane is impossible because there is no water access. In 1997, this traditional view was challenged for the first time by the identification of membrane-bound transcription factor site-2 protease (S2P),[15] which shows unusual proteolytic activity by cleaving sterol regulatory element-binding protein (SREBP) at its hydrophobic Site-2 within a membrane-spanning domain.[16] Almost at the same time, mutations in two other genes, i.e. *PSEN1* and *PSEN2*, named after ‘presenile’ as they appear in very early onset cases, were uncovered in the FAD patients without *APP* mutations, which cause the disease in an autosomal dominant way as well as *APP* mutations.[17–21] Moreover, FAD mutations in either *APP, PSEN1* or *PSEN2* elevates Aβ42/40 ratio promoting an aggregation prone Aβ profile, suggesting APP and Presenilins (PSENs) are involved in the same or similar mechanisms for Aβ production.[22,23] Finally, studies using *PSEN 1* and *2* knock-out models revealed that PSENs are essential for γ-secretase activity generating Aβ peptide.[24,25] Further studies confirmed this finding by the identification of two transmembrane aspartic acid residues in the catalytic core of PSEN,[26] the demonstration of a similar enzymatic role of PSEN on Notch[27,28] and finally the cross-linking of transition-state γ-secretase inhibitors to PSEN.[29,30]

1.1.2 Heterogeneity of γ-secretase complexes

Several years after the identification of PSEN as essential entity of γ-secretase activity, three other proteins, i.e. Nicastrin (NCT),[31] Anterior pharynx defective-1 (APH1)[32] and Presenilin enhancer-2 (PEN2),[33] were sequentially revealed to be essential for this proteolytic function exerted by PSEN. Now, it is well-known that γ-secretase activity is mediated by a family of intramembranous tetrameric protease complexes, each consisting of either one of the two PSEN (PSEN1 and PSEN2) and either one of the two APH1 (APH1A and APH1B) subunits and one subunit of PEN2 and one of NCT.[34–36] In human, two PSEN variants, i.e. PSEN1 and PSEN2, together with two APH1 variants, i.e. APH1A and APH1B, collectively generate four main different γ-secretase complexes, whereas in rodent a third APH1c variant that differs only in 5 amino acids from APH1b exists explaining why in rodents six different complexes were identified.[37,38] Additionally, splicing variants of PSEN[39–43] and APH1[44,45] have been

reported in mammalian cells adding even more complexity to γ-secretase heterogeneity.

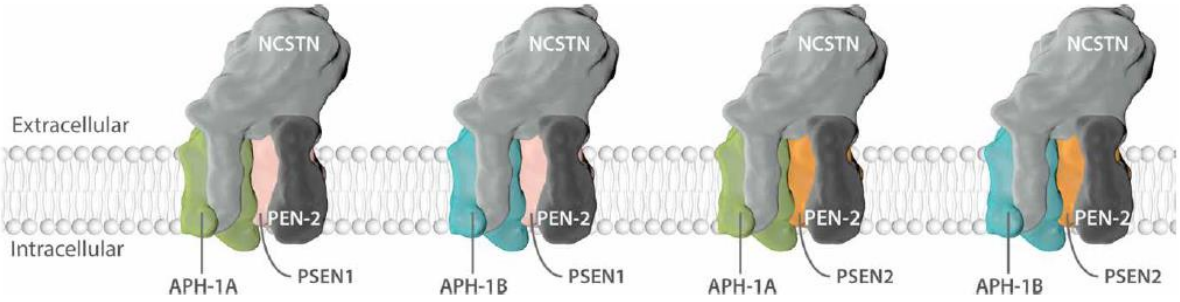


Figure 2. Schematic representation of the four different tetrameric γ-secretase complexes that exist in human. All complexes contain NCT, PEN-2, and either PSEN1 or PSEN2 and APH1A or APH1B. **Adapted from** *Habets, et al. 2019.*[46]

Until now, it remains largely unknown why cells express so many different γ-secretase complexes and whether they play different roles in cell biology. While γ-secretase is the key point of Aβ production and inhibition of this activity provides a promising target for anti-Aβ therapy in AD,[24] it is clear that indiscriminate inhibition of all γ-secretases would cause severe side effects. For instance, a phase III trial of the γ-secretase inhibitor Semagacestat (LY450139) in AD was halted not only because of the Notch-related skin, gastrointestinal and immunological side effects, but especially also the deterioration of cognition.[47] Until now no good explanation for this cognitive deterioration has been provided.[48] Interestingly, PSEN2 has been reported to be directed by its unique motif (E_{16}RTSLM_{21}) to late endosomes/lysosomes via the trans-Golgi network (TGN)/endosomal adaptor complex protein (AP) complex AP-1 in a phosphorylation-dependent manner and selectively cleaving the co-localized substrates, different to PSEN1 which broadly distributes in the cell.[49] This suggests that different γ-secretase complexes might have complex-specific subcellular localizing properties and substrate selectivity, and therefore may be specifically targeted to spare side effects when contemplating lowering-Aβ therapy. Indeed, MRK560, a PSEN1-selective γ-secretase inhibitor[50] has promising therapeutic potential in preclinical experiments in both AD[51] and T-cell Acute lymphoblastic leukemia (T-ALL)[46] models, without showing any Notch-related phenotypes as reported in the Semagacestat trial.[47] APH1 variants have been reported to contribute to the different Aβ profiles, with APH1B containing complexes prone to produce longer Aβ peptides compared to APH1A.[52] However, a potent APH1A- or APH1B-selective γ-secretase inhibitor is

currently unavailable,[53] making that the therapeutic potential of APH1B-selective inhibition in AD remains questioned.

1.1.3 The controversy of γ-secretase function in cell biology

γ-Secretases cleave a wide range of integral membrane proteins (See table 1 at the end of Introduction section and ref[54]). During this process, the intracellular domains of the substrates are released, with many of those appear to regulate cell signaling.[55] The best known example is Notch, whose intracellular domains released by γ-secretase translocate to cytoplasm and nucleus and regulate expression of a series of down-stream genes in development and cancer.[27,46] Moreover, γ-secretase limits the inflammatory response through the processing of LRP1,[56] while γ-secretase cleavage of SIRPα enhances inflammatory signaling.[57] To date, γ-secretase cleavage of at least 61 substrates has been linked to various signaling mechanisms.[54] Similar signaling is performed by other intramembranous proteases, such as the rhomboids and S2P, and was baptized "regulated intramembrane proteolysis (RIP)".[58] Most importantly, signaling mediated by RIP is irreversible, in contrast to other signaling mechanisms like phosphorylation.[55]

Despite evidence for the role of γ-secretases in intracellular signaling, clearing membrane bound protein stubs generated by ectodomain shedding is the other main task of γ-secretase function.[59] The "proteasome of the membrane" hypothesis, raised almost two decades ago by Kopan et al.,[59] suggests mainly a clearance function of γ-secretase in cell biology, and is still implicitly accepted in the field. Indeed, γ-secretases have the property to trim their substrates in the membrane, removing hydrophobic amino acids, resulting ultimately in the release of small peptides into the extracellular milieu.[60–62] The function of many of these peptides remains unknown, but the Aβ peptides cleaved from APP shows important pathological relevance in the context of AD.[22,63–66] γ-Secretases generate a spectrum of Aβ peptides by a progressive processing mechanism that shortens the initially ε-cleavage-generated Aβ49 or Aβ48 peptide (the numbers indicate the number of amino acids) by removing consecutively tripeptides or tetrapeptides (Figure 3).[60,67,68] *PSEN* mutations alter the carboxypeptidase activity of γ-secretase by destabilizing the substrate-enzyme interaction, resulting in a relative shift of long versus short Aβ.[69] These longer Aβ fragments act as seeds for Aβ oligomerization and amyloid plaque formation.[70]

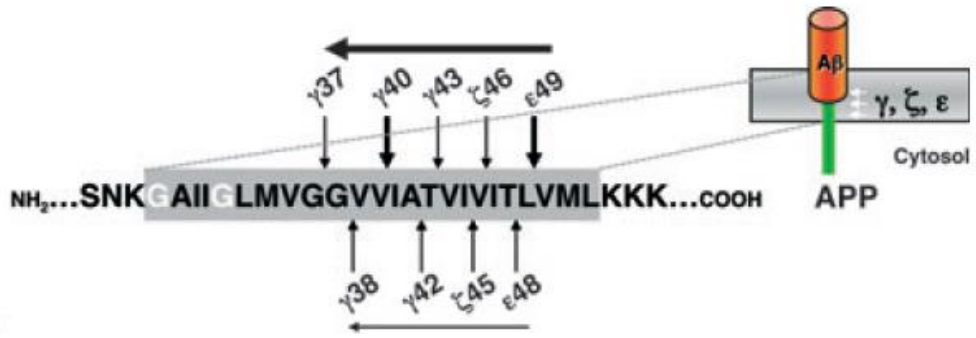


Figure 3. Stepwise APP cleavage of γ-secretase. The individual γ-secretase cleavage sites in the APP transmembrane domain (TMD) are depicted by thick (major cleavage sites) and thin (minor cleavage sites) vertical arrows. Horizontal arrows indicate the direction of the cleavages. The major product line (ε49 – γ37), which generates Aβ40 as principal Aβ species, is depicted with a thick horizontal arrow. The minor product line (ε48 – γ38), which gives rise to the pathogenic Aβ42, is depicted with a thin horizontal arrow. **Adapted from** *Lichtenthaler, et al. 2011.*[68]

Apparently, the controversy on γ-secretase biological function is largely due to the lack of knowledge of the γ-secretase substrate proteome and whether their proteolytic processes would collectively contribute to signaling mechanisms or merely to degradation of membrane bound fragments in a specific cellular context. To address this question, it is required the determination of the total substrate proteome in each experimental condition and the evaluation of the effects of γ-secretase deficiency in a systemic way. However, this progress has been largely limited by the current strategies for γ-secretase research.

1.1.4 The obstacles in γ-secretase research methodology

The first obstacle of investigating the physiological function of γ-secretase is the lack of an unbiased approach for the large-scale endogenous substrate identification. Progress in other fields of intramembrane proteolysis illustrates the importance of such unbiased approaches to understand the role(s) of those proteases, while currently none of them is applicable to study γ-secretase.

A group of membrane-bound proteases that mostly cleave single-pass transmembrane proteins at the extracellular surface of cell membrane and release the ectodomains of those proteins into the extracellular milieu is termed “sheddases”.[68,71,72] While the secretome generated by these sheddases plays essential roles in both physiological and pathophysiological conditions, unbiased identification of the secretome had been challenging. This is largely due to the low abundance of those shedded peptides and

the high abundance of other confounding peptides in the cell culture media, which severely compromised the utility of mass spectrometry (MS).[73] Since approximately a decade ago, this problem has been successfully solved by using the secretome protein enrichment with click sugars (SPECS) method, which consists of metabolic labelling of cellular glycoproteins with azido sugars followed by copper-free click chemistry-mediated biotinylation of cellular glycoproteins.[73,74] By using SPECS, a large number of glycosylated membrane proteins have been identified as substrates of BACE1,[73] SPPL3[75] and ADAM10,[76] accordingly. These studies provided important insights for the understanding of physiological roles of these sheddases, for instance the identification of ADAM10 substrates in mouse primary neurons revealed fundamental role of the enzyme in axon targeting and synapse function in the brain.[76] Interestingly, γ-secretase has been reported to directly cleave some substrates (i.e. BCMA,[77] NRADD,[78] SYT7,[79] and TNFRSF12A[80]), shedding their ectodomain into the extracellular environments. While from this point of view γ-secretase can be considered as a sheddase as well, evidences from the majority of currently known γ-secretase substrates point out that a prior ectodomain-shortening step on the precursor is most often required for a protein to be cleaved by γ-secretase.[54,81,82] Therefore, SPECS is predicted to identify only a limited number of γ-secretase substrates which likely contain naturally short ectodomains and do not require a prior cleavage by other secretases.

An elegant method directly links serine- or cysteine-proteases to their substrates by introducing a 2,3-diaminopropionic acid (Dap) substitution into the catalytic site, enabling the formation of a hydrolysis resistant substrate-enzyme intermediate through a stable amide bond.[83,84] The enzyme-substrate complexes can be recovered and analyzed by MS. Novel substrates of the intramembrane cleaving Rhomboid RHBDL4 were identified demonstrating its role in non-canonical secretion of endoplasmic reticulum-resident chaperones.[85] However, aspartyl proteases, for instance γ-secretase, use their catalytic aspartate residues to interact with water and the carbonyl oxygen of the scissile amide bond does not involve the formation of an acyl-enzyme intermediate.[86] Therefore, this approach cannot be used for the identification of γ-secretase substrates.

In silico approaches are another way to unbiasedly identify novel substrates for intramembrane cleaving proteases, illustrated by a study of the signal peptidases

complex (SPC).[87] SPC is a family of membrane-integral serine proteases whose canonical role is to cleave off N-terminal signal peptides.[88] Surveying the human proteome for the presence of a specific Ala-X-Ala motif characteristic for the cleavage sites of SPC,[89] candidate cleavage sites were found in 1,297 membrane proteins, but in regions outside of the canonical site at the N-terminus.[87,90] Subsequent validation experiments showed that SPC can cleave those sites when they become exposed because of protein misfolding.[87] Thus, this study revealed an unexpected novel degradation function of SPC in addition to its well-known signaling function.[88] Unlike SPC, γ-secretase substrates do not share such easily identifiable consensus cleavage sequences,[54,81,82] making prediction of their substrates unreliable. Artificial intelligence methods linking sequence features with predicted conformational structures might provide a solution,[91] but direct experimental identification of novel substrates using unbiased screening approaches will be important to feed such analysis.

Blocking γ-secretase activity in a cell line using small-molecule chemical inhibitors such as Semagacestat and monitoring the accumulation of substrate carboxy-terminal fragments (CTFs) is one of the most commonly used strategies for γ-secretase substrate identification. The main problem hampering the development of an unbiased approach for γ-secretase substrate identification is that MS cannot discriminate full-length (FLs) unprocessed precursors from accumulating γ-secretase substrates (the CTFs). An ideal strategy to solve this problem is to first fractionate the CTFs from their FLs based on their different molecular weights (MW.FL > MW.CTF) and then to quantify these proteins/fragments separately with MS. Tracing back to 2008, Hemming., et al. reported the first attempt to identify γ-secretase substrate unbiasedly by combining the conventional fractionation approach (SDS-PAGE) with MS.[82] They treated Hela cells with γ-secretase inhibitor (DAPT), purified membrane proteins, separated the CTF and FL proteins using SDS-PAGE, cut the gel into fractions and performed in-gel digestion, and eventually sequenced those samples using MS. By quantifying the accumulation of peptides derived from CTF upon DAPT treatment, this study identified at the end only 13 endogenous γ-secretase substrates in Hela cells. Likely due to the low yield of such unbiased approach, to date, most studies of γ-secretase substrates have been still performed in the traditional way, which are largely limited to known proteins for which antibodies are available or in which epitope tags were engineered.[54] We reason that, in the study reported by Hemming., et al., the low

membrane proteins abundance from each fractions after a serial purifying processes might have eventually caused this limited outcome. Therefore, a better fractionation approach with higher loading capacity before fractionation and/or avoiding multi-step protein purification after fractionation might improve this strategy.

The second obstacle of γ-secretase research, which is a conceptual problem with most studies on the biology and pharmacology of γ-secretase, is their reductionist approach. Researchers have often confused the concept of “the function of γ-secretase” with “the function of a certain substrate via γ-secretase”. Most studies focus on analyzing the intracellular signaling of one specific substrate at a time.[54] Indeed these studies have led to important insights into the function of different substrates, e.g. Notch[27] and APP,[24] but they do not really tackle the question of the physiological function of the protease itself. To really understand the physiological function of γ-secretase, one needs to take into account that the net effect of γ-secretase inhibition is the integrated response of all affected signaling pathways in the cellular context at that point in time. Very little work has been done to investigate this question in a systemic way.

With the development of single-cell RNA sequencing (scRNA-seq) technologies, researchers now are able to perform unbiased, high-throughput, and high-resolution transcriptomic analysis of individual cells from complex tissues,[92] like brain samples.[93] We speculate that this approach would provide a good integrated read-out for the overall context-dependent γ-secretase function, e.g. evaluating effects of blocking the processing of γ-secretase proteomes in brain cells exposed to different brain environments.

1.2 Microglia

1.2.1 The guardians of central nervous system?

Microglia are resident macrophages of central nervous system (CNS) that constantly survey brain parenchyma.[94,95] They originate from embryonic yolk sac, migrate into CNS during development, and stay resident for years or even decades dependent on species and local microenvironments.[96–99] Microglia have been considered as long-lived cells but this does not mean that they always survive through adulthood and have limited proliferation, like neurons. Instead, they can undergo turnover at a context-dependent rate by self-renewal in both heathy and disease brain conditions.[98,100,101]

For example, mouse neocortical resident microglia have a median lifetime of over 15 months in homeostatic conditions, but they undergo at least threefold increased proliferation in AD contexts.[98]

Microglia morphologically appear various in different cell states. In healthy brains, “homeostatic state” microglia are ramified with multiple long branches and protrusions dynamically sensing the local brain microenvironment.[94] Upon acute and small brain injuries, microglia in the vicinity of lesions (< 90 μm) get activated rapidly (within the first several minutes post injury), and show protruded processes around the injury sites and more rounded cell somas.[94,102] Chronic stimuli, for instance amyloid plaques and neurofibrillary tangles, change microglial morphology from a ramified to an amoeboid shape.[103]

As a group of phagocytes, one of the key biological features of microglia is their engulfment capacity.[104] Microglia are responsible for the clearance of abnormal extracellular materials including apoptotic cells,[105,106] protein aggregates,[107] myelin debris[108] and microbes[109] in brain. They play a protective role in maintaining brain homeostasis but may act in a detrimental way in AD and other brain disorders.[110–113]

During development, microglia prune excess synapses mediated by the classical complement cascade,[114,115] which is vital important for the formation of mature neural circuits in the brain. However, it has been reported that this physiological microglial function can be inappropriately reactivated and mediates synapse loss in AD brains.[116,117] Synapse loss is an early hallmark of AD and correlates with cognitive impairment,[118–120] while the underlying molecular signals driving this pathological process remained largely unknown. A recent study revealed that perivascular secreted phosphoprotein 1 (SPP1/osteopontin) is the key modulator of microglia mediated synapse engulfment and that ablation of SPP1 prevents synapse loss in an AD mouse model.[121] Intriguingly, while synapse loss is detrimental for cognition in AD, it has been reported that microglial selective engulfment of apoptotic synapses via phosphatidylserine (PtdSer) - TREM2 signal protects neural homeostasis from neuronal hyperactivity in the pre-plaque brains of an AD mouse model.[122] These study suggested that SPP1 and TREM2 both function as upstream modulators of the complement-mediated microglia phagocytosis of synapses but may have divergent contributions to the disease at different stages.

The role of microglia on amyloid pathology in AD remains elusive. By introducing the suicide gene *HSVTK* into microglia under the *CD11b* promoter in an AD rodent model, Grathwohl et al. showed that deletion of microglia does not stop the plaque formation and cannot ameliorate amyloid-associated neuritic dystrophy.[123] Interestingly, another study focusing on the same scientific question reports different results. Shabestari et al. utilized the FIRE mouse model, which is entirely deficient of microglia because of a specific deletion of the microglial-associated fms intronic regulatory element (FIRE) in *Csf1r* enhancer but retains meningeal and perivascular macrophages, and reported that absence of microglia leads to cerebral amyloid angiopathy (CAA) instead of parenchymal plaques, increased brain calcification and hemorrhages, and premature lethality in 5xFAD-FIRE mice.[124]

During bacterial meningitis, e.g. *Streptococcus pneumoniae* infection, microglia phagocytose the pathogens, initiate the immune response and recruit periphery leukocytes to the infection sites.[125] However, the role of microglia involvement in this antibacterial defenses is controversial, because the inflammatory response triggered by microglia-derived cytokines e.g. TNF-α, lL-6, IL-12, etc., may contribute to the deleterious neuronal damage and even lethal cerebral edema.[109,126]

1.2.2 Dynamic players in the cellular phase of Alzheimer's disease

The fundamental hallmarks of AD consist of extracellular amyloid plaques, intracellular neurofibrillary tau tangles (NFTs), neuroinflammation, granulovacuolar degeneration (GVD) and neuronal loss. The "amyloid cascade hypothesis" posits that Aβ deposition is the direct cause of AD which initiates a cascade leading progressively to tau pathology, neuroinflammation, neuronal loss, and, ultimately, dementia.[127,128] Over the past years, large-scale genome-wide association (GWAS) and other genetic studies revealed that the gene variants associated with LOAD are highly enriched in myeloid lineage cells, suggesting these cells, including microglia as the predominant immune cell type in brains, are key modulators in AD etiology.[129–137] From this point of view, AD is not just a neurological disease but is more like an inflammatory disease which may be largely contributed by microglia dysfunction. Indeed, the rather linear and neuron-centric "amyloid cascade hypothesis" cannot adequately explain the long time window between the biochemical changes, i.e. amyloid plaques and neuronal tangles, and the occurrence of clinical symptoms in AD.[138]

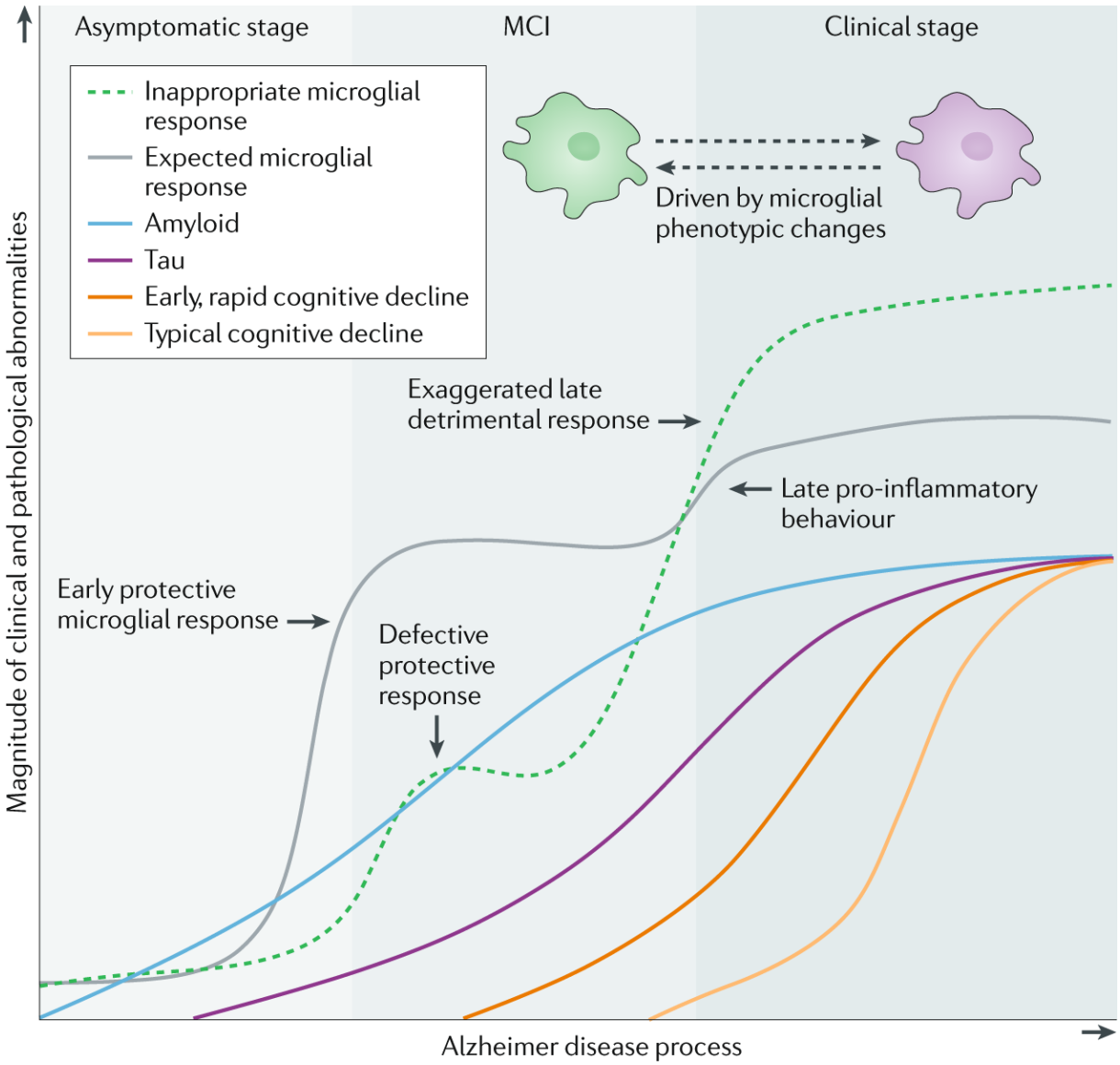


Figure 4. Dynamic changes in microglial activation affect Alzheimer's disease progression. Current evidences, collected from human post-mortem studies, human neuroimaging studies as well as animal model studies, as nicely summarized in ref[139], suggest that, at the early, asymptomatic, stage of AD, the initial microglial response is protective overall. However, as AD progresses, chronic activation causes phenotypic changes in microglia and shifts their behaviour towards a pro-inflammatory phenotype, which causes damage to neuronal networks. Inappropriate microglial responses can occur in individuals with defective protective functions owing to genetic or acquired factors such as microglial priming. Microglia in those individuals might have a weak initial protective response, a quicker transition to phenotypes that are detrimental overall and an exaggerated late-stage deleterious inflammatory response. Individual susceptibility to Alzheimer disease (in terms of more profound clinical presentation at a given pathological stage) might therefore be partly determined by microglial behaviour. MCI, mild cognitive impairment. **Adapted from** *Leng & Edison, et al. 2021.*[139]

The concept of “the cellular phase of AD” that emphasizes complex multiple-cell-type interactions taking place in between “the biochemical phase” and “the clinical phase” has received increasing attention in the field.[138] The cellular phase hypothesis proposes that Aβ deposition acts as a trigger for cellular inflammatory-like reactions which encompass microglia, astroglia, oligodendrocytes, vascular cells and tau reactivity in the neurons and suggests that these cellular processes become self-sustaining, much like a chronic inflammation becomes independent from the initial trigger. Indeed, a spatial transcriptomic study conducted by our colleagues in the lab revealed that, in an AD mouse model, early transcriptomic alterations are mainly involved with myelin and oligodendrocyte genes (OLIGs), whereas a multicellular gene co-expression network of plaque-induced genes (PIGs) involving the complement system, oxidative stress, lysosomes and inflammation is prominent in the later phase of the disease.[140] Therefore, microglia are undoubtedly important participants in the cellular phase of AD, and manipulating microglia biological functions, e.g. enhancing phagocytosis of Aβ plaques, might be promising for AD therapy.[141–143]

By applying high-throughput single-cell transcriptomic approaches in mouse or chimeric models of aging and neurodegenerative disease, several research groups characterized a specific microglial transcriptional phenotype that is called disease-associated microglia (DAM).[144–147] This subpopulation of microglia highly express a series of AD risk genes, such as *Apoe*, *Trem2, Ctsb* and *Ctsd, etc*., as described in the above mentioned genetic studies, which demonstrates a high relevance of DAM for AD. Moreover, pseudo-time trajectory analysis implied a progressive microglia state transition in these AD models from a homeostatic transcriptional phenotypic state (HM) to the activated DAM state. Most importantly, enhancing DAM response by administration of an agonistic anti-TREM2 antibody[148] or an agonistic anti-CLEC7A antibody[149] has shown promising amyloid plaque clearing effects in AD mouse models. At least 7 other important microglia cell states have been described in the context of AD, for instance antigen-presenting response microglia (HLA), interferon response microglia (IRM), transitioning response microglia (TRM), Ribosomal response microglia (Ribo), cytokines response microglia (CRM), transitioning cytokines response microglia (tCRM) and cycling and proliferating microglia (CPM), demonstrating the heterogeneity of microglia differentiated into multiple response

states.[144,145,147,150] However, the functional relevance of microglia in these specific transcriptomic states, comparing to DAM, remains largely unexplored.

1.2.3 γ-Secretase substrates participate in microglia biology

We referred to the most recent review literature[54] that compiled 149 reported γ-secretase substrates and complemented the list to 161 by searching for the related peer-reviewed articles in Pubmed (See Table 1). Interestingly, although these so far reported γ-substrates were investigated in various cell types or tissues, we found 52 out of the 161 are encoded by genes that are part of the transcriptional changes defining specific microglia states in AD models.[145,150]

Colony stimulating factor 1 receptor (CSF1R) is a tyrosine kinase transmembrane receptor vital for microglial survival[151] and is highly expressed in homeostatic (HM) microglia. It has been reported that inhibitors blocking CSF1R signaling effectively reduced the proliferation of microglia and attenuated neurodegeneration in both amyloid[152] and tau[153] mouse models of AD. Exposure of macrophages to lipopolysaccharide (LPS) induces rapid degradation of CSF1R via γ-secretase cleavage, which results in the release of its soluble ICD containing the tyrosine kinase domain into cytosol.[154] While the Toll-like receptors have been shown to be responsible for LPS induced macrophage activation, whether the released CSF1R ICD is involved in this signaling process remains unknown.[155]

All of the three members (TYRO3, AXL and MERTK) of TAM receptor tyrosine kinase family have been reported to be cleaved by γ-secretase.[156] TYRO3 is prominently expressed by neuron but not in microglia.[157] Macrophages recognize the so-called “eat-me” signals that are prominently provided by phosphatidylserine (PtdSer) and phagocytose apoptotic cells via cell surface receptors including AXL and MERTK.[105] Both AXL and MERTK have been shown to be responsible for microglial phagocytosis of Aβ plaques, and the microglia in *Axl*$^{-/-}$*Mertk*$^{-/-}$ *APP/PS1* mice were blunted to respond to the amyloid pathology.[157] Interestingly, *Axl* is highly expressed in DAM, while *Mertk* is highly expressed in HM.

Signal regulatory protein α (SIRPα) is a membrane immunoreceptor that is highly expressed in myeloid lineage cells[158] and get upregulated in DAM cells in a chimeric AD model.[150] Upon binding with its ligand CD47, a multi-pass transmembrane protein

expressed by many different cell types, phosphorylation occurs in the cytoplasmic immunoreceptor tyrosine-based inhibitory motif (ITIM) of SIRPα, resulting in inhibition of NF-κB signaling in macrophages.[159] Host cells, for instance erythrocytes and platelets, express CD47 as the "don't eat me" signal that negatively regulates the phagocytosis mediated by macrophages.[160,161] It has been reported that LPS and TNFα induce the rapid proteolysis of SIRPα by γ-secretase, which releases the SIRPα-ICD into cytosol.[57] In the other way around, ectopic overexpression of the ITIM-containing SIRPα-ICD resulted in enhanced STAT-1 and NF-κB pathway activation, suggesting a negative regulation of "don't eat me" signal mediated by γ-secretase.[57,159]

Another known substrate of γ-secretase in microglia is TREM2[162] which carries major genetic risk of AD.[131,163] TREM2 is of pivotal importance in the DAM response of microglia to amyloid plaques, and deleting *Trem2* causes a blockage of this putatively protective microglia response.[144,164,165] TREM2 signaling is mediated by its adaptor protein TYROBP. The latter contains an immunoreceptor tyrosine-based inhibitory motif (ITAM) which get phosphorylated upon ligand-TREM2 interaction and recruits Syk protein kinase to regulate mitogen-activated protein kinase (MAPK) and phospholipase Cγ (PLCγ)-dependent signaling pathways.[166] It has been proposed that γ-secretase inhibition accumulates the membrane-bound TREM2-CTF which might trap TYROBP and compete its binding with the functional full length TREM2.[167] Thereby, without adequate binding with its adaptor, the TREM2 downstream signaling transduction might be attenuated upon γ-secretase inhibition. However, this hypothesis requires the precondition of a slower turnover of TYROBP than TREM2, which means TREM2 should be always more abundant than TYROBP. It is not clear whether this is true in the real situation. Therefore, whether and how TREM2 signaling transduction is mediated by γ-secretase remains largely unclear.

Glycoprotein non-metastatic melanoma protein B (GPNMB) is a single-pass type I glycoprotein with substantial sequence homology to premelanosome protein (PMEL), both of which are cleaved by γ-secretase.[168,169] *GPNMB* is one of the top highly expressed DAM marker genes in both human and mouse microglia in AD as revealed by single-cell transcriptomic studies.[144,145,150] Biochemical measurements also reveal that elevated GPNMB co-localizes with a distinct population of microglia cells that cluster around amyloid plaques in sporadic AD brains.[170] GPNMB expression is elevated also in the white matter of Nasu-Hakola disease (NHD) brains, which are

patients with loss of function mutations of TREM2 or TYROBP.[171] Moreover, GPNMB is vital for the internalization of α-synuclein (αSyn) in stem cell derived neurons.[172] While the role of GPNMB in microglia is far to clear, its homologue PMEL is highly expressed in melanocytes, and its proteolytic process has been studied as the physiological model of amyloid formation.[173] BACE2 has been reported to act as a sheddase to release a luminal fragment containing the so-called Mα fragments, whose oligomerization and aggregation further form the pigmented fibrils in the melanosomes of pigment cells.[174] *Bace2*$^{-/-}$ mice show abnormal melanogenesis represented by a coat color defect (Figure 5A). γ-secretase seems not directly involved in the proteolytic processes that generate Mα fragments, and so far no clear evidence has shown that the cleavage of PMEL-CTF via γ-secretase is involved in signaling processes.[173] However, it has been reported that mutations in and near the transmembrane domain alter PMEL amyloid formation.[175] Interestingly, we found that the γ-secretase inhibitor Semagacestat treated *App*$^{NL\text{-}G\text{-}F}$ mice showed a clear coat color defect as well (Figure 5B), suggesting the involvement of γ-secretase in the process of melanogenesis, likely via a signaling event. Therefore, it will be interesting to study in the future whether γ-secretase cleavage on GPNMB plays a signaling role in microglia biological functions in AD.



Figure 5. Coat color defects in *Bace2*$^{-/-}$ mice and Semagacestat treated *App*$^{NL\text{-}G\text{-}F}$ mice. **A.** Coat color defect of *Bace2*$^{-/-}$ mouse compared with its *WT* and *Bace1*$^{-/-}$ littermates. **B.** Coat color defects in Semagacestat treated *App*$^{NL\text{-}G\text{-}F}$ mice (Bi and Bii) compared with the Vehicle treated control littermate (Biii). *App*$^{NL\text{-}G\text{-}F}$ mice were treated with Semagacestat in a dose of 60 mg/kg weight per day in diet for 4 weeks. **Figure 5A is adapted from** *Rochin, et al. 2013.*[174]

Many other microglia proteins besides exemplified above are cleaved by γ-secretase (See Table 1). It should be noticed that most of substrates listed in this table were identified in various cell models and in a biased way (i.e. candidate substrate approach). We predict that by using an unbiased γ-secretase substrate identification approach we will be able to have a systemic understanding of the role of γ-secretase in microglia. This will not only enrich the knowledge of γ-secretase biology but might also provide novel targets for AD therapy.

Table 1. Full list of reported γ-secretase substrates updated to February 2023. We compiled in total 161 transmembrane proteins that undergo γ-secretase cleavage by searching in Pubmed for the related peer-reviewed articles published until Februray 2023 using the key words “gamma secretase AND (substrate OR cleavage OR process OR shedding)”. Proteins are sorted alphabetically by their short names. The table displays the protein ID according to the organism where it was initially identfied and indicates the ID of its most similar orthologue in mouse and human, according to the Mouse Genome Informatics (MGI) website (URL: http://www.informatics.jax.org)[176]. Proteins listed in this table are single-pass type I membrane proteins unless specifically indicated differently. NA: not available. *: single-pass type II membrane protein. **: single-pass type III membrane protein. ***: multi-pass membrane protein. We refer to the recent human microglia single-cell RNA sequencing study[150] for the annotation of human proteins encoded by genes that are among the top differentially expressed genes (DEGs) in the specific human microglia states. For the mouse proteins we refer to the microglia single-cell RNA sequencing study.[145] DEGs are the genes most significantly upregulated or downregulated in a particular microglia cell state vs cells in the other states. |avg_Log2FC| > 0.1. adj_P-value < 0.05 using Bonferroni correction. HM: homeostatic microglia; DAM: disease associated microglia; HLA: antigen-presenting response microglia; IRM: interferon response microglia; Ribo: Ribosomal response microglia; CRM: cytokines response microglia; Trans-CRM: transitioning cytokines response microglia. CPM: cycling and proliferating microglia. The name of microglia states are highlighted in red if the corresponding DEGs are up-regulated in the specific cell states, while the name of microglia states are highlighted in blue if the corresponding DEGs are down-regulated in the specific cell states.

No.	Protein name	Original identified organism and ID	Human ortholog ID	Involved cell state human sc	Mouse ortholog ID	Involved cell state mouse sc	Reference
1.	ACP2	Human (P11117)	P11117	IRM Ribo	P24638	H1M DAM TRM	177
2.	ACE2	Human (Q9BYF1)	Q9BYF1		Q8R0I0		178
3.	ADAM10	Mouse (O35598)	O14672	Ribo	O35598	H1M DAM TRM	179
4.	Alcadein α	Human (O94985)	O94985	Ribo	Q9EPL2		180
5.	Alcadein β	Human (Q9BQT9)	Q9BQT9		Q99JH7		180
6.	Alcadein γ	Human (Q9H4D0)	Q9H4D0		Q9ER65		180
7.	APLP1	Mouse (Q03157)	P51693		Q03157		181
8.	APLP2	Human (Q06481)	Q06481	HM Trans-CRM DAM HLA Ribo CRM	Q06335	DAM H1M H2M	181

9.	apoER2	Mouse (Q924X6)	Q14114		Q924X6		182
10.	APP	Mouse (P12023)	P05067	Ribo	P12023		24
11.	AXL	Human (P30530)	P30530	DAM IRM Ribo	Q00993	DAM IRM TRM H1M H2M	156,183
12.	BCMA**	Human (Q02223)	Q02223		O88472		77
13.	Betacellulin	Human (P35070)	P35070		Q05928		184
14.	Betaglycan	Rat (P26342)	Q03167		O88393		185
15.	CACHD1	Mouse (Q6PDJ1)	Q5VU97		Q6PDJ1		186
16.	Cadherin-6B	Chicken (Q90762)	P55285		P97326		187
17.	CADM1	Mouse (Q8R5M8)	Q9BY67		Q8R5M8	DAM H1M H2M	188
18.	CAR	Human (P78310)	P78310		P97792		189
19.	CD147	Human (P35613)	P35613	Ribo	P18572	DAM TRM H1M	190
20.	CD200	Human (P41217)	P41217		O54901		191
21.	CD43	Human (P16150)	P16150	Ribo	P15702		192
22.	CD44	Human (P16070)	P16070		P15379	DAM	193
23.	CD99	Human (P14209)	P14209	HM HLA Ribo	Q8VCN6		194
24.	CSF1R	Mouse (P09581)	P07333	HM Trans-CRM DAM HLA IRM Ribo	P09581	H1M H2M DAM TRM	195
25.	CX3CL1	Human (P78423)	P78423		O35188		196
26.	CXCL16	Human (Q9H2A7)	Q9H2A7	DAM HM Ribo	Q8BSU2	DAM CRM H1M H2M	196
27.	DCC	Rat (Q63155)	P43146		P70211		197
28.	Delta1	Mouse (Q61483)	O00548		Q61483		198–200
29.	Desmoglein-2	Human (Q14126)	Q14126		O55111		82

30.	DNER	Human (Q8NFT8)	Q8NFT8		Q8JZM4		82
31.	DR6	Human (O75509)	O75509	DAM HLA Ribo	Q9EPU5		201
32.	DSCAM	Mouse (Q9ERC8)	O60469		Q9ERC8		202
33.	DSCAML1	Mouse (Q4VA61)	Q8TD84		Q4VA61		202
34.	Dystroglycan	Human (Q14118)	Q14118		Q62165		82
35.	E-Cadherin	Mouse (P09803)	P12830		P09803		203
36.	EpCAM	Human (P16422)	P16422		Q99JW5		204
37.	EphA2	Human (P29317)	P29317		Q03145	CPM DAM	156
38.	EphA3	Mouse (P29319)	P29320		P29319		205
39.	EphA4	Rat (D3ZZK3)	P54764		Q03137		206
40.	EphA5	Human (P54756)	P54756		Q60629		156
41.	EphA7	Human (Q15375)	Q15375		Q61772		156
42.	EphB2	Mouse (P54763)	P29323	IRM	P54763		207
43.	EphB3	Human (P54753)	P54753		P54754		156
44.	EphB4	Human (P54760)	P54760		P54761		156
45.	EphB6	Human (O15197)	O15197		O08644		156
46.	Ephrin-B1	Mouse (P52795)	P98172	Ribo	P52795	H1M DAM	208
47.	Ephrin-B2	Mouse (P52800)	P52799	Ribo	P52800		209
48.	ErbB4	Human (Q15303)	Q15303		Q61527		210
49.	F11R	Human (Q9Y624)	Q9Y624		O88792	H2M DAM TRM	177
50.	FGFR3	Mouse (Q61851)	P22607		Q61851		211
51.	FGFR4	Human (P22455)	P22455		Q03142		156

52.	FLT1	Bovine (F1MDD9)	P17948		P35969	DAM H1M H2M	212
53.	Frizzled-2***	Fruit fly (Q9VVX3)	Q14332		Q9JIP6		213
54.	GHR	Mouse (P16882)	P10912		P16882		214
55.	GLG1	Human (Q92896)	Q92896	Ribo	Q61543		177
56.	GluR3***	Mouse (Q9Z2W9)	P42263		Q9Z2W9		215
57.	GnT-V*	Human (Q09328)	Q09328	Ribo	Q8R4G6	H1M DAM TRM	216
58.	GPNMB	Human (Q14956)	Q14956	DAM HM HLA CRM Trans-CRM	Q99P91	DAM H1M H2M	168
59.	HER2	Human (P04626)	P04626		P70424		217
60.	HLA-A2	Human (P01892)	P04439	HLA IRM HM Ribo Trans-CRM	NA		218
61.	IFNαR2	Human (P48551)	P48551	Ribo	O35664	DAM	219
62.	IGF1R	Human (P08069)	P08069		Q60751		220
63.	IL11R	Human (Q14626)	Q14626		Q64385	DAM	221
64.	IL1R1	Human (P14778)	P14778		P13504	DAM	222
65.	IL1R2	Human (P27930)	P27930		P27931		223
66.	IL6R	Human (P08887)	P08887	HLA Ribo	P22272	H1M DAM TRM	224
67.	INSR	Human (P06213)	P06213		P15208	H1M H2M TRM	225
68.	Ire1α	Human (O75460)	O75460		Q9EQY0		226
69.	Ire1β	Human (Q76MJ5)	Q76MJ5		Q9Z2E3		226
70.	Jagged1	Rat (Q63722)	P78504	HM Trans-CRM DAM HLA IRM Ribo CRM	Q9QXX0		200
71.	Jagged2	Human (Q9Y219)	Q9Y219		Q9QYE5		198

72.	KCNE1	Human (P15382)	P15382		P23299		227
73.	KCNE2	Human (Q9Y6J6)	Q9Y6J6		Q9D808		227
74.	Klotho	Human (Q9UEF7)	Q9UEF7		O35082		228
75.	L1	Mouse (P11627)	P32004		P11627		229
76.	LAR	Human (P10586)	P10586		A2A8L5		230
77.	LDLR	Human (P01130)	P01130		P35951	DAM H1M H2M	177
78.	LRP1	Human (Q07954)	Q07954	Ribo	Q91ZX7	H1M H2M DAM IRM TRM	231
79.	LRP1b	Human (Q9NZR2)	Q9NZR2		Q9JI18		232
80.	LRP6	Human (O75581)	O75581		O88572		233
81.	Megalin	Opossum (Q6E0K3)	P98164		A2ARV4		234
82.	MERTK	Human (Q12866)	Q12866	HM DAM HLA IRM Ribo CRM	Q60805	H1M H2M DAM TRM	156
83.	MET	Human (P08581)	P08581		P16056		235
84.	MUC1	Human (P15941)	P15941		Q02496		236
85.	MUSK	Human (O15146)	O15146		Q61006		156
86.	N-cadherin	Human (P19022)	P19022		P15116		237
87.	Nectin-1α	Mouse (Q9JKF6)	Q15223		Q9JKF6		238
88.	Nectin-3	Mouse (Q9JLB9)	Q9NQS3		Q9JLB9		239
89.	Neogenin	Human (Q92859)	Q92859		P97798		240
90.	Neuregulin-1	Mouse (Q6DR98)	Q02297		Q6DR98		241
91.	Neuregulin-2	Mouse (P56974)	O14511		P56974		242
92.	Neurexin-1-β	Rat (Q63373)	P58400		P0DI97		243

93.	Neurexin-2-β	Rat (Q63376)	P58401		E9Q7X7		243
94.	Neurexin-3-β	Human (Q9HDB5)	Q9HDB5		Q8C985		244
95.	Neuroligin-1	Rat (Q62765)	Q8N2Q7		Q99K10		245,246
96.	Neuroligin-2	Rat (Q62888)	Q8NFZ4		Q69ZK9		245
97.	NG2	Mouse (Q8VHY0)	Q6UVK1		Q8VHY0	DAM	247
98.	NGL-3	Rat (P0CC10)	Q9NT99		P0C192		248
99.	NLRR3	Human (Q9H3W5)	Q9H3W5		Q8CBC6		249
100.	Notch-1	Mouse (Q01705)	P46531	Ribo	Q01705	H1M TRM	27
101.	Notch-2	Mouse (O35516)	Q04721		O35516	H1M DAM TRM	250
102.	Notch-3	Mouse (Q61982)	Q9UM47		Q61982		250
103.	Notch-4	Mouse (P31695)	Q99466		P31695	H1M	250
104.	NPR-C	Mouse (P70180)	P17342		P70180		82
105.	NRADD**	Mouse (Q8CJ26)	NA		Q8CJ26		78
106.	p75NTR	Human (P08138)	P08138		Q9Z0W1		251
107.	PAM	Rat (P14925)	P19021		P97467		252
108.	PDPN	Human (Q86YL7)	Q86YL7	DAM IRM CRM HM Trans-CRM Ribo	Q62011		253
109.	Pianp	Mouse (Q6P1B3)	Q8IYJ0		Q6P1B3	DAM	254
110.	PLXDC2	Human (Q6UX71)	Q6UX71	DAM IRM Ribo	Q9DC11	DAM H2M	82
111.	Pmel17	Human (P40967)	P40967		Q60696		169
112.	Polycystin-1***	Human (P98161)	P98161		O08852	H1M TRM	255
113.	Polyductin	Human (P08F94)	P08F94		E9PZ36		256
114.	PRiMA	Mouse (Q810F0)	Q86XR5		Q810F0		257

115.	Protocadherin-12	Human (Q9NPG4)	Q9NPG4	Ribo	O55134		258
116.	Protocadherin-α4	Rat (Q767I8)	Q9UN74		O88689		259
117.	Protocadherin-γ-A1	Rat (I6LBW6)	Q9Y5H4		Q91XZ0		259
118.	Protocadherin-γ-A3	Mouse (Q91XY5)	Q9Y5H0		Q91XY5		260
119.	Protocadherin-γ-C3	Mouse (Q91XX1)	Q9UN70		Q91XX1		260
120.	Protogenin	Chicken (Q589G5)	Q2VWP7		Q2EY15		261
121.	PTK7	Human (Q13308)	Q13308		Q8BKG3		262
122.	PTPRT	Mouse (Q99M80)	O14522		Q99M80		263
123.	Ptprζ	Rat (Q62656)	P23471		B9EKR1		264
124.	PVRL2	Mouse (P32507)	Q92692	IRM Ribo	P32507		177
125.	RAGE	Human (Q15109)	Q15109		Q62151		265
126.	Robo1	Human (Q9Y6N7)	Q9Y6N7		O89026		266
127.	RPTPκ	Mouse (P35822)	Q15262		P35822		267
128.	RPTPμ	Mouse (P28828)	P28827		P28828	H1M H2M TRM	267
129.	RYK	Human (P34925)	P34925	Ribo	Q01887		268
130.	SEZ6	Mouse (Q7TSK2)	Q53EL9		Q7TSK2		269
131.	SEZ6L	Human (Q9BYH1)	Q9BYH1		Q6P1D5		177
132.	SEZ6L2	Human (Q6UXD5)	Q6UXD5		Q4V9Z5		177
133.	SIRPα	Human (P78324)	P78324	DAM Ribo	P97797		57
134.	SorCS1	Human (Q8WY21)	Q8WY21		Q9JLC4		270,271
135.	SorLA	Human (Q92673)	Q92673	IRM Ribo	O88307		270–272
136.	Sortilin	Human (Q99523)	Q99523	Ribo	Q6PHU5	H1M DAM TRM	270

137.	Syndecan-1	Human (P18827)	P18827		P18828		82
138.	Syndecan-2	Human (P34741)	P34741		P43407		82
139.	Syndecan-3	Human (O75056)	O75056		Q64519	DAM IRM H1M H2M	273
140.	SYT7**	Mouse (Q9R0N7)	O43581		Q9R0N7		79
141.	TIE1	Human (P35590)	P35590		Q06806		274
142.	TMEFF2	Human (Q9UIK5)	Q9UIK5		Q9QYM9		275
143.	TNFR1	Human (P19438)	P19438	HM Trans-CRM DAM HLA Ribo	P25118	TRM	276
144.	TNFRSF12A	Human (Q9NP84)	Q9NP84		Q9CR75	CRM	80
145.	TREM2	Human (Q9NZC2)	Q9NZC2	DAM IRM Ribo	Q99NH8	DAM TRM H1M H2M	162
146.	TRKA	Human (P04629)	P04629		Q3UFB7		156
147.	TRKB	Mouse (P15209)	Q16620		P15209		277
148.	TROP2	Mouse (Q8BGV3)	P09758		Q8BGV3		278
149.	TYRO3	Human (Q06418)	Q06418		P55144		156
150.	Tyrosinase	Mouse (P11344)	P14679		P11344		279
151.	TYRP1	Mouse (P07147)	P17643		P07147		279
152.	TYRP2	Mouse (P29812)	P40126		P29812		279
153.	Vasorin	Human (Q6EMK4)	Q6EMK4		Q9CZT5		82
154.	VE-cadherin	Human (P33151)	P33151		P55284		280
155.	VEGFR2	Human (P35968)	P35968		P35918		281
156.	VEGFR3	Human (P35916)	P35916		P35917		156
157.	VGSC β1	Mouse (P97952)	Q07699		P97952		282
158.	VGSC β2	Human (O60939)	O60939		Q56A07		282,283

159.	VGSC β3	Mouse (Q8BHK2)	Q9NY72	Q8BHK2	[282]
160.	VGSC β4	Mouse (Q7M729)	Q8IWT1	Q7M729	[282]
161.	VLDLR	Mouse (P98156)	P98155	P98156	[284]

Chapter 2: Research objectives

The general goal of this project is to systemically investigate the biological function of γ-secretase by profiling its endogenous substrate proteome and evaluating the effects of its deficiency in microglia.

Specific objectives:

- We aim to develop an unbiased proteomic approach for high-throughput identification of γ-secretase substrates.
- We aim to evaluate the effects of γ-secretase deficiency on microglia transcriptional cell states in different cellular contexts using scRNA-seq.

Chapter 3: Materials and Methods

3.1 Key Resources Table

REAGENT or RESOURCE	SOURCE	IDENTIFIER
Antibodies		
Anti-APP-c20 (B63.3)	De Strooper's lab,[285] KU Leuven	N/A
Anti-PSEN1-NTF (B19)	De Strooper's lab,[286] KU Leuven	N/A
Anti-APH1A-CTF (B80.3)	De Strooper's lab,[287] KU Leuven	N/A
Anti-Nicastrin (9C3)	De Strooper's lab,[285] KU Leuven	N/A
Anti-PEN2-NTF (B126)	De Strooper's lab,[288] KU Leuven	N/A
Anti-hPSEN1-NTF (MKAD 3.5)	Marc Mercken,[289] Mitsubishi Kasei Institute of Life Sciences	N/A
Anti-PSEN2-CTF (D30G3)	Cell Signaling Technology	Cat#9979; RRID:AB_10829910
Anti-APH1B (Anti-APH1b/c)(L82)	De Strooper's lab,[290] KU Leuven	N/A
Anti-APLP2 (W2CT)	David Walsh, University College Dublin	N/A
Anti-Syndecan 3 (2E9)	Guido David, KU Leuven	N/A
Anti-LRP1 (EPR3724)	Epitomics	Cat#2703-1
Anti-GAPDH	HyTest	Car#5G4-6C5; RRID:AB_1616722
Anti-β-ACTIN	Sigma	Cat#A5441; RRID:AB_476744
Anti-ATP1A1	Novus Bio	Cat#NB300-146; RRID:AB_2060979
Anti-FLAG (M2)	Sigma	Cat#F3165; RRID:AB_259529
Anti-GFP	Abcam	Cat#Ab13970; RRID:AB_300798

Anti-Amyloid β (N) (82E1)	IBL	Cat#10323; RRID:AB_1630806
Goat anti-mouse IgG-HRP	Bio-Rad	Cat#170-6516; RRID:AB_11125547
Goat anti-rabbit IgG-HRP	Bio-Rad	Cat#170-6515; RRID:AB_11125142
Donkey anti-mouse IgG-AF647	Invitrogen	Cat#A31571; RRID:AB_162542
Donkey anti-chicken IgG-AF488	Jackson Immunolabs	Cat#703-545-155; RRID:AB_2340375
Anti-human CD11b MicroBeads	Miltenyi	Cat#130-093-634
Anti-mouse CD11b-PE (REA592)	Miltenyi	Cat#130-113-806; RRID:AB_2751172
Anti-mouse CD45-BV421	BD Biosciences	Cat#563890; RRID:AB_2651151
Anti-mouse Hashtag 1 (A0301)	BioLegend	Cat#155801; RRID:AB_2750032
Anti-mouse Hashtag 2 (A0302)	BioLegend	Cat#155803; RRID:AB_2750033
Anti-mouse Hashtag 3 (A0303)	BioLegend	Cat#155805; RRID:AB_2750034
Anti-mouse Hashtag 4 (A0304)	BioLegend	Cat#155807; RRID:AB_2750035
Anti-human Hashtag 1 (A0251)	BioLegend	Cat#394601; RRID:AB_2750015
Anti-human Hashtag 2 (A0252)	BioLegend	Cat#394603; RRID:AB_2750016
Anti-human Hashtag 3 (A0253)	BioLegend	Cat#394605; RRID:AB_2750017
Anti-human Hashtag 4 (A0254)	BioLegend	Cat#394607; RRID:AB_2750018
Anti-human Hashtag 5 (A0255)	BioLegend	Cat#394609; RRID:AB_2750019

Anti-human Hashtag 6 (A0256)	BioLegend	Cat#394611; RRID:AB_2750020
Anti-human Hashtag 7 (A0257)	BioLegend	Cat#394613; RRID:AB_2750021
Anti-human Hashtag 8 (A0258)	BioLegend	Cat#394615; RRID:AB_2750022
Anti-human Hashtag 9 (A0259)	BioLegend	Cat#394617; RRID:AB_2750023
Anti-human Hashtag 10 (A0260)	BioLegend	Cat#394619; RRID:AB_2750024
Anti-human Hashtag 12 (A0262)	BioLegend	Cat#394623; RRID:AB_2750025
Anti-human Hashtag 13 (A0263)	BioLegend	Cat#394625; RRID:AB_2750026
Biological Samples		
Human brain tissue	Tom Theys, UZ Leuven	https://www.uzleuven.be/nl
Chemicals, Peptides, and Recombinant Proteins		
Semagacestat	Jassen Pharmaceuticals	LY-450139
Tamoxifen	Sigma	Cat#T5648-1G
Rock inhibitor	Sigma	Cat#Y-27632
L-Glutamine	Sigma	Cat#G7513
N-acetyl-L-cysteine	Sigma	Cat#A7250
Human insulin	Sigma	Cat#I9278
Apo-transferrin	Sigma	Cat#T1147
Sodium selenite	Sigma	Cat#S9133
Cholesterol	Sigma	Cat#C4951
Heparin sulfate	Ams bio UK	Cat#GAG-HS01
Recombinant Human BMP4	Peprotech	Cat#120-05
Recombinant Human SCF	Peprotech	Cat#300-07
Recombinant Human VEGF	Peprotech	Cat#100-20

Recombinant Human M-CSF	Peprotech	Cat#300-25
Recombinant Human IL-3	Peprotech	Cat#200-03
Recombinant Human IL34	Peprotech	Cat#200-34
TGFβ1	Peprotech	Cat#100-21
CX3CL1	Peprotech	Cat#300-31
SuperScript™ II Reverse Transcriptase	Invitrogen	Cat#18064
Oligo(dT)12-18	Invitrogen	Cat#18418012
RNaseOUT™	Invitrogen	Cat#10777-019
dNTP Mix	Invitrogen	Cat#18427089
DTT	Sigma	Cat#3483-12-3
SensiFAST Sybr No Rox Mix 2x	Meridian	Cat#BIO-98005
Percoll	GE Healthcare	Cat#17-5445-02
Red Blood Cell Lysis Buffer	Biolegend	Cat#420301
Fixable Viability Dye eFluor™ 506/780	eBioscience	Cat#65-2860-40
Actinomycin D	Sigma	Cat#A1410
Protease inhibitor cocktail	Roche	Cat#11697498001
Critical Commercial Assays		
Neural Tissue Dissociation Kit (P)	Miltenyi	Cat#130-092-628
RNeasy® Micro Kit	QIAGEN	Cat#74004
Bradford Protein Assay	Bio-Rad	Cat#5000001
TransIT®-LT1 Transfection Reagent	Mirus	Cat#MIR 2305
GELFREE 8100 10% Cartridge Kit	Expedeon	Cat#SKU 42105
Single-cell gene expression profiling kit	10X Genomics	Cat#CG000204_ChromiumNextGEMSingleCell3_v3.1

Deposited Data		
Original images and blots	This paper	http://dx.doi.org/10.17632/kgzzfrm272.1
Proteomics dataset	This paper	PXD039238
Single-cell dataset	This paper	GSE245391
Transcriptomics dataset	Mancuso et al.[146]	GSE137444
Transcriptomics dataset	Sala Frigerio et al.[145]	GSE127893
Transcriptomics dataset	Hasselman et al.[147]	GSE133433
Transcriptomics dataset	Keren-Shaul et al.[144]	GSE98969
Transcriptomics dataset	Friedman et al.[291]	GSE89482
Experimental Models: Cell Lines		
H9 stem cell line	De Strooper's lab	WAe009-A; https://hpscreg.eu/cellline/WAe009-A
HEK293T/17	ATCC	Cat#CRL-11268
Experimental Models: Organisms/Strains		
Mouse: *C57BL/6J*	The Jackson Laboratory	Cat#000664
Mouse: *App*$^{NL\text{-}G\text{-}F}$	Takaomi Saido,[292] RIKEN Center for Brain Science	N/A
Mouse: *Cx3cr1*$^{CreERT2/WT}$	The Jackson Laboratory[293]	Cat#021160
Mouse: *Aph1a*$^{fl/fl}$*b*$^{-/-}$*c*$^{fl/fl}$	De Strooper's lab[287]	Cat#030985
Mouse: *Cx3cr1*$^{CreERT2/WT}$ x *Aph1a*$^{fl/fl}$*b*$^{-/-}$*c*$^{fl/fl}$	This paper	N/A
Mouse: *Cx3cr1*$^{CreERT2/WT}$ x *Aph1a*$^{fl/fl}$*b*$^{-/-}$*c*$^{fl/fl}$ x *App*$^{NL\text{-}G\text{-}F}$	This paper	N/A
Oligonucleotides		
See Table S4 for Primer pairs of qPCR	This paper	N/A

Recombinant DNA		
pcDNA3.1+ hTNFRSF1B/C-(K)DYK	GenScript	Cat#OHU19055D
pcDNA3.1+ hCD300A/C-(K)DYK	GenScript	Cat#OHU05929D
pcDNA3.1+ hMILR1/C-(K)DYK	GenScript	Cat#OHu15096D
pLKO.1-puro-CMV-TurboGFP™	Sigma	Cat#SHC003
Software and Algorithms		
ImageJ	NIH	https://imagej.nih.gov/ij/
Image Studio Lite Ver 5.2	LI-COR	https://www.licor.com/bio/image-studio/
Prism 9	GraphPad	https://www.graphpad.com/scientificsoftware/prism/
FCS Express 7	De Novo Software	https://denovosoftware.com/
NIS-Elements AR (5.41.01)	Nikon	https://www.microscope.healthcare.nikon.com/en_AOM/products/software/nis-elements
Inkscape (0.92.4)	"Inkscape's Contributors" and "The Inkscape Project"	https://inkscape.org/
GIMP (2.10.18)	GNU Image Manipulation Program	https://www.gimp.org/
BioRender	BioRender	https://www.biorender.com/
R (v4.1.0)	R Core Team and the R Foundation for Statistical Computing	https://www.r-project.org/
Cell Ranger (v6.0.1)	10x Genomics	https://support.10xgenomics.com/single-cell-gene-expression/software/
Seurat (v4.0)	Satija lab[294]	https://satijalab.org/seurat/
MaxQuant (v 1.6.10.43)	MaxQuant	https://www.maxquant.org/

3.2 Experimental Model And Study Participant Details

3.2.1 Mice

C57BL/6J mice (JAX stock #000664), *App*$^{NL-G-F}$ mice (obtained from Dr. Takaomi Saido)[292], *Cx3cr1*$^{CreERT2/wt}$ mice (JAX stock #021160)[293] and *Aph1a*$^{fl/fl}$*b*$^{-/-}$*c*$^{fl/fl}$ mice (JAX stock #030985)[287] were bred and maintained in local facilities. *Cx3cr1*$^{CreERT2/wt}$ mice and *Aph1a*$^{fl/fl}$*b*$^{-/-}$*c*$^{fl/fl}$ mice were crossed to generate the tamoxifen-inducible microglia-specific γ-secretase conditional KO mice (*Cx3cr1*$^{CreERT2/wt}$ x *Aph1a*$^{fl/fl}$*b*$^{-/-}$*c*$^{fl/fl}$). This strain was further crossed with *App*$^{NL-G-F}$ mice to generate the mice with AD background (*Cx3cr1*$^{CreERT2/wt}$ x *Aph1a*$^{fl/fl}$*b*$^{-/-}$*c*$^{fl/fl}$ x *App*$^{NL-G-F}$). 3-month-old *Cx3cr1*$^{CreERT2/wt}$ x *Aph1a*$^{fl/fl}$*b*$^{-/-}$*c*$^{fl/fl}$ mice, 3-month-old and 7-month-old *Cx3cr1*$^{CreERT2/wt}$ x *Aph1a*$^{fl/fl}$*b*$^{-/-}$*c*$^{fl/fl}$ x *APP*$^{NL-G-F}$ mice were used for the single-cell RNA sequencing experiment. 6-Month-old *Cx3cr1*$^{wt/wt}$ x *Aph1a*$^{fl/fl}$*b*$^{-/-}$*c*$^{fl/fl}$ x *APP*$^{NL-G-F}$ mice were used for tamoxifen control. For brevity reasons, in the following texts we called tamoxifen-treated and vehicle-treated *Cx3cr1*$^{CreERT2/wt}$ x *Aph1a*$^{fl/fl}$*b*$^{-/-}$*c*$^{fl/fl}$ mice as *GS*^{iΔMG} and *GS*^{WT}mice, separately. We called tamoxifen-treated and vehicle-treated *Cx3cr1*$^{CreERT2/wt}$ x *Aph1a*$^{fl/fl}$*b*$^{-/-}$*c*$^{fl/fl}$ x *APP*$^{NL-G-F}$ mice as *App*$^{NL-G-F}$*-GS*^{iΔMG} and *App*$^{NL-G-F}$*-GS*^{WT}mice, separately. We called tamoxifen-treated and vehicle-treated *Cx3cr1*$^{wt/wt}$ x *Aph1a*$^{fl/fl}$*b*$^{-/-}$*c*$^{fl/fl}$ x *APP*$^{NL-G-F}$ mice as *App*$^{NL-G-F}$*-TAM_QC* and *App*$^{NL-G-F}$*-Ctrl_QC* mice, separately. 5-month-old *C57BL/6J* mice were used for detection of γ-secretase subunits in microglia. Both female and male animals were used in experiments. Littermates of the same sex were randomly assigned to experimental groups. Mice were housed in groups of 2-4, under a 14 h light (7 am to 9 pm) and 10 h dark cycle at 21°C, with food and water *ad libitum*. All experiments were conducted according to protocols approved by the local Ethical Committee of Laboratory Animals of the KU Leuven (government license LA1210579, ECD project number P177/2020) following local and EU guidelines.

3.2.2 Primary human microglia

For human microglia isolation, temporal neocortex tissues were obtained from a 2-year old male and a 22-year old female patient. Both patients were diagnosed with epilepsy and underwent a neurosurgical resection at UZ Leuven. Samples were collected at the time of surgery and transferred on ice to the laboratory for tissue processing within 10 min post-sampling. All procedures were conducted in accordance with the protocols approved by the local Ethical Committee (protocol number S61186).

3.2.3 H9MG

We used *in vitro* human microglia-like cells generated from H9 embryonic stem cells (WA09, purchased from WiCell) according to the serum- and feeder-free protocol for hPSC-derived monocytes/macrophages.[295] Bohlen et al. optimized microglia medium conditions and developed TIC medium that mainly contains three astrocyte-derived key components TGF-β, IL-34 and cholesterol.[296] We adapted these two protocols described above to generate H9MG (Figure S1).

Briefly, H9 embryonic stem cells were expanded in Essential 8 medium with its supplement (A1517001, Gibco) in matrigel-coated 6-well plates. At day 0, H9 stem cells were dissociated with Accutase (A6964, Sigma-Aldrich) and suspended in mTeSR-1 medium with its supplement (#85850, Stemcell Technologies). Then, ~1 million cells were seeded in a 96-well u-bottom ultra-low adherence plate (#650979, Greiner Bio-one) and supplemented with Rock inhibitor (Y-27632, Sigma-Aldrich) and cytokines (50 ng/mL BMP4, 20 ng/mL SCF and 50 ng/mL VEGF). We spun the plate at 100 g for 3 minutes to pellet cells on the bottom of the wells. From day 1 to day 3, the medium was daily changed. At day 4, embryonic bodies (EBs) were collected from the plates and transferred to a T175 flask. Each flask contained 192 EBs in 40 mL differentiation medium (X-VIVO15, 100 ng/mL M-CSF, 25 ng/mL IL3, 2 mM Glutamax, 100 U/mL Pen/Strep and 0.055 mM β-mercaptoethanol). The differentiation medium was changed when it got yellow. From day 18 onward, the H9-derived monocyte-like cells (H9MC) were visible in the supernatant, and the non-adherent H9MC could be collected weekly. All the H9MC used in this study were collected from day 18, day 25 and day 32. The harvested H9MC were then transferred to the microglia TIC medium (DMEM F12, 2 mM L-Glutamine, 5 µg/mL N-acetyl-L-cysteine, 5 µg/mL human insulin, 100 µg/mL apo-transferrin, 100 ng/mL sodium selenite, 1.5 µg/mL cholesterol, 1 µg/mL heparin sulfate, 50 ng/mL M-CSF, 50 ng/mL IL34, 25 ng/mL TGFβ1, 10 ng/mL CX3CL1) for 7-day further maturation to H9MG. All cytokines used in this study were purchased from Peprotech. Using this combined protocol, we were able to generate ≥ 300 million H9MG in a T175 flask within 39 days.

3.2.4 HEK293T cell line

HEK293T cells were cultured in Dulbecco's modified Eagle's medium/F-12 (Invitrogen), 10% fetal bovine serum (GIBCO). Cells were maintained in a humidified incubator at 37°C with 5% CO_2.

3.3 Method Details

3.3.1 Mice

While *Cx3cr1*$^{CreERT2/WT}$ targets not only microglia but also other myeloid linage cells[297], for instance circulating monocytes, the tamoxifen inducible recombinase activity[293] allows us to induce the KO after embryo development (1 month old in this study) and analyse the cells months later (2-6 month later in this study). Microglia originate from the yolk sac and self-renew in the brain,[97,101] while monocytes derive from bone-marrow and undergo fast turnover. Several studies have shown that the Cre modified monocytes can be replaced within 1 month upon withdraw of tamoxifen but Cre modified microglia stay permanently in the brain.[149,293] Therefore, mice were treated with tamoxifen (single dose of 2 mg /kg per day) or vehicle (corn oil) by i.p. injection for 5 consective days at 1 month of age and sacrificed at the indicated time points. For mouse microglia isolation and histology, mice were terminally anesthetized with an overdose of sodium pentobarbital and transcardially perfused with heparinized PBS.

3.3.2 Isolation of human and mouse primary microglia

The procedures of human and mouse primary microglia isolation are as previously described.[146] Briefly, tissues were subjected to dissociation using the Neural Tissue Dissociation Kit (P) (#130-092-628, Miltenyi) following the manufacturer's specifications. The cell suspension was filtered over a 70-µm cell strainer (#542070, Greiner) with ice-cold FACS buffer (PBS, 2% FCS, 2 mM EDTA). The filtered suspension was further centrifuged at 300g at 4 °C for 15 min. We suspended the cell pellet with 30% Percoll (#17-5445-02, GE Healthcare) and spun the suspension at 300g at 4 °C for 15 min. Myelin layers were formed on top of the supernatant and were removed with a Pasteur pipette.

For human microglia isolation, the cell pellets were first suspended in 1x Red Blood Cell Lysis Buffer (#420301, Biolegend) and incubated for 5 min on ice with occasional

shaking. Then, the reaction was stopped by diluting with sufficient ice-cold PBS. The cell suspension was centrifuged at 300g at 4 °C for 15 min, and pellets were suspended in FACS buffer with anti-human CD11b MicroBeads (1:10, #130-093-634, Miltenyi) at 4 °C for 15 min. Microglia were washed and sorted on a Miltenyi MACS Magnetic Separator. CD11b positive fraction (microglia) and CD11b negative fraction (non-microglia cell types) were collected separately. Western blot analysis was performed for the quality control of microglia purity (not shown). At the end, ~1.5 million human primary microglia were collected from each tissue sample and lysed for detection of γ-secretase subunits.

For mouse microglia isolation, the cell pellet was suspended in FACS buffer with anti-mouse CD11b-PE (1:50, REA592, Miltenyi), anti-mouse CD45-BV421 (1:500, #563890, BD Biosciences) and the cell viability marker e780 (1:2000, #65-2860-40, eBioscience) and incubated at 4 °C for 30 min. For the single-cell experiments, we added a specific hashtag antibody (A0301-A0304, Biolegend) for each individual sample during the antibody incubation. Microglia were washed and sorted on a Miltenyi MACSQuant Tyto cell sorter. Alive microglia expressing CD11b and medium level CD45 but e780 negative were sorted. At the end, ~2 million microglia sorted from equally pooled brain cell suspension from three *C57BL/6J* mice were lysed for detection of γ-secretase subunits (WB). ~15,000 microglia from each GS^{KO}, GS^{WT}, *TAM_QC* or *Ctrl_QC* mouse were sorted for the single-cell mRNA library preparation. FACS data were analyzed using FCS express software.

3.3.3 RNA isolation, reverse transcription and real-time qPCR

RNA from different stages of microglia-like cell differentiation was isolated using the RNeasy Micro Kit (#74004, QIAGEN) according to the manufacturer's instructions. Reverse transcription of 200 ng (mRNA) from each sample was performed using the Superscript II reverse transcriptase (#18064, Invitrogen) according to the manufacturer's instructions. Real-time semi-quantitative PCR was performed using the SensiFast Sybr No-Rox kit (BIO-98020, Bioline). All qPCR primers are indicated in Table S4. Mean expression of two housekeeping genes (18S and GAPDH) was used for all normalizations. The expression level of the genes are shown in ΔCt.

3.3.4 Expression and validation of novel γ-secretase substrates

HEK293T cells were transiently transfected with the recombinant plasmids pcDNA3.1+ hTNFRSF1B/C-(K)DYK, pcDNA3.1+ hCD300A/C-(K)DYK, pcDNA3.1+ hMILR1/C-(K)DYK and the positive transfection control pLKO.1-puro-CMV-TurboGFP, separately, using TransIT®-LT1 Transfection Reagent (Mirus). 36 hours after the transfection, cells were treated with 90 nM Semagacestat or DMSO for 16 hours and then collected for immunoblotting analysis using a FLAG M2 antibody (Sigma).

3.3.5 Immunoblotting

Cells for western blotting were washed in ice-cold PBS and then lysed in STE buffer (250 mM sucrose, 5 mM Tris-HCL, 1 mM EGTA, pH7.4) supplemented with protease inhibitor (Roche) and 1% Triton X-100 (Sigma) for 20 minutes in ice. Cell extract was centrifuged at 14, 000 rpm for 20 min and supernatant was collected and subjected to protein concentration measurement. Equal amount of protein in each sample mixed with NuPAGE LDS Sample Buffer (Invitrogen) was loaded on 4 to 12% Bis-Tris gels for SDS-PAGE. Resolved proteins were transferred on PVDF membranes. Membranes were blocked in 5% skimmed milk in TBS with 0.1% Tween 20 at RT for 45 minutes. The following primary antibodies were used in the study: APP-c20 (B63.3), PSEN1-NTF (B19), APH1A-CTF (B80.3), NCT (9C3), PEN2-NTF (B126) have been described.[285–288] PSEN1-NTF (1:1,000, MKAD 3.5) was a gift from Marc Mercken; PSEN2 (1:1,000, D30G3, Cell Signaling); APH1B (human) or APH1b/c (mouse) (1:1,000, L82) was generated in the laboratory by immunizing rabbits with a QDKNFLLYNQRSR peptide;[290] APLP2 (1:1,000, W2CT) was a gift from D. Walsh, and Syndecan3 (1:1,000, 2E9) was a gift from G. David; LRP1 (1:15,000, EPR3724, Epitomics), GAPDH (1:10,000, 5G4, HyTest); β-ACTIN (1:10,000, A5441, Sigma). ATP1A1 (1:1,000, NB300-146, Novus Bio); FLAG M2 (1:1,000, F3165, Sigma). The membrane was incubated with primary antibody solution at 4 °C overnight. Then we washed the membrane with TBST 3 times and incubated it with the HRP-labeled secondary antibody at RT for 1h. Secondary antibodies are goat polyclonal anti-mouse IgG-HRP conjugate (1:10,000, #170-6516, Bio-Rad), goat polyclonal anti-rabbit IgG-HRP conjugate (1:10,000, #170-6515, Bio-Rad). We washed the membrane with TBST 3 times and TBS 2 times. Eventually, blots were imaged by using the ImageQuant LAS 4000 mini biomolecular imager (GE Healthcare).

3.3.6 Immunofluorescence staining of brain sections

The PBS perfused mouse brain samples were fixed overnight with 4% PFA in PBS. Brains were then embedded in 4% Top Vision low-meltingpoint agarose (Thermo Fisher Scientific) and cut into 35 µm thick coronal sections using a vibratome (Leica VT1000S). The sections were blocked and permeabilized in a PBS based buffer supplemented with 5% donkey serum and 0.3% triton x100 for 1.5 hours at room temperature. After blocking, the sections were incubated in the blocking buffer based primary antibody solution (GFP (1:1,000, Ab13970, abcam); 82E1 (1:200, #10323, IBL)) gently agitated overnight at 4°C. The next day, sections were washed three times for 5 minutes in PBST (0.3% triton x100 in PBS). The sections were incubated with the blocking buffer based secondary antibody solution (Donkey anti-mouse AF647 (1:500, A31571, Invitrogen) and Donkey anti-chicken AF488 (1:500, 703-545-155, Jackson Immunolabs)) gently agitated for two hours at room temperature. The sections were then stained with DAPI solution (1/5,000 in PBS) gently agitated for 15 minutes at room temperature. Finally, the sections were washed three times for 5 minutes in PBST and mounted onto glass slides using the Glycergel mounting media and allowed to dry at room temperature.

3.3.7 Gamma-secretase Substrate Identification (G-SECSI) workflow

Step 1. γ-secretase Inhibition

Semagacestat was solubilized in DMSO and then diluted in the culture medium with final DMSO dilution by volume 1/1000. At day 6 in TIC, H9MG were refreshed with 2 µM Semagacestat containing microglia TIC medium for 16 hours. H9MG cultured in TIC medium containing 0.1% DMSO were used as control.

Step 2. Membrane protein purification

Cells were washed twice with ice-cold washing buffer (PBS supplemented with protease inhibitor cocktail (#11697498001, Roche)). Then, cells were mechanically detached from the dishes or flasks with a cell scraper and collected in ice-cold washing buffer. Cells were pelleted by centrifugation at 800g for 10 min and re-suspended with STE buffer (250 mM sucrose, 5 mM Tris-HCL, 1 mM EGTA, pH7.4) supplemented with protease inhibitor without detergent. 10 µL STE buffer was used per mg pellet. Then, we used a cell cracker with a bead of 8.010 mm diameter to homogenize the cells. Cell

suspension was pushed through the cracker with syringes (20 times) to achieve a complete homogenization. Cell homogenate was centrifuged at 800g for 10 min to remove nuclei, and subsequently the supernatant was spun at 15,000g for 10 min to reduce the mitochondria content. Then, the remaining supernatant was collected and spun at 100,000g for 1 h to pellet the membrane fraction. The membrane pellet was washed with 100 mM Na_2CO_3 (pH 11.3) for 10 min and was spun at 100,000g for 0.5 h to pellet the membranes again. All steps were done at 4°C or on ice.

Step 3. Molecular weight-based protein fractionation and quality control

Molecular weight-based protein fractionation

The membrane pellets were re-suspended in STE buffer without detergent, and the protein concentrations were determined using a Bradford Protein Assay (Bio-Rad). To fractionate membrane proteins by their molecular weights, we used GELFREE 8100 Fractionation System with a GELFREE 8100 10% Cartridge Kit (SKU 42105, Expedeon) following the manufacturer's recommendations. Briefly, purified membrane proteins were mixed with Sample Buffer (from the kit) supplemented with 1M DTT (#3483-12-3, Sigma) and heated at 95°C for 5 min for denaturation. Then, samples were cooled down and loaded. 4 channels of the cartridge were used for each pair of samples (Semagacestat treated and control) from each batch, with 300 µg membrane proteins loaded in each channel and 2 channels for each sample. Then, the cartridge was placed on the instrument, and the fractionation programme as indicated in Table S5 was started. During each pause of the procedure, protein fractions in the collection chambers were transferred by using a multichannel pipette and collected in clean Eppendorf tubes on ice. The collection chambers were washed twice by using Running Buffer (from the Kit). After the washing, 100 µL fresh Running Buffer was added to the collection chamber, and the fractionation programme was continued. The first fraction collected during the first pause of the programme was discarded as the manufacturer suggested, since it contains mainly small debris. Finally, twelve fractions from each sample were collected and stored at -80°C.

Ponceau staining and Western blotting

Membrane protein (1 µg) from the whole purified membrane protein lysate as well from each fraction generated by GELFREE 8100 fractionation system was loaded on a 4-12% NuPAGE Bis-Tris gel (NP0323BOX, ThermoFisher) for SDS-PAGE. After transfer to a nitrocellulose membrane, we performed Ponceau staining. After 1 min staining,

the membrane was washed 3 times with distilled water and was then imaged. The membrane was incubated in blocking buffer (5% skimmed milk powder in TBS with 0.1% Tween 20) at RT for 45 min. We first probed the membrane with a primary C-terminal specific antibody against LRP1 (EPR3724, Epitomics). The membrane was incubated with primary antibody solution at 4 °C overnight. Then we washed the membrane with TBST 3 times and incubated it with the HRP-labeled secondary antibody at RT for 1h. We washed the membrane with TBST 3 times and TBS 2 times. Eventually, blots were imaged by using the ImageQuant LAS 4000 mini biomolecular imager (GE Healthcare).

Step 4. MS and CTF identification

Sample preparation for mass spectrometry

H9MG fractionated membrane samples were prepared for mass spectrometry using s-trap mini columns (Protifi). Membrane pellets were solubilized in 5% SDS, 10mM TCEP (tris (2-carboxyethyl) phosphine) and 50mM TEAB (triethylammonium bicarbonate). Samples were alkylated with 20 mM iodoacetamide for 1 hour. Samples were loaded onto s-trap columns following the manufacturer's instructions and columns were washed 5 times with 100mM TEAB pH 7.1 in 90% methanol. Proteins were digested with trypsin (1:20 enzyme to protein) in 100 mM ammonium bicarbonate at 47 °C for 2 hours. Peptides were eluted from the mini column by sequential washes with 80ul 100mM ammonium bicarbonate followed by 80ul 0.2% formic acid and lastly with 80ul 0.2% formic acid in 50% acetonitrile. Peptides were dried and suspended in 45µl of 1% formic acid for analysis by mass spectrometry.

Liquid chromatography mass spectrometry analysis

H9MG membrane derived peptides were analyzed using an Exploris 480 (Thermo Scientific) mass spectrometer coupled with a Dionex Ultimate 3000 RS (Thermo Scientific). LC buffers were the following: buffer A (0.1% formic acid in Milli-Q water (v/v)) and buffer B (80% acetonitrile and 0.08% formic acid in Milli-Q water (v/v). For all samples 15 µL of the suspended peptides was loaded at 10 µL/min onto a trap column (100 µm × 2 cm, PepMap nanoViper C18 column, 5 µm, 100 Å, Thermo Scientific) equilibrated in 2% buffer B. The trap column was washed for 5 min at the same flow rate and then the trap column was switched in-line with a Thermo Scientific, resolving C18 column (75 µm × 50 cm, PepMap RSLC C18 column, 2 µm, 100 Å).

Peptides were eluted from the column at a constant flow rate of 300 nl/min with a linear gradient from 5% buffer B to 35% buffer B in 125 min and then to 98% buffer B by 127 min. The column was then washed with 98% buffer B for 20 min. The data was acquired using an easy spray source operated in positive mode with spray voltage at 2.6 kV, and the ion transfer tube temperature at 250°C. The MS was operated in DDA mode. A scan cycle comprised a full MS scan (m/z range from 335-1800), orbitrap resolution set to 60000, AGC target set to custom, normalised AGC target at 300%, maximum injection time mode set to custom, maximum injection time at 25 ms, microscan set to 1 and source fragmentation disabled. Data of full MS scan were acquired in profile mode. MS survey scan was followed by 20 MS/MS scan events using the following parameters: multiplex ions set to false, isolation window set to 1.4, collision energy mode set to fixed, collision energy type set to normalized, HCD collision energies set to 30%, orbitrap resolution 15000, first mass 110, AGC target set to standard, maximum injection time mode set to custom, maximum injection time set to 40, microscan set to 1. Data for MS/MS DDA scan event were acquired in profile mode. Two blanks were run between each sample to reduce peptide carry-over.

Processing and analysis of proteomics data

Raw mass spectrometry data files were searched and quantified with the MaxQuant software package (version 1.6.10.43). Proteins and peptides were identified using Uniprot canonical databases. The following search parameters were set: oxidation of methionine and N terminal acetylation were set as variable modifications, carbamidomethylation of cysteine was set as a fixed modification, protein and peptide false discovery rate of 0.01.

In silico determination of carboxyterminal fragment

Single-pass membrane proteins can be categorized into 4 sub-types (www.uniprot.org), including single-pass type I and type III membrane proteins which both have a N-terminus located at the extracellular side and a C-terminus located at the cytosolic side, and single-pass type II and type IV membrane proteins which have reversed topology. Among all previously identified single-pass membrane γ-secretase substrates (Table 1), 154 out of 158, are single-pass type I membrane proteins. From the four remaining substrates, BCMA[77], NRADD[78] and SYT7[79] are single-pass type III membrane proteins containing natural short ectodomains. Thus the preferred topology of γ-secretase substrates seems to be N-terminus outside. The fourth one is β 1,6 N-

acetylglucosaminyltransferase V (GnT-V)[216] that is the only reported single-pass type II membrane protein to be cleaved by γ-secretase. Only three multi-pass membrane proteins, Glutamate Receptor Subunit 3 (GluR3), Polycystin-1 (PC1) and Frizzled-2 (FZ2), have been reported to be cleaved by γ-secretase.[213,215,255] It remains unclear whether these multi-pass proteins become only substrates after cleavage by other enzymes which then generate a single-pass membrane protein fragment, or what exactly is further required to make such proteins a substrate for γ-secretase. Given the complexity of single-pass type II membrane proteins and multi-pass membrane proteins, we focus here only on single-pass type I and III membrane proteins.

The extracellular domain of the CTF that are substrates of γ-secretase are in general less than 50 amino acids (aa) long, while proteins with an extracellular domain larger than 200 aa are not processed by γ-secretase.[81] We used therefore a conservative threshold of 60 aa for the predicted length of the extracellular domain of the γ-secretase substrates, meaning that we considered the part starting from the carboxyl-terminus up to 60 aa beyond the transmembrane domain of the single-pass type I/III membrane protein as theoretical threshold for the determination of the length of the CTF.

Step 5. Spectral pattern visualization of target protein

Data normalization

We processed the raw intensity values from the proteomics data by a two-step normalization method. Firstly, we normalized every raw intensity value by the sum of raw intensities from the same fraction to rule out the differences possibly caused by loading error of the injection to MS. Then, each value out from the first step normalization was multiplied by the mean fraction weight between two conditions.

Faceted bar plot

We show the relative abundance of each detected tryptic peptide in a faceted bar plot for each protein separately. The relative abundance of a specific peptide in the 12 fractions were aligned in a row, while the relative abundance of different peptides in the same fraction were aligned in a column. These different rows which show the unique tryptic peptides for each protein are sorted by the location of their first aa residue along the full-length protein. The location of the first aa residue is indicated at the right side of the rows, and are ordered from the amino-terminus down to the carboxyl terminus. The different columns are reflecting the 12 elution batches from left

(small) to right (large) molecular weight fractions. We indicate with a double blue line the transmembrane domain (TMD) according to www.uniprot.org, and with a single green line the 60 aa above the double green line which indicates the predicted start of CTF.

3.3.8 Preparation of H9MG single-cell samples

We seeded H9MC collected from D25 as described above in 12-well plates (500,000 cells/well). We grew them in TIC medium for 7 days, TIC medium was refreshed every two days. At Day 7, we pre-treated H9MG with 2 µM Semagacestat or DMSO for 22 h. We added 200 ng/mL LPS or PBS during the last 6 hours of the experiment. For the collection, we added 500 µL Accutase (#07922, Stemcell) with 5 µM Actinomycin D (A1410, Sigma) in each well and incubated the plate at 37 ℃ for 6 min. We rinsed the cells with cold PBS with 5 µM ActD and collected cells in a clean Eppendorf tube on ice. We spun the cell suspension at 300g for 5min and suspended the cells with cold FACS buffer. We spun down the cell pellets and incubated each of the 12 samples with a specific hashtag antibody (A0251-A0260, A0262 and A0263, Biolegend) at 4 ℃. After 30 min, we washed the cells in cold FACS buffer. We spun down the cell pellets again and suspended cells in FACS buffer.

3.3.9 Single-cell mRNA libraries preparation and sequencing

H9MG libraries

We measured the concentration of the cell suspensions on a LUNA cell counter and eventually pooled ~2,000 cells from each of the 12 samples together (4 conditions: n = 3 samples per condition). We equally divided the pool into 2 and prepared them into 2 cDNA libraries using the 10X Genomics single-cell gene expression profiling kit following the manufacturer's protocol (CG000204_ChromiumNextGEMSingleCell3_v3.1). All cDNA libraries were then sequenced on a DNBSEQ PE100 sequencing platform.

Mouse microglia libraries

We suspended the cells in a final concentration of 1000 cells/µl. We pooled ~2,000 cells from each of the 3 - 4 samples (each labeled with a specific hashtag antibody, Biolegend) for one cDNA library. For single cell encapsulation, custom microfluidics as described previously[298] was used instead of the standard 10x GEM generation chips.

The custom HyDrop chip provided an improved encapsulation efficiency of >75% and better control of droplet formation due to the imaging capabilities of the platform. It helps in preventing the run failure due to chip clogging. The workflow of the HyDrop chip allowed combining two 10x reactions into a single run[298] which enabled us to target for 12000 cell recovery per experimental time point. After single-cell encapsulation, library preparation followed the manufacturer's protocol (CG000204_ChromiumNextGEMSingleCell3_v3.1). All cDNA libraries were then sequenced on a DNBSEQ PE100 sequencing platform.

3.4 Quantification And Statistical Analysis

3.4.1 Quantitative analysis of the abundance of the CTFs

Reference plot for calculating molecular weight in the collected fractions

The mean and the 95% confidence interval (CI) of the protein sizes in each fraction was calculated using the data (size and location) from all detected known γ-secretase substrates (See supplementary Table S6). We connected the 95% CIs across all 12 fractions which is the red shadow overlaying part of the reference plot in Figure 6D. By using the reference plots and the predicted size of FL and CTF of each protein (by number of aa), we can deduce the putative location of the FL and CTF of the protein amongst the different fractions, and therefore deduce the location of the green vertical dotted line. For each protein, the peptides derived from the FL protein are in the fractions beyond the vertical green dotted line, and the peptides derived from putative CTF fragments are at the left side of that line and below the green horizontal line, so called quadrant 3 or Q3 (see Figure 6C and E).

γ-Secretase substrate identification

We quantified the relative total signal in Q3 of the each plot. We consider a protein a substrate of γ-secretase if (1) the increase of CTF upon Semagacestat treatment of the target protein was detected in at least 3 out of 4 independent experiments; (2) the value of Q3 in the Semagacestat treated condition is at least 1.2 fold larger than the value of Q3 in the control condition; (3) $P.adj < 0.05$, using student t test followed by Benjamini-Hochberg false discovery rate correction, $n = 3$ or 4.

3.4.2 Functional and Pathway Enrichment Analysis of Candidate Substrates

Candidate substrates identified in the H9MG cells were tested for enrichment of Gene Ontology (GO) Biological Process (BP) and Molecular Function (MF) terms, as well as KEGG pathways, using the clusterProfiler package (v4.2.2). Enriched terms were identified using the *enrichGO()* and *enrichKEGG()* functions, with the parameters qvalueCutoff = 0.05, minGSSize = 100, and pAdjustMethod = "BH". Top GO enrichments were visualized by grouping the 50 most significant terms by semantic similarity, as calculated by the *calculateSimMatrix()* and *reduceSimMatrix()* functions.

3.4.3 Single-cell sequencing data analysis

Alignment, pre-processing, and clustering

H9MG: The 10x Genomics Cell Ranger software (version 6.0.1) was used to align reads to the GRCh38 human reference genome, demultiplex cellular barcodes, and quantify unique molecular identifiers (UMI) and Hashtag oligos (HTO). The UMI and hashtag count matrices for each of the libraries were loaded into the Seurat package (v4.1.1). Genes whose transcripts were identified in less than 3 cells were immediately removed from the expression matrices. Cell barcodes were filtered to include only those detected in both RNA and HTO data. The HTO assays were normalized using the centered log-ratio (CLR) transformation. Seurat's *HTODemux()* function was run with default parameters on the hashtag-count matrices to demultiplex cells into their samples of origin. Cells that could not be assigned to an HTO and cells that were positive for more than one HTO were deemed as negatives and inter-sample doublets, respectively, and removed from further analysis. In the remaining 22,987 demultiplexed singlet, intra-sample doublets were identified and removed using DoubletFinder (v2.0.3). Further quality filtering was performed such that only cells meeting the following cutoffs were retained: < 20% mitochondrial reads, > 5,000 counts, < 65,000 counts, and > 2,000 unique genes. In total, n = 21,851 cells were used for further downstream analysis.

All H9MG single-cell transcriptomes were initially clustered jointly, using Seurat's canonical correlation analysis (CCA) to integrate the RNA transcript counts from the two libraries. In brief, gene counts from each of the libraries were log-normalized for library size and the 2,000 most variable genes were identified using a variance-

stabilizing transformation. The *FindIntegrationAnchors()* function was used to identify anchors for the joint dataset and the data was integrated using the *IntegrateData()* function. The integrated data was scaled using *ScaleData()* and a principal component analysis (PCA) was performed with the *RunPCA()* function. Uniform Manifold Approximation and Projection (UMAP) embeddings were created using the *RunUMAP()* function, using the first 29 principal components (PCs) as input for the non-treated cells and 30 PCs for the treated cells (as determined through the visual inspection of a Scree plot). A shared nearest neighbor (SNN) graph was constructed using Seurat's *FindNeighbors()* function, again using 29 and 30 PCs, respectively. Seurat's *AddModuleScore()* function was used to score cells according to their expression of the Friedman proliferating gene set.[291] Cells for which this score was greater than 0 were classified as proliferating. Proliferating cells were removed and the remaining transcriptomes were re-clustered following the above procedure (Figure 9B).

Next, the non-proliferating H9MG transcriptomes were clustered separately depending on the presence or absence of LPS treatment, using the same integration and dimensionality techniques as described in the joint clustering procedure. The UMAP of steady state non-proliferating cells was created using the first 23 PCs and clustered using the same number of PCs, with a resolution of 0.12 (Figure 9D). The UMAP of LPS-treated non-proliferating cells was created and clustered using 15 PCs, with a resolution of 0.15 (Figure 9I).

***In vivo* microglia**: The same alignment and cellular barcode demultiplexing procedures were followed for the *in vivo* microglia harvested from the *C57BL/6J* background (*$GS^{i\Delta MG}$, GS^{WT}*) mice and *$App^{NL\text{-}G\text{-}F}$* background (*$App^{NL\text{-}G\text{-}F}$-$GS^{i\Delta MG}$, $App^{NL\text{-}G\text{-}F}$-$GS^{WT}$*, *$App^{NL\text{-}G\text{-}F}$-Ctrl_QC, and $App^{NL\text{-}G\text{-}F}$-TAM_QC*) mice. In this instance, reads were aligned to the GRCm38 mouse reference genome. The lincRNAs Gm42418 and AY036118 were removed from the expression matrices, as they overlap a locus that harbors an Rn45s sequence repeat, and may thus obtain inflated expression counts from contaminating 18S rRNA. After demultiplexing cells into samples of origin based on the presence of Hashtag oligos, 9,556 and 46,730 cells were retained from the *C57BL/6J* background mice (n = 8) and *$App^{NL\text{-}G\text{-}F}$* background mice (n = 24), respectively. The cells were further filtered to remove cells with either high/low number of read counts and expressed genes, cells with mitochondrial content > 10%, or intra-sample doublets as identified by DoubletFinder.

For the *C57BL/6J* background mice, the remaining 7,922 single microglia transcriptomes were integrated by library using Seurat's anchor-based integration workflow (as described in the H9MG processing section). The first 20 PCs were used to generate a UMAP and create a SNN graph. The cells were clustered with a resolution of 0.25. Clusters of cells determined to be non-microglial (based on high expression of non-microglial cell-type markers and low expression of microglial markers) and a low-quality cluster (as determined by low UMI counts and high mitochondrial content) were removed. Furthermore, one $GS^{i\Delta MG}$ sample with a low number of remaining microglial transcriptomes (n = 8) was removed from further analysis. Integration, scaling, and dimensionality reduction was repeated on the remaining 7,285 microglial single cell transcriptomes. 20 dimensions were used for dimensionality reduction. Unbiased clustering by the Louvain algorithm with a resolution of 0.15 identified 4 clusters (Figures 10B-C).

For the $App^{NL\text{-}G\text{-}F}$ background mice, the remaining 41,856 RNA transcript counts (Figure S7A) from three libraries were similarly integrated using integration anchors. The first 26 PCs and a resolution of 0.25 were used to generate a UMAP and cluster the cells (Figure S7B). Non-microglial and low-quality clusters were removed (Figures S7C and E). Integration, scaling, and dimensionality reduction was repeated on the remaining 37,884 microglial single cell transcriptomes. 15 dimensions were used for dimensionality reduction. Unbiased clustering by the Louvain algorithm with a resolution of 0.35 identified 9 clusters (Figure S8A). Clusters 0 and 1 were merged, as their marker genes revealed similar homeostatic microglia state profiles (Figures S8B and 10B).

Gene module enrichment visualization

To calculate and visualize the enrichment of gene sets of interest (i.e. markers for microglial states and sets of differentially expressed genes) for each cell, we used Seurat's *AddModuleScore()* function. In brief, this function calculates the activity of a gene set in each cell by comparing the mean abundance level of the genes of interest against the average abundance of sets of random control genes which have a similar average expression level. The calculated scores were visualized on the UMAP. Density plots were created using the Nebulosa package (v1.0.2).

Differential Expression analysis

Differential expressions between clusters and between conditions were performed on the normalized counts using the *FindMarkers()* and *FindAllMarkers()* functions provided within the Seurat package. Min.pct values were set to 0.1. P-values were calculated using the Wilcoxon rank-sum test and were corrected for multiple testing using the Bonferroni method. Seurat's *DotPlot()* and *DoHeatmap()* functions, as well as the ComplexHeatmap package (v1.10.2), were used to visualize the relative expression levels of marker genes on either a per-cell or a per-cluster basis.

Pseudotime analysis

Count matrices and UMAP embeddings were loaded into Monocle 3 (v1.0.0, using SeuratWrappers' *as.cell_data_set()* to convert the Seurat object into a Monocle object. The *learn_graph()* and *order_cells()* functions were used to fit a principal graph, identify trajectories of interest, and assign pseudotime values along the trajectories. Statistical significance of pseudotime values between each of the two conditions being compared was determined using a t-test.

Gene Set Enrichment Analyses

Gene Set Enrichment Analysis (GSEA) was performed using the clusterProfiler package (v4.2.2). The outputs of differential expression analyses between conditions (as obtained by Seurat's *FindMarkers()* function) were ranked according to each gene's signed log10(p-value). clusterProfiler's *GSEA()* function was used to calculated gene set enrichment scores based on the ranked list. The following parameters were used: *nPerm* = 1000, *minGSSize* = 10, *maxGSSize* = 500, *pvalueCutoff* = 0.05, *pAdjustMethod* = "BH". The enrichments scores of gene sets in the ranked list of differentially expressed genes were visualized using *gseaplot()* function from the enrichPlot package (v1.10.2) (Figures S6C and F).

3.4.4 Imaging and quantitative analysis of the Immunofluorescent images

Confocal images were obtained using a Nikon AX Confocal Microscope System driven by NIS-Elements AR (5.41.01) software. For excitation, 405 nm, 488 nm, 561 nm, 640 nm laser lines were used. All the stained sections were imaged by a 4x or 20x objective. Roughly, 8-12 Z-step sections within 15-25 µm thickness were obtained from each sample. All images used for a particular comparative analysis were acquired using the

same acquisition parameters. The representative images (in Figure 12H) were processed by FIJI/Image J software using maximum intensity projections of the Z-stack images. The microglia ($EYFP^+$) area, the density of microglial puncta ($EYFP^+$ puncta with diameter > 30 μm), the overlapped microglia and plaque ($EYFP^+82E1^+$) area and the total plaque ($82E1^+$) area were quantified using NIS-Elements AR (5.41.01) software. The quantification were performed using a semi-automated house-made macro in NIS-Elements AR software. Briefly, the maximum intensity projections of the Z-stack images were used, and the number of counts and the positive area of either microglia or plaques were identified with threshold function and normalized by the area of interest. All the quantification results were generated using the measurement of the whole cortical region of the brain coronal sections. For all the quantitative analysis, two sections (one anterior section without hippocampus and one posterior section with hippocampus) were randomly selected from each individual animal, stained and imaged as described above. 5 animals in each condition were used for the quantification.

3.5 Resource Availability

Materials availability

Materials and reagents used in this study are listed in the key resources table. Reagents generated in this study are available upon request.

Data and code availability

- Mass spectrometry data files and MaxQuant analysis files generated in this study have been deposited at the ProteomeXchange data repository and are publicly available as of the date of publication. The accession number is indicated in the key resources table. Please notice that the fraction 2-13 in the raw data are referring to the fraction 1-12 in the figures in this paper, since the first fraction generated from the GELFREE 8100 Fractionation System was not included for further analysis according to the manufacturer's recommendations.
- Single-cell RNA-seq data files generated in this study have been deposited at Gene Expression Omnibus (GEO) database and are publicly available as of the

date of publication. The accession number is indicated in the key resources table.

- This paper analyzes existing, publicly available data. The accession numbers for the datasets are listed in the key resources table.
- Original western blot images and microscopy data have been deposited at Mendeley and are publicly available as of the date of publication. The DOI is listed in the key resources table.
- This paper does not report original code.
- Any additional information required to reanalyze the data reported in this paper is available from the lead contact upon request.

Additional Resources

We generated faceted bar-plots of the 359 detected specific single-pass type I and type III membrane proteins from H9MG in this study. The faceted bar-plots are accessible on our website https://data.bdslab.org.

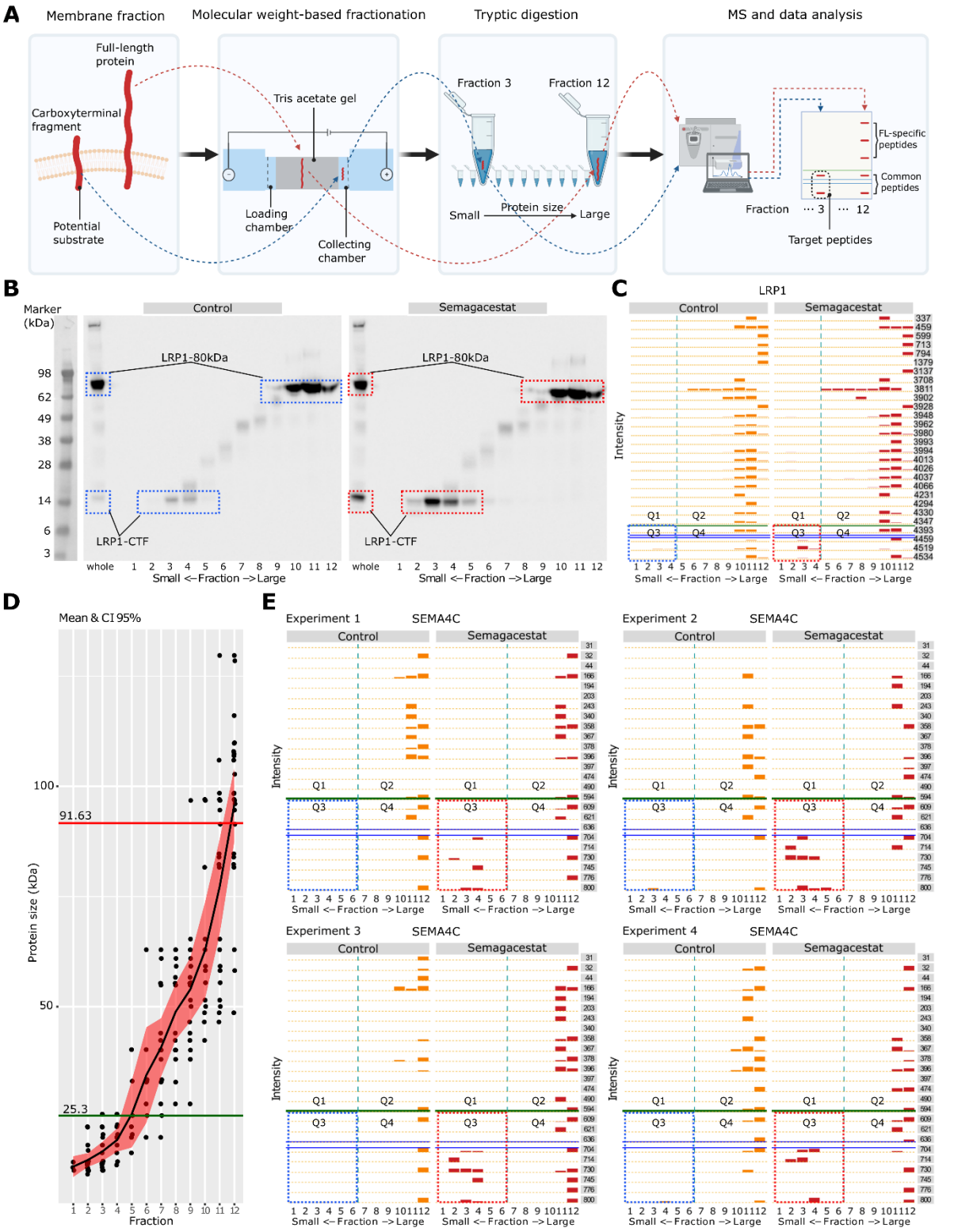
Chapter 4: Results

4.1 Identification and characterization of γ-secretase substrate proteome in H9MG cells

4.1.1 G-SECSI to identify substrates of γ-secretase

We developed an unbiased γ-Secretase Substrate Identification (G-SECSI) method to identify novel substrates in microglia (Figure 6A). H9MG (Figure S1) express the full spectrum of γ-secretase enzymes similar to primary human and mouse microglia (Figures S2). We prepared the membrane fractions that were fractionated on a Gel-Eluted Liquid Fraction Entrapment Electrophoresis[299,300] system to separate full-length (FL) proteins from their carboxyterminal fragments (CTF) which accumulate when γ-secretase inhibitors are used. The different fragments of LRP1, a known substrate of γ-secretase, distributed nicely over the different fractions (Figure 6B). The LRP1 80 kDa fragment (generated by furin cleavage of the 600 kDa protein)[301] distributes in fraction 10-12 and remains unchanged in treated and control conditions. In fraction 3-4 of the Semagacestat treated sample a clear accumulation of LRP1-CTF is seen, in contrast to the faint bands in the control condition. Thus, the fractionation method allowed us to separate efficiently the CTF that accumulates after γ-secretase inhibition from the FL protein.

We next analyzed each fraction by MS and obtained a visual representation of the peptide distribution over the different fractions in faceted bar plots, exemplified in Figure 6C. The plots show the relative abundance of all the tryptic peptides per fraction identified for a particular protein, ranked according to their position in the FL protein (Meth. 3.3.7 Step 5). These plots thus provide a semi-quantitative overview of all identified peptides and their localization in the protein. The peptides generated from the LRP1-CTF migrate in quadrant (Q) 3, while the same peptides when generated from the LRP1-80kDa protein, migrate in Q4. Notice that the carboxyterminal peptides of LRP1 mainly detected in Q4 in the untreated condition accumulate after Semagacestat treatment in Q3. These Q3 peptides are confirmed to be derived from the 14 kDa LRP1-CTF by γ-secretase cleavage (Figure 6B). Thus, by analyzing the tryptic peptides in each fraction and quantifying their distribution in Q3 we can assess whether a membrane-bound protein is a candidate γ-secretase substrate or not.



(Legend continued on next page)

Figure 6. γ-Secretase substrate identification using G-SECSI. A, Schematic representation of G-SECSI procedure. Proteins are fractioned according to molecular weight (MW). Mass spec on the different fractions allows to assign identified peptides to either the carboxyterminal fragments (CTF) or to the full length protein (FL). **B,** Western blot analysis of LRP1, a known γ-secretase substrate. Equal volume of each fraction was loaded and the resulting blot was probed with LRP1 C-terminal specific antibody (EPR3724). The lane at the left side displays the unfractionated lysate. **C,** Faceted barplot showing the relative abundance of each detected peptide of LRP1 in the corresponding fraction as identified by mass spec analysis. At the right side the position of the first aa of each specific peptide in LRP1-FL is indicated. The green horizontal line shows the start of the LRP1-CTF (Meth. 3.3.7 Step 5). The blue double horizontal liness indicate the borders of the transmembrane domain (TMD) based on UniprotKB.[302] The green verticle line separates the fractions in which LRP1-CTF derived peptides (left side) and LRP1 80 kDa fragment derived peptides distribute. Q3 is quadrant 3 region defined by the horizontal and vertical green lines, where LRP1-CTF derived peptides should be detected. **D,** Reference plot showing the mean and the 95% confidence interval of the protein size in each fraction. This plot is generated using MW. and distribution of the fragments of known substrates detected in the different fractions. **E,** Faceted barplot of previously unknown γ-secretase substrate SEMA4C. The faceted barplots were derived from four independent experiments. Control (left) and Semagacestat treated (right) samples are indicated. The green horizontal line and blue double horizontal lines are as above. Q3 defines the area where SEMA4C-CTF derived peptides should distribute.

4.1.2 Identification of novel γ-secretase substrates in H9MG

We repeated 4 independent G-SECSI experiments using H9MG (Figure S3A). We loaded 600 µg membrane protein and collected twelve fractions per run. We identified and quantified 60,044 ± 5,417 (mean ± SD) peptides per experiment and assigned them to 6,009 ± 86 (mean ± SD) proteins, of which about 50% were membrane proteins (Figure S3B). Eventually, we extracted the single-pass type I and type III membrane protein subset covered by 4,285 ± 734 (mean ± SD) peptides assigned to 343 ± 10 (mean ± SD) specific proteins per experiment for further analysis.

Figure 6E shows the results obtained for the novel γ-secretase substrate human Semaphorin-4C (SEMA4C). *Sema4c* becomes upregulated in microglia after spinal cord injury and might play a role in microglia mediated wound recovery.[303] The double blue horizontal lines indicate that the transmembrane domain (TMD) of SEMA4C is between aa 664 and aa 684. The single green horizontal line indicates the position of aa 604 which is the putative start of the CTF. The predicted size of SEMA4C-FL (based on the number of aa) is 91.6 kDa and therefore should distribute in fraction 11-12, and the predicted SEMA4C-CTF of 25.3 kDa should distribute in fraction 3-6 (Figure 6D and 6E). The green vertical dotted line between fraction 6 and 7 separates the peptides in Q4 derived from SEMA4C-FL and the peptides in Q3 derived from SEMA4C-CTF. The peptides accumulate in Q3 when Semagacestat is used, indicating that the SEMA4C-CTF in the control conditions is cleaved by γ-secretase.

We performed this analysis for the 359 detected specific single-pass type I and type III membrane proteins from H9MG. The faceted bar-plots are accessible on our website https://data.bdslab.org. We compared the relative abundance of the CTF-derived peptides in Semagacestat vs. Control conditions and identified in total 85 γ-secretase substrate candidates, of which 59 proteins (69%) were previously unknown (Table S1). The identified substrates are indicated in the volcano plot (Figure 7A, threshold: P.adj < 0.05 and Foldchange ≥ 1.2), and the relative abundance of their potential CTF-derived peptides across the 4 biological replicates are indicated in the heatmap (Figure 7B) which also demonstrates the high reproducibility of this method over the four independent experiments.

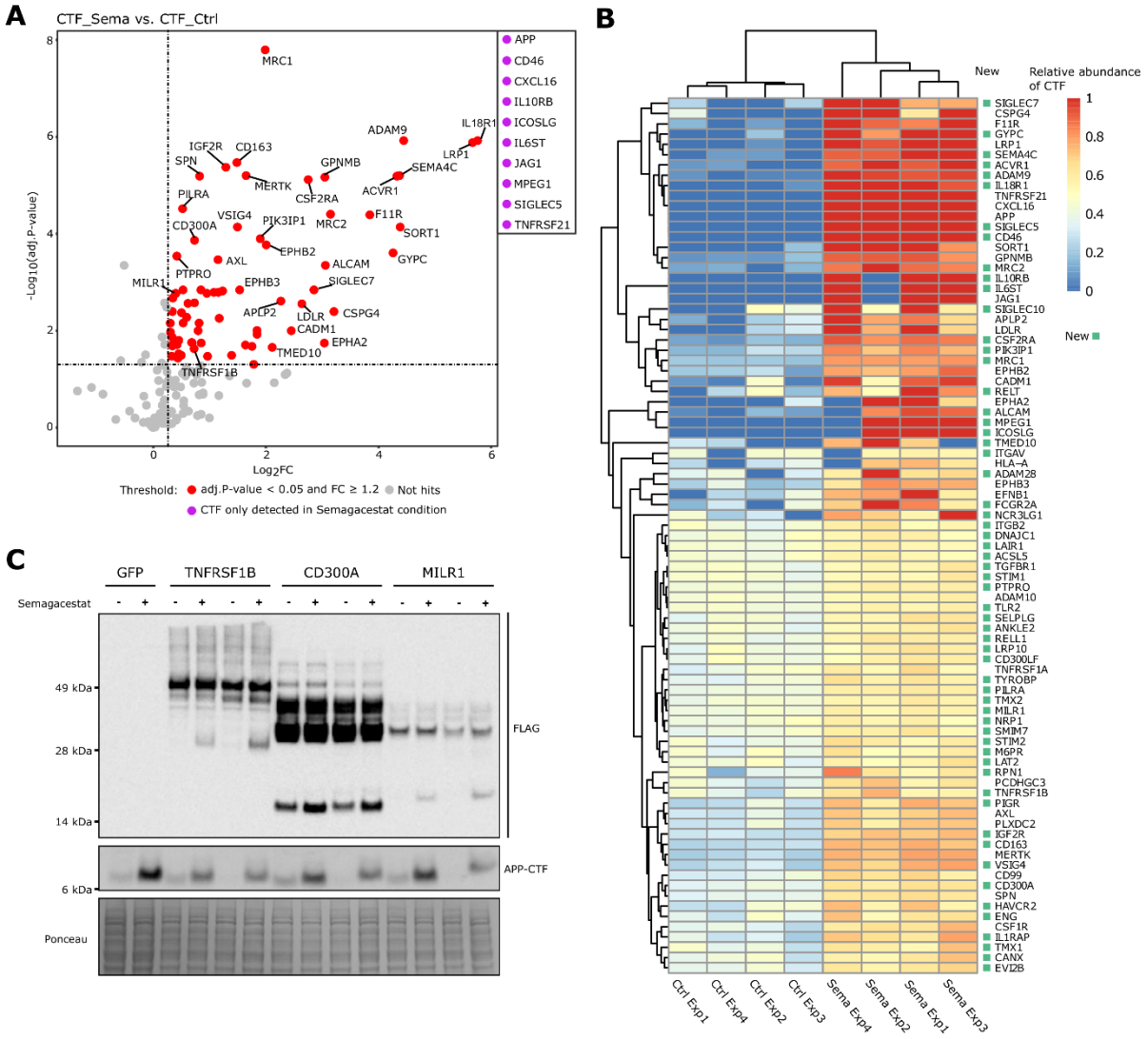


Figure 7. Overview of γ-secretase substrates in H9MG human microglia-like cells. A, Volcano plot showing the relative increase of CTF peptides in the presence of Semagacestat versus control. Proteins accumulating CTF only after treatment with semagacestat are indicated by purple dots in the insert at the top right. Every substrate has been confirmed in at least 3 out of 4 independent experiments and with fold change ≥ 1.2 and P.adj < 0.05, using student t test followed by Benjamini-Hochberg false discovery rate correction. **B**, Heatmap of the relative abundance of CTF proteins identified as γ-secretase substrates over four experiments. Previously unknown substrate candidates are indicated with green squares (left side of protein names). **C**, Validation of identified novel γ-secretase substrates. TNFRSF1B, CD300A and MILR1 cDNA tagged with FLAG were expressed in HEK293T cells and extracts were analyzed by Western blots using FLAG M2 mAb. Empty vector expressing GFP was used as negative and endogeneous APP-CTF accumulation as positive control. Ponceau staining is shown as loading control.

4.1.3 Validation of the identified novel γ-secretase substrates

We selected three novel candidates from the list, i.e., TNFRSF1B (FC = 1.66, P.adj = 0.0234), CD300A (FC = 1.67, P.adj = 0.0001) and MILR1 (FC = 1.32, P.adj = 0.0017), which are slightly above the threshold for assigning them as γ-secretase substrates (Figure 7A). We cloned the cDNA of these candidates and inserted a FLAG epitope into their carboxyl termini. We transfected the plasmids in HEK293T cells, treated the cells with Semagacestat or DMSO for 16 hours, and analyzed the cell lysates by western blot (Figure 7C). Probing the membrane with the FLAG antibody revealed a 29 kDa band from TNFRSF1B, a 20 kDa band from CD300A and a 20 kDa band from MILR1 that accumulate upon Semagacestat treatment. These results show that even the candidates that were identified at the lower threshold of the assay are reliable γ-secretase substrates.

4.1.4 γ-Secretase substrates are central in intracellular microglial signaling

Gene ontology (GO) analysis suggests that the identified γ-secretase substrates are involved in various microglial biological processes, including proliferation, phagocytosis, cytokines production, axon guidance and migration (Table S2). “Transmembrane receptor protein kinase activity” (P.adj = 1.36E-09) and “Cytokine binding” (P.adj = 1.36E-09) are the most significantly enriched molecular function GO terms (Table S2). Accordingly, 6 receptor tyrosine kinases (AXL, CSF1R, EPHA2, EPHB2, EPHB3 and MERTK) were identified (Table S1). Furthermore, 4 interleukin receptors (IL10RB, IL18R1, IL1RAP, IL6ST), 3 tumor necrosis factor receptors (TNFRSF1A, TNFRSF1B, TNFRSF21) and 2 colony stimulating factor receptors (CSF1R, CSF2RA) are in the “Cytokine-cytokine receptor interaction” pathway (Table S3). Interestingly, 53 out of 85 (62%) substrates are encoded by genes that are part of the transcriptional changes defining specific microglia states in AD models (Figure 8).[145,147,150] Half of these substrates (26/53) are encoded by homeostatic (HM) genes. Sixteen substrates are encoded by typical “disease associated microglia” or DAM genes (e.g. *GPNMB*, *GYPC*), HLA-microglia genes (e.g. *HLA-A*, *PILRA*) and “Interferon response Microglia” or IRM genes (e.g. *TLR2*, *CD163*). Proteins harboring the immunoreceptor tyrosine-based activation motif (ITAM: GPNMB, FCGR2A, TYROBP) or the immunoreceptor tyrosine-based inhibitory motif (ITIM: CD300A,

CD300LF, MILR1, LAIR1, PILRA) are also identified as γ-secretase substrates (Table S1). ITAM- and ITIM-bearing receptors are known to play distinct roles in activating and inhibitory signaling transduction in microglia.[304,305] Hence, our findings suggest a role of γ-secretase in maintaining a dynamic equilibrium between different cellular signals via cleaving distinct substrates in microglia. We reasoned that investigating the overall profile of the transcriptomes of the microglia would provide a good integrated read-out for the overall context-dependent effect of blocking the processing of >85 γ-secretase substrates.

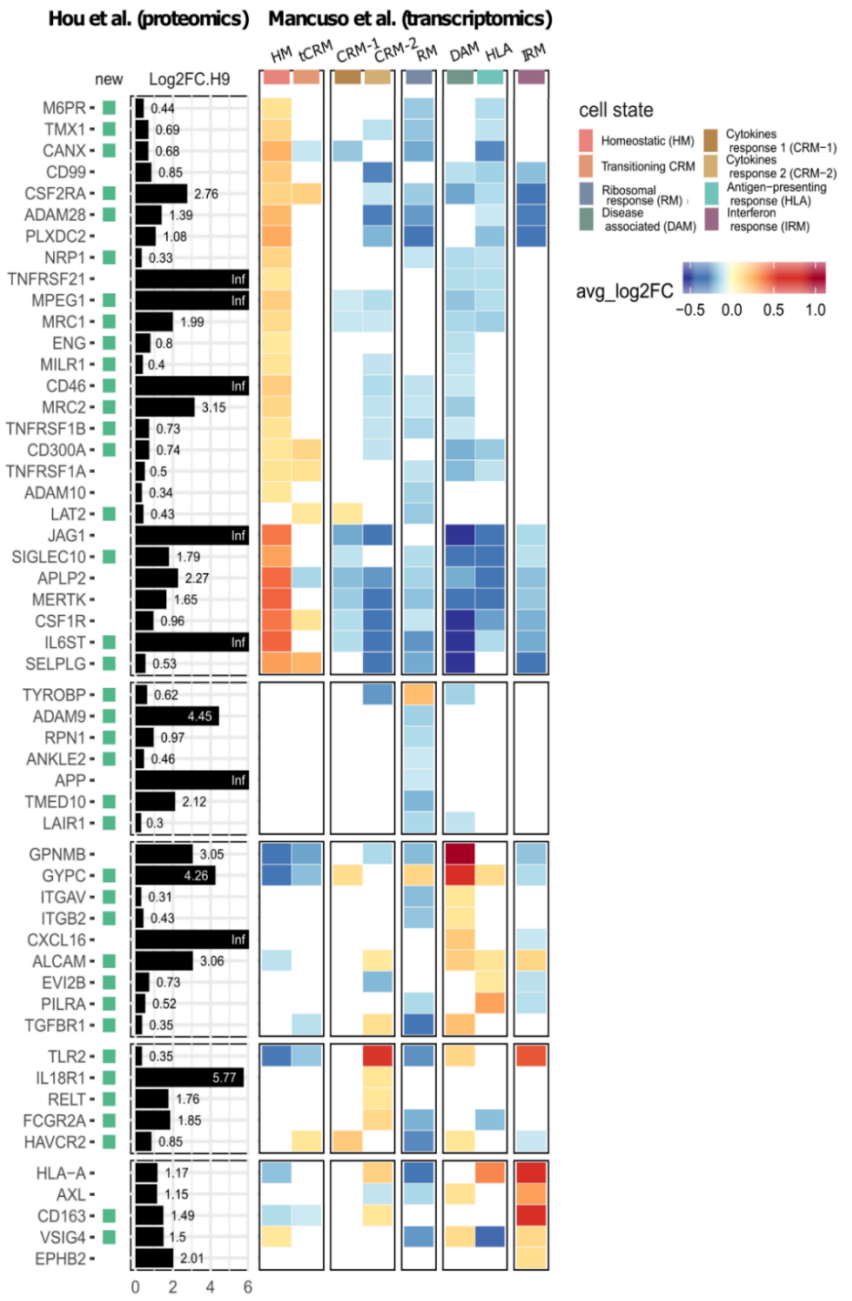
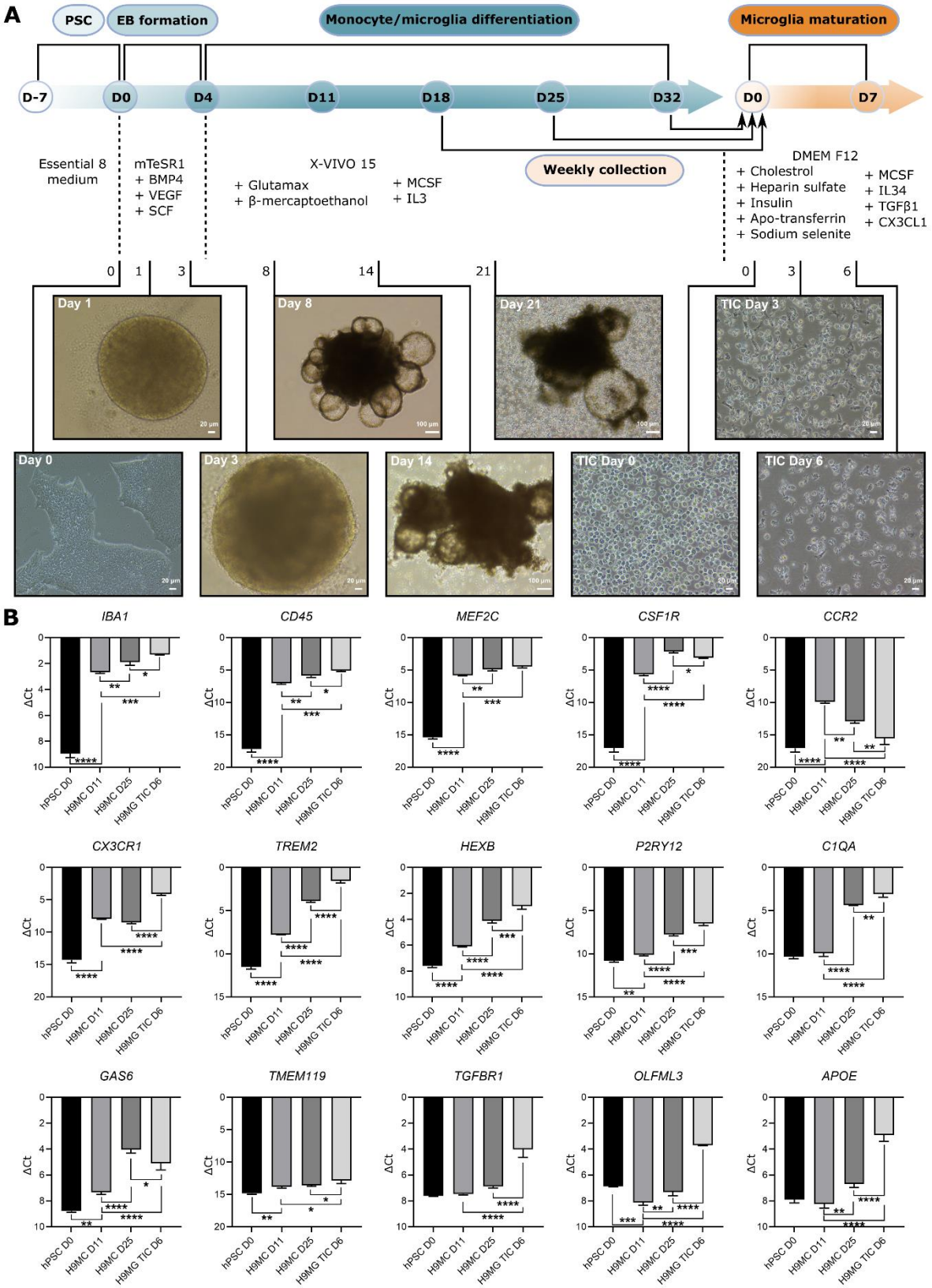
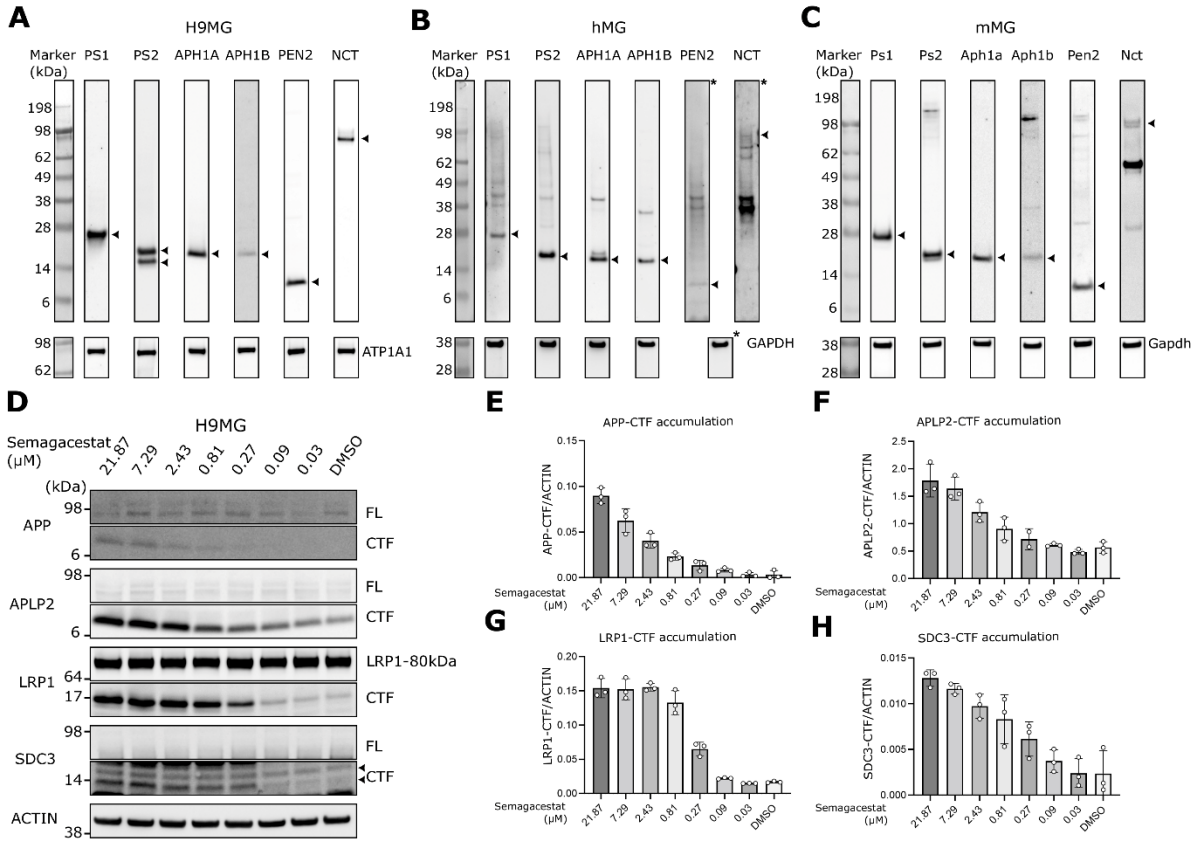


Figure 8. γ-Secretase substrates are highly involved in microglia cell state regulation. Combined plots showing substrates encoded by human microglia cell state-defining genes organized per cell state as defined by Mancuso et al.[150] Cell state-defining genes are the most significantly up- or down-regulated genes in a particular microglia cell state *vs*. cells in the other states. |avg_Log2FC| > 0.1 using Bonferroni correction (P.adj < 0.05). The black bars represent the Log2FC of the CTF relative abundance of the substrates in Semagacestat condition *vs.* Control condition. The heatmap summarizes the differential expression (Log2FC, colour scale) of the corresponding genes in the particular cell states (each cluster compared to all others). HM: homeostatic; (t)CRM: (transitioning) cytokine response; RM: ribosomal; DAM: disease associated; HLA: HLA response; IRM: interferon response.



(Legend continued on next page)

Figure S1. Workflow and quality control of H9MG differentiation, related to Method 3.2.3. **A,** Schematic of the protocol for H9MG differentiation. Four main stages of differentiation, i.e. Pluripotent Stem Cell (PSC), Embryonic Body (EB) formation, monocyte (H9MC)/microglia (H9MG) differentiation and microglia maturation are discerned. Notice the different culturing medium used at each stage. Representative pictures are shown. **B,** Quality control of H9MG differentiation showing qRT-PCR results of 15 marker genes in cells collected at 4 different points of the differentiation timeline (hPSC D0, H9MC D11, H9MC D25 and H9MG TIC D6). At day 11, general myeloid lineage marker genes (*IBA1*, *CD45*, *MEF2C* and *CSF1R*) and some monocyte/microglia marker genes (*CCR2, CX3CR1, TREM2 and HEXB*) are already highly expressed in the cells compared to the H9 stem cells from which they are derived. With further differentiation, more microglia-specific marker genes (*P2RY12*, *C1QA* and *GAS6*) become highly expressed whereas the monocyte-specific gene *CCR2* significantly goes down. Once the cells become cultured in TIC medium, other microglia marker genes (*TMEM119*, *TGFBR1*, *OLFML3* and *APOE*) become highly expressed, while *CCR2* becomes further downregulated indicating the mature microglia phenotype acquired in TIC medium. ΔCt values are normalized by the average Ct value of GAPDH and 18S. Data are shown as mean ± SD. n = 3. One-way ANOVA followed by Tukey's post hoc test. *P < 0.05; **P < 0.01; ***P < 0.001; ****P < 0.0001.



(Legend continued on next page)

Figure S2. Expression of γ-secretase subunits and known substrates in microglia/H9MG, related to Method 3.3.5. A-C, Western blot analysis of the expression of the 4 γ-secretase subunits and their homologues in human microglia-like cells derived from H9 stem cells (H9MG, **A**), human microglia directly isolated from human brain (hMG, **B**) and mouse microglia directly

isolated from mouse brain (mMG, **C**). GAPDH was used as loading control for whole cell lysate samples, and plasma membrane protein ATP1A1 was used as loading control for purified membrane samples. In mouse the Aph1b gene is duplicated (hence an Aph1c gene). Both genes only differ in 5 aa. Here Aph1b indicates the two subunits.[287] * For the blotting of PEN2 from hMG, the membrane used for NCT blotting was stripped and re-probed with PEN2 antibody. **D,** Western blot analysis of the known γ-secretase substrates APP, APLP2, LRP1 and SDC3 in H9MG treated with increasing concentrations of Semagacestat. **E-H,** Quantification of CTF accumulation of the known γ-secretase substrates in panel **D**. Data are normalized by ACTIN expression and are presented as mean ± SD. n = 3.

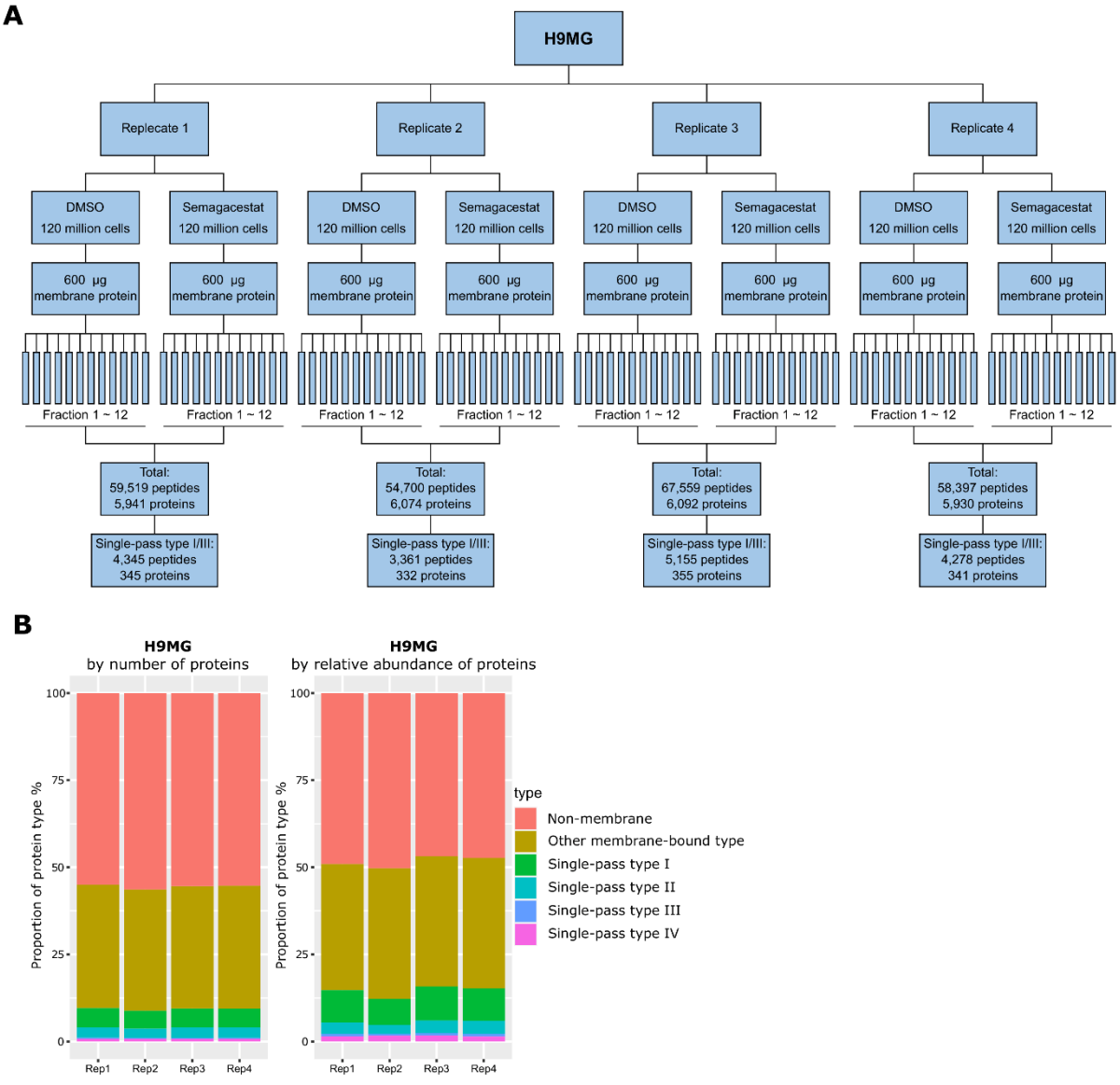


Figure S3. Summary of preparations for γ-secretase substrates identification, related to Figure 7. A, In total 4,800 µg purified membrane proteins (~600 µg from ~120 million cells for each sample) were run in four experiments and fractionated over 96 fractions. The numbers of identified peptides and proteins as well as their single-pass type I/III membrane protein subsets in each experiment are indicated. **B**, Stacked bar plots showing the proportion of different protein types in H9MG samples by protein number (left panel) and relative protein abundance (right panel).

4.2 Effects of γ-secretase deficiency on microglia transcriptional cell states

4.2.1 γ-Secretase inhibition causes substantial changes of microglia transcriptomes but does not affect the strong cell state response to LPS *in vitro*

We analyzed the single-cell transcriptomes of H9MG before and after Semagacestat treatment under *in vitro* cell culture conditions. We performed a second experiment in parallel treating cell cultures with lipopolysaccharide (LPS), asking whether a strong γ-secretase independent signal could overcome the transcriptional changes induced by Semagacestat. The LPS response is largely mediated by the specific receptor TLR4[306] which is not cleaved by γ-secretase (Figure S4).

We obtained a total of 17,006 single transcriptomes across the four different conditions: normal cell culture (Ctrl), Semagacestat treated (Sema), LPS treated (LPS) and Semagacestat/LPS treated (SemaLPS) (Figures 9A-B and S5). As expected, LPS treatment induced a strong response[307] (Figure 9B). Semagacestat treatment did not alter LPS induced gene expression (Figure 9C). Thus, LPS drives the cell state independently of γ-secretase activity.

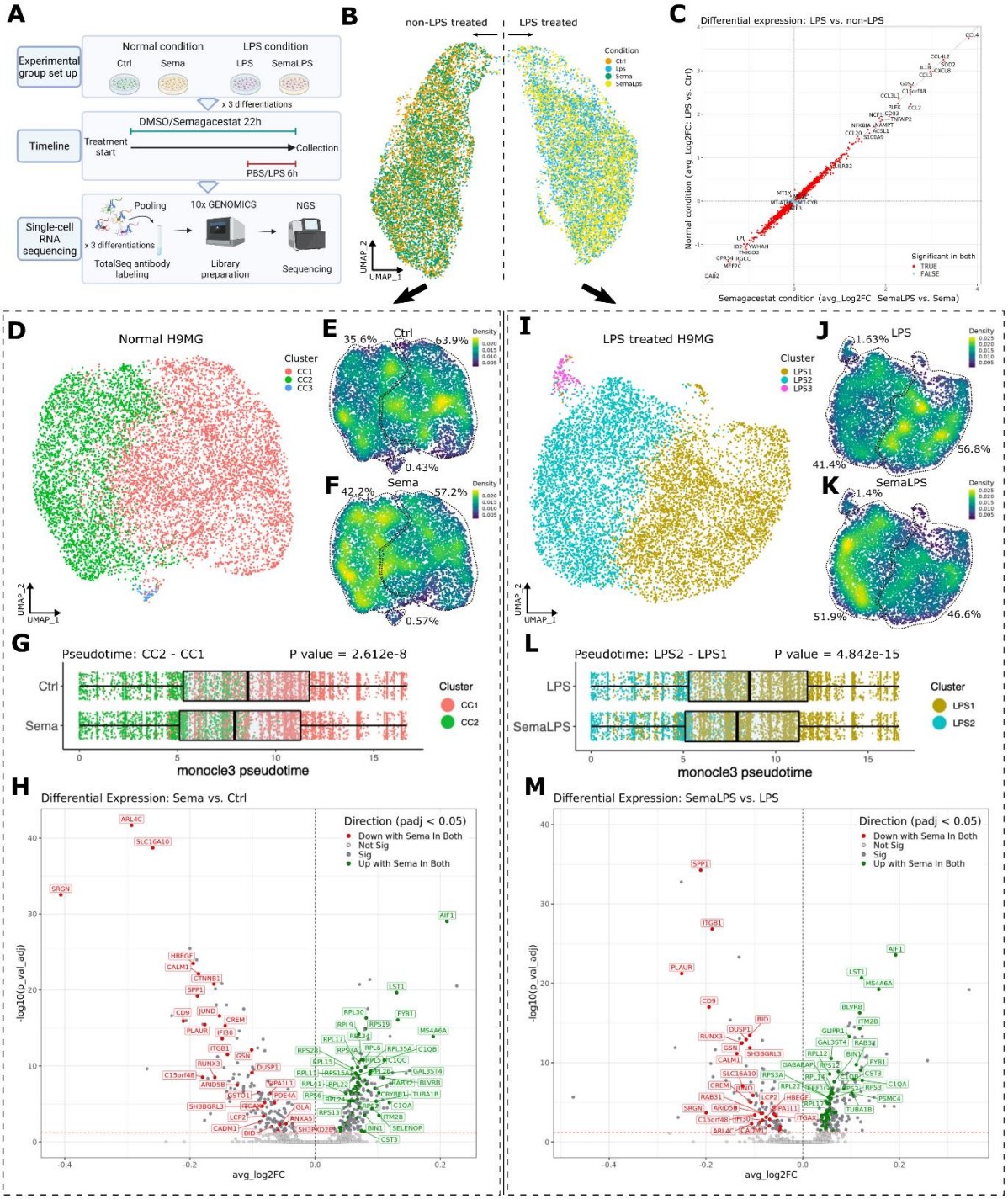
We separated the 8,611 and 8,395 single H9MG transcriptomes in the normal and the LPS stimulated conditions, respectively, and analyzed those individually. Using unbiased clustering, we identified cell clusters CC1, CC2 and CC3 in the normal culture condition (Figure 9D) and LPS1, LPS2 and LPS3 in the LPS stimulated condition (Figure 9I). Semagacestat treatment mildly shifted the distribution of cells between cluster CC1 and CC2 (Figures 9E-F) and between cluster LPS1 and LPS2 (Figures 9J-K). We analyzed the top expressed genes in these clusters (Figures S6A-B and S6D-E). Cells in cluster CC2 and LPS2 expressed higher typical HM genes (such as *C1QA, MAF* and *NAIP*) and HLA genes (such as *MS4A6A*, *HLA-DMB* and *HLA-DRB1*) compared to their counterparts, CC1 and LPS1 expressing higher typical DAM genes (such as *CD9*, *SPP1* and *ORL1*). Trajectory analysis with Monocle 3, aligning cells along the trajectories from CC2 to CC1 and from LPS2 to LPS1, confirmed rather mild effects on cell states caused by Semagacestat treatment (Figures 9G and 9L).

The impact of Semagacestat treatment on gene expression becomes however evident in gene differential expression (DE) and gene set enrichment (GSEA) analyses. These

analyses demonstrate that 350 genes are significantly (P.adj < 0.05) up- or down-regulated in Sema cells compared to Ctrl cells (Figures 9H and S6C), while 267 genes are significantly up- or down-regulated in the SemaLPS vs. LPS conditions (Figures 9M and S6F). Notably, in both control and LPS conditions, Semagecestat induces up-regulation of HM genes (e.g. *C1QA*, *MAF*, *NAIP*, etc.) and down-regulation of DAM genes (e.g. *CD9*, *SPP1*, *OLR1*, etc.)[147,150] (Figure S6C and S6F). Thus, γ-secretase seemingly regulates the expression levels of a similar set of genes in control and under LPS stress.

(Figure shown on next page)

Figure 9. γ-Secretase inhibition alters microglial steady-state signaling *in vitro*. A, H9MG cells were collected for single-cell RNA sequencing from four conditions: Ctrl (vehicle), Sema (Semagacestat), LPS (vehicle treatment for 22h with last 6 hours exposure to LPS) and SemaLPS (Semagacestat treatment for 22h with last 6 hours exposure to LPS). n = 3 independent differentiations per condition. **B,** Uniform manifold approximation and projection (UMAP) showing 17,006 single H9MG passing quality control after removal of the proliferative subpopulation. Cells are colored according to the four different conditions. **C,** Quadrant plot showing the similarity of the LPS response in the vehicle (Y axis) and in the Semagacestat condition (X axis). Wilcoxon rank-sum test, P values adjusted with Bonferroni correction (P.adj < 0.05). **D-F,** UMAPs showing 8,611 single H9MG transcriptomes from Ctrl and Sema treated conditions retrieved from panel **B**. Two main (CC1, CC2) and a small (CC3) cluster are identified (**D**). Density plots showing the distribution of H9MG cells across the three clusters in Ctrl (**E**) and Sema (**F**) conditions. **G**, Plots showing the delayed phenotypic trajectory of H9MG cells caused by γ-secretase inhibition (pseudotime ordering with Monocle 3 and colored by the cell states shown in **D**). **H,** Volcano plot showing the gene differential expression in non-proliferative H9MG cells in Sema vs Ctrl. Wilcoxon rank-sum test, P values adjusted with Bonferroni correction (P.adj < 0.05). The genes up- and down-regulated by Semagacestat in both the non-LPS condition (**H**) and the LPS condition (**M**) are colored in green and red, respectively. **I-K,** UMAPs showing 8,395 single H9MG transcriptomes from LPS and SemaLPS conditions retrieved from panel **B**. Two main (LPS1, LPS2) and a small (LPS3) cluster are identified (**I**). Density plots showing the distribution of H9MG cells across the three clusters in LPS (**J**) and SemaLPS (**K**) conditions. **L**, Plots showing delayed phenotypic trajectory of H9MG cells caused by γ-secretase inhibition (pseudotime ordering with Monocle 3 and colored by the cell states shown in **I**). **M,** Volcano plot showing the gene differential expression in SemaLPS vs LPS. Wilcoxon rank-sum test, P values adjusted with Bonferroni correction (P.adj < 0.05). The genes up- and down-regulated by Semagacestat in both the non-LPS condition (**H**) and the LPS condition (**M**) are colored in green and red, respectively.

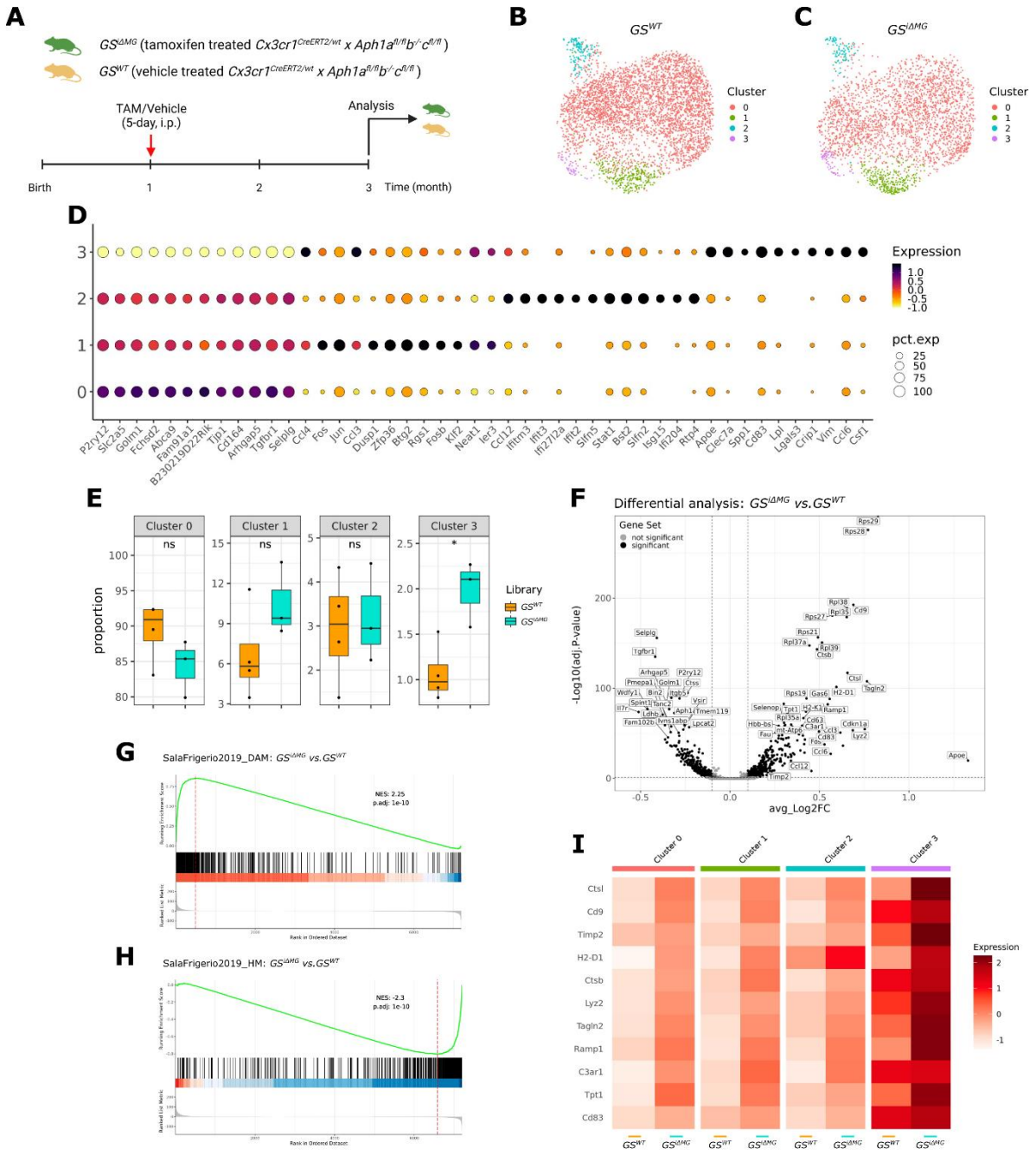


(Legend shown on last page)

4.2.2 γ-Secretase deficiency alters cell signaling in microglia *in vivo*

We crossed the *Cx3cr1*$^{CreERT2/WT}$ mice[293] with the *Aph1a*$^{fl/fl}$*b*$^{-/-}$*c*$^{fl/fl}$ mice[287] to generate the microglia-specific γ-secretase conditional KO mice (*GS*^{iΔMG}, Figure 10A). We induced the knockout at 1 month of age by treating the mice for 5 consecutive days with tamoxifen. We analyzed the single-cell transcriptomes of 7,285 microglia from 3-month-old mice and obtained 4 microglia clusters (Figure 10B-C). While a very small cluster 3 marked by the relatively high expression of DAM genes was significantly enriched with *GS*^{iΔMG} microglia (Figure 10D-E), the overall effects of γ-secretase deficiency on cell states is limited as it was in the cell culture experiments.

In contrast, DE and GSEA analyses revealed that 919 genes were significantly differentially regulated (P.adj < 0.05, abs(avg_Log2FC) > 0.1) by γ-secretase deficiency. Those genes that were up-regulated had a stronger DAM profile, while those that were down-regulated were more homeostatic (Figures 10F-H). DE analysis between *GS*^{iΔMG} and *GS*^{WT} microglia on a per-cluster basis showed that representative DAM genes (*e.g. Ctsl, Cd9, Timp2, H2-D1, Ctsb, Lyz2)* were consistently upregulated in the *GS*^{iΔMG} condition across all clusters (Fig 10I). This suggests that disrupting γ-secretase modulates the global gene expression of a cluster of genes associated with microglia activation,[144,145,291] without changing overall cell states as determined by the Louvain clustering algorithm.



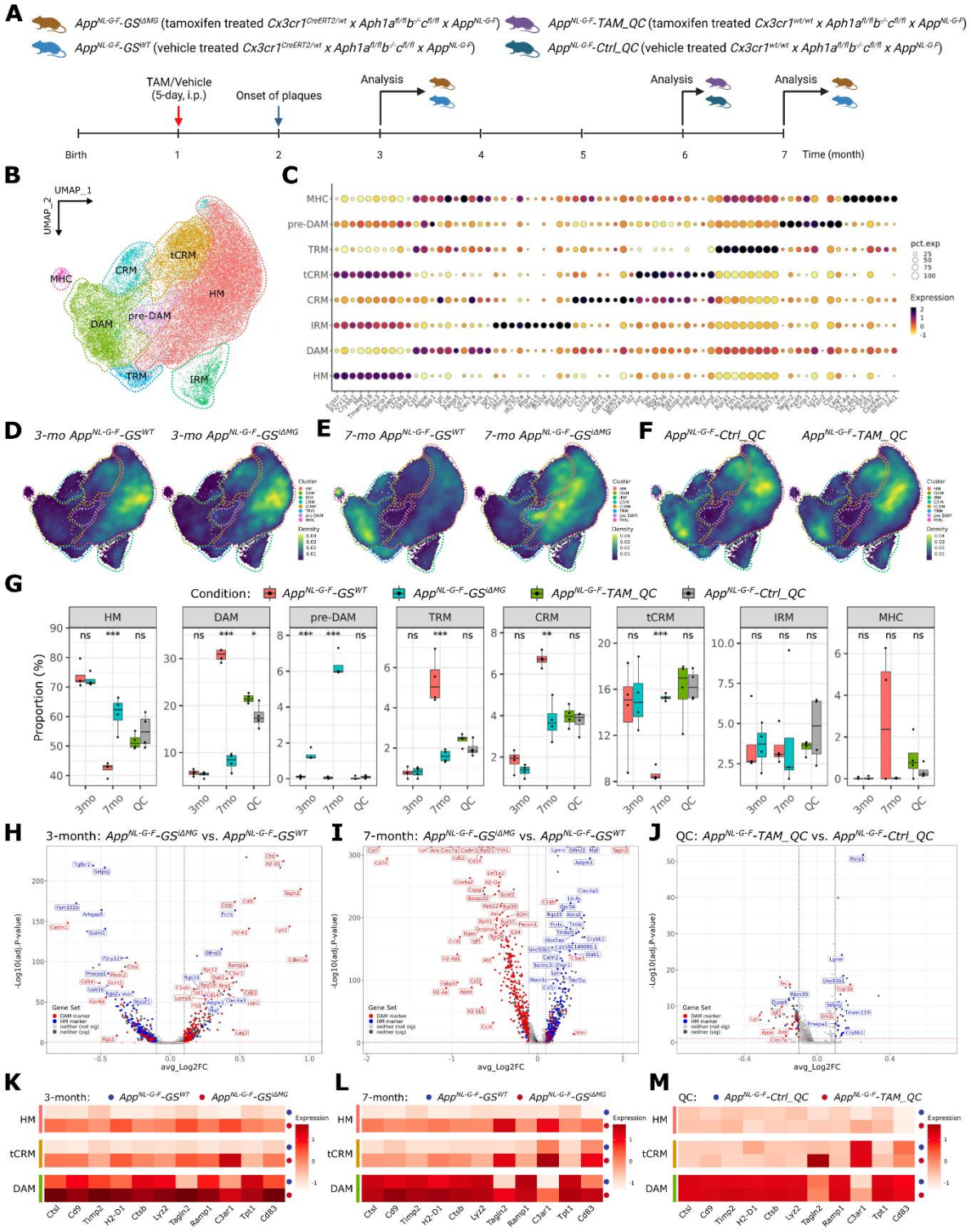
(Legend continued on next page)

Figure 10. γ-Secretase deficiency alters microglial signaling *in vivo*. A, Mice were treated with tamoxifen or vehicle at 1 month of age and sacrificed at 3 months. **B-C,** UMAP showing 4,376 single mouse microglia from 4 *GS*^{WT} mice (**B**) and 2,909 single mouse microglia from 3 *GS*$^{i\Delta MG}$ mice (**C**). **D,** Top 10 differentially expressed genes per cluster. The size of each dot represents the percentage of cells expressing the indicated gene within the cluster and the color represents the scaled and normalized average expression of the indicated gene. **E,** Box plots showing proportion of cells across the clusters. Multiple unpaired Student's t test corrected by Bonferroni method. n = 3-4 biological replicates per condition. *P < 0.1; ns, not significant. **F,** Volcano plots showing the gene differential expression in mouse microglia of *GS*$^{i\Delta MG}$ vs. *GS*^{WT}. Wilcoxon rank-sum test, P values adjusted with Bonferroni correction (P.adj

< 0.05). **G-H,** GSEA Enrichment Score curves. Gene set enrichment analysis (GSEA) for the gene differential expression in mouse microglia of $GS^{i\Delta MG}$ vs. GS^{WT} was performed using HM and DAM gene sets[144,145] as reference. The DAM gene set is significantly enriched in genes that are up-regulated (**G**) and the HM gene sets is significantly enriched in genes that are down-regulated (**H**) in γ-secretase deficient cells. **I,** Heatmap showing the relative expression of the representative genes (identified in **F**) in $GS^{i\Delta MG}$ vs. GS^{WT} across all the identified clusters.

4.2.3 γ-Secretase deficiency impedes the formation of activated microglial cell states in *App*$^{NL\text{-}G\text{-}F}$ mice

Given the preponderance of the γ-secretase substrates involved in AD-related microglia cell states (Figure 8) and the altered HM and DAM genes expression in the *in vitro* (Figure 9) and *in vivo* (Figure 10) experiments, we decided to investigate the effects of γ-secretase deficiency on microglia exposed to amyloid plaques. We further crossed the $GS^{i\Delta MG}$ mice with the $App^{NL\text{-}G\text{-}F}$ model for AD[292] to generate the $App^{NL\text{-}G\text{-}F}$-$GS^{i\Delta MG}$ mice. We reasoned that the transcriptomic alterations we recorded previously in healthy conditions might be more easily picked up as cell state transitions in a disease model.[144,145,291] The tamoxifen-induced KO mice ($App^{NL\text{-}G\text{-}F}$-$GS^{i\Delta MG}$), the vehicle treated control mice ($App^{NL\text{-}G\text{-}F}$-$GS^{WT}$), as well as the mice for tamoxifen induced artefact controls ($App^{NL\text{-}G\text{-}F}$-*TAM_QC* and $App^{NL\text{-}G\text{-}F}$-*Ctrl_QC*) are indicated in Figure 11A. We induced the knockout at 1 month of age with tamoxifen and analyzed the single-cell transcriptomes of 37,884 microglia (Figure S7) from 3-month-old mice and from 6/7-month-old mice which show mild and advanced amyloid pathology, respectively. Unbiased clustering using Seurat resulted in 6 main clusters (Figures 11B-C), named homeostatic (HM), cytokine response (CRM), transitioning cytokine response (tCRM), interferon response (IRM), transition response (TRM) and disease-associated (DAM) microglia, referring to previous work [144–146,150,291] (Figures S8A-C). A small novel “pre-DAM” cluster whose partially overlapping HM and DAM signature represents an intermediate cell state (Figures 11B-C) is of particular interest, because it is only seen in the $App^{NL\text{-}G\text{-}F}$-$GS^{i\Delta MG}$ mice (Figure S8D). Moreover, pre-DAM cells highly express the subset of DAM genes (*e.g. Ctsl, Cd9, Timp2, Ctsb, Lyz2*) that represent the disrupted microglial signaling shown in the $GS^{i\Delta MG}$ mice in Figure 10, while the expression levels of other known DAM signature genes (e.g. *B2M*, *Axl*, *Cst7*, *Lpl*, *Lilrb4a*) are not as pronounced (Figure S8E).



(Legend continued on next page)

Figure 11. γ-Secretase deficiency perturbs microglia cell states in AD mouse brains. A, Mouse microglia for single-cell RNA sequencing were isolated from mice with 2 genotypes (*Cx3cr1*$^{CreERT2/WT}$ x *Aph1a*$^{fl/fl}$*b*$^{-/-}$*c*$^{fl/fl}$ x *App*$^{NL-G-F}$ and *Cx3cr1*$^{WT/WT}$ x *Aph1a*$^{fl/fl}$*b*$^{-/-}$*c*$^{fl/fl}$ x *App*$^{NL-G-F}$). Mice were treated with tamoxifen or vehicle at 1 month of age before Aβ plaques are formed and were sacrificed at one of the 3 indicated time points (3, 6 and 7 months). **B,** UMAP of the 37,884 single mouse microglia from 24 mice (6 conditions x 4 biological replicates per condition) passing quality control and after removal of non-microglial subpopulations. Eight

clusters are indicated: Homeostatic microglia (HM), Cytokine response microglia (CRM), transitioning cytokine response (tCRM), Inteferon response microglia (IRM), Disease-associated microglia (DAM/ARM), Immature DAM (pre-DAM), Transitioning response microglia (TRM), and Antigen presenting response microglia (MHC). Annotation is based on previous studies[145,146,150] (See Figure S8**A-C**). **C,** Top 10 differentially expressed genes in each identified cluster. **D-F,** Density plots showing the distribution of mouse microglia across the 8 clusters in *App$^{NL\text{-}G\text{-}F}$-GS^{WT}* and *App$^{NL\text{-}G\text{-}F}$-GS$^{i\Delta MG}$* mice at 3 months (**D**) and 7 months (**E**), and *App$^{NL\text{-}G\text{-}F}$-Ctrl_QC* and *App$^{NL\text{-}G\text{-}F}$-TAM_QC* at 6 months (**F**). **G,** Box plots showing proportion of cells across all clusters in the different conditions, two-way ANOVA followed by Tukey's multiple comparison test. n = 4 biological replicates per condition. *P < 0.1; **P < 0.01; ***P < 0.001; ns, not significant. **H-J,** Volcano plots showing the gene differential expression in mouse microglia of *App$^{NL\text{-}G\text{-}F}$-GS$^{i\Delta MG}$* vs. *App$^{NL\text{-}G\text{-}F}$-GS^{WT}* at 3 months (**H**) and 7 months (**I**), and also *App$^{NL\text{-}G\text{-}F}$-TAM_QC* vs. *App$^{NL\text{-}G\text{-}F}$-Ctrl_QC* at 6 months (**J**). Wilcoxon rank-sum test, P values adjusted with Bonferroni correction (P.adj < 0.05). The genes above the threshold and belonging to the previously decribed DAM/ARM and HM[144,145] are colored in red and blue, respectively. **K-M,** Heatmaps showing the relative expression of the representative genes (identified in *GS$^{i\Delta MG}$*, Figure 10**I**) across the main clusters in mouse microglia of *App$^{NL\text{-}G\text{-}F}$-GS$^{i\Delta MG}$* vs. *App$^{NL\text{-}G\text{-}F}$-GS^{WT}* at 3 months (**K**) and 7 months (**L**), and also *App$^{NL\text{-}G\text{-}F}$-TAM_QC* vs. *App$^{NL\text{-}G\text{-}F}$-Ctrl_QC* at 6 months (**M**).

We compared the single microglia transcriptomes in the 6 indicated conditions (n=4 animals per condition). The shifts in microglia distribution across different cell states caused by γ-secretase deficiency were mild at 3 months but obvious at 7 months (Figures 11D-E). The relative proportions of DAM, CRM and TRM were significantly reduced in *App$^{NL\text{-}G\text{-}F}$-GS$^{i\Delta MG}$* mice compared to *App$^{NL\text{-}G\text{-}F}$-GS^{WT}* mice at 7 months, whereas HM and tCRM were significantly increased (Figure 11G). Interestingly, the pre-DAM cluster was significantly enriched in both 3-month and 7-month *App$^{NL\text{-}G\text{-}F}$-GS$^{i\Delta MG}$* mice compared to their age-matched *App$^{NL\text{-}G\text{-}F}$-GS^{WT}*mice (Figure 11G). DE analysis between microglia of *App$^{NL\text{-}G\text{-}F}$-GS$^{i\Delta MG}$* mice and microglia of *App$^{NL\text{-}G\text{-}F}$-GS^{WT}* mice at 7 months echoed the reduced proportion of the DAM cluster revealed the upregulation of HM genes and the downregulation of DAM genes (Figure 11I). A DE analysis of microglia transcriptomes between the two γ-secretase conditions on a per-cluster basis confirmed that the same group of genes (*e.g. Ctsl, Cd9, Timp2, Ctsb, Lyz2*) were consistently upregulated in the *App$^{NL\text{-}G\text{-}F}$-GS$^{i\Delta MG}$* groups at both 3 and 7 months across the main clusters (Figures 11K-L). Thus, disrupting γ-secretase has a general effect on all the γ-secretase deficient microglia, as in the cell cultures and the control mice, next to its blocking effect on cell state transitions driven by the amyloid plaques.

Tamoxifen treatment alone, comparing *App^{NL-G-F}-TAM_QC* and *App^{NL-G-F}-Ctrl_QC* samples, showed only mild effects, with a small decrease in the DAM cluster but no effects in other clusters (Figures 11F-G). DE analysis also confirmed that the tamoxifen induced artefact was limited (Figure 11J) and did not affect the expression of genes regulated by γ-secretase (*e.g. Ctsl, Cd9, Timp2, Ctsb, Lyz2*)(Figure 11M).

To exclude the potential effect of the genetic modification (floxed *Aph1a/c* alleles and *Aph1b* knockout)[287] on microglia cell states in the AD context, we compared the tamoxifen-untreated *App^{NL-G-F}* x *Aph1Floxed* mice (*App^{NL-G-F}-GS^{WT}*) and the *App^{NL-G-F}* mice at 12 months of age. We analyzed 5,999 single microglia transcriptomes from the *App^{NL-G-F}* x *Aph1Floxed* mice and 7,185 transcriptomes from the *App^{NL-G-F}* mice. All the typical microglia transcriptomic cell states (HM, DAM, CRM, IRM and TRM) as previously described[145] were identified and annotated in the UMAP (Figures S9A-C). The genetic modification in the *App^{NL-G-F}* x *Aph1Floxed* mice did not significantly change the distribution of microglia across the different cell states compared to the age-matched *App^{NL-G-F}* mice (Figures S9A-D). This confirms that the alterations observed in the experiments above can be attributed to γ-secretase deficiency induced by tamoxifen treatment and not to the genetic construct as such.

Taken together, the results indicate that γ-secretase deficiency alters the expression of a series of specific genes in microglia in different cell environments and majorly impedes the formation of *in vivo* activated microglia cell states induced by amyloid plaque exposure (DAM, TRM, CRM), as evidenced in 7-month vs. 3-month-old animals.

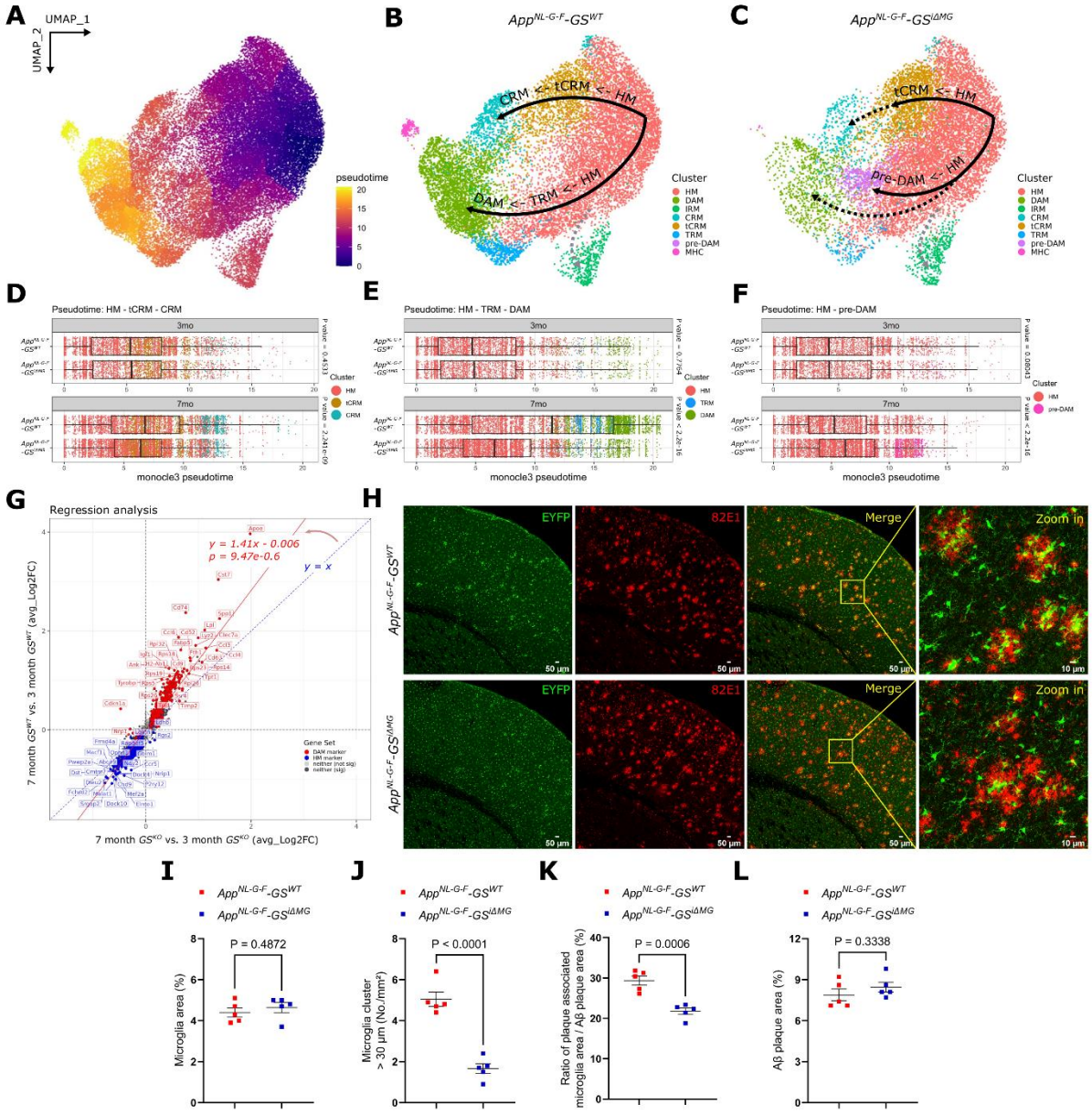
4.2.4 γ-Secretase deficiency blocks *in vivo* microglia in a pre-DAM state in response to amyloid pathology

Using Monocle 3 and assuming a transition from the homeostatic to other cell states (Figure 12A), two major pseudo-time trajectories from HM towards DAM and CRM emerge (Figures 12B-C). These align with previously reported human microglial responses in a chimeric AD model.[150] A third trajectory towards IRM (grey dotted line) was not further considered, as the IRM cell state was not affected by γ-secretase deficiency (Figure 11G). Particularly at 7 months microglia distributions along the HM-tCRM-CRM and the HM-TRM-DAM axes are shifted towards higher pseudotime values in *App^{NL-G-F}-GS^{WT}* mice H9MG, while in *App^{NL-G-F}-GS^{iΔMG}* mice they reside mostly in HM, tCRM and pre-DAM states (Figures 12D-F). Regression analysis comparing the

transcriptomic profiles of microglia in 7-month vs. 3-month brains in the deficient or control γ-secretase condition (Figure 12G) confirms a significantly attenuated age-dependent microglia activation in the *App*$^{NL\text{-}G\text{-}F}$-*GS*$^{i\Delta MG}$ mice. Of note, age here reflects increased amyloid plaque accumulation.

TREM2 is cleaved by γ-secretase,[162] important for TREM2 down-stream signaling.[167] TREM2-KO blocks microglia in a so-called DAM1 state in *TgAD* mice.[144] DAM1 expresses only a subset of the DAM program and lacks the Trem2-dependent lipid metabolism (*Lpl*, *Ccl6*) and phagocytic pathway genes (*Axl*. *Clec7a*, *Ctsl*) characteristic of a full DAM response.[144] pre-DAM microglia accumulate when DAM is abolished in *App*$^{NL\text{-}G\text{-}F}$-*GS*$^{i\Delta MG}$ mice, leading us to wonder if pre-DAM is a DAM1-like state. Interestingly, while the low expression of *Axl*, *Cst7*, *Lpl* and *Lilrb4a* in pre-DAM aligns with what has been described in DAM1, the high expression of *Cd9*, *Ctsl*, *Spp1* and *Timp2* in pre-DAM conflicts with the reported DAM1 features (Figure S8E). We next performed a Pearson's correlation analysis between the fold changes of genes in pre-DAM vs. DAM identified in this study and DAM1 vs. DAM2 identified previously by Keren-Shaul et al. but find only a weak correlation (Figure S8F, R = 0.35). Therefore, the perturbation of microglia states caused by γ-secretase deficiency is distinct from that previously reported in the *Trem2* KO condition.[144]

We finally compared morphological microglia phenotypes and amyloid pathologies in 7-month *App*$^{NL\text{-}G\text{-}F}$-*GS*$^{i\Delta MG}$ and *App*$^{NL\text{-}G\text{-}F}$-*GS*^{WT} mice using immunofluorescent staining. The total area covered by microglia (EYFP^{+}) is similar between the two genotypes (Figures 12H-I). However, while the γ-secretase potent microglia formed large clusters around the plaques, γ-secretase deficient microglia remained nicely distributed in a tilted fashion in the presence of amyloid plaques (Figure 12H and 12J-K). There was no clear difference in amyloid plaque load (Figure 12L). Taken together, consistent with the single-cell transcriptomic analysis, γ-secretase deficiency blocks microglial response to Aβ plaques.



(Legend continued on next page)

Figure 12. γ-Secretase deficiency blocks microglia in a pre-DAM state in response to amyloid pathology. A, UMAP showing the phenotypic trajectory of *in vivo* microglia in response to amyloid pathology obtained by an unbiased pseudotime ordering with Monocle 3. **B-C,** UMAPs showing 13,694 single mouse microglia from 3 and 7 month *App*$^{NL\text{-}G\text{-}F}$-*GS*^{WT} mice (**B**), and 11,835 single mouse microglia from 3 and 7 month *App*$^{NL\text{-}G\text{-}F}$-*GS*$^{i\Delta MG}$ mice (**C**). Arrows indicate the potential microglia activation routes determined by pseudotime analysis (**D-F**) based on Mancuso et al.[150] **D-F** Distribution of cells from *App*$^{NL\text{-}G\text{-}F}$-*GS*^{WT} and *App*$^{NL\text{-}G\text{-}F}$-*GS*$^{i\Delta MG}$ mice along the three indicated transcriptional trajectories: HM - tCRM - CRM (**D**), HM - TRM - DAM (**E**) and HM - pre-DAM (**F**), colored by clusters (shown in **B** and **C**). **G,** Quadrant plot showing age-dependent microglial gene differential expression in *App*$^{NL\text{-}G\text{-}F}$-*GS*^{WT} mice (Y axis) and in *App*$^{NL\text{-}G\text{-}F}$-*GS*$^{i\Delta MG}$ mice (X axis). Linear regression analysis was performed on the Log2FC of differentially expressed genes in the *App*$^{NL\text{-}G\text{-}F}$-*GS*^{WT} mice 7 mo vs. 3 mo and the *App*$^{NL\text{-}G\text{-}F}$-*GS*$^{i\Delta MG}$ mice 7 mo vs. 3 mo comparisons (lm(*App*$^{NL\text{-}G\text{-}F}$-*GS*^{WT} 7 mo vs. 3 mo ~ *App*$^{NL\text{-}G\text{-}F}$-*GS*$^{i\Delta MG}$ 7 mo vs. 3 mo)). To determine if the obtained slope was different from y=x, the t-

statistic was calculated by taking the absolute value of 1 (the slope of y=x) minus the calculated slope and dividing it by the standard error. The p-value was obtained from this test statistic. **H,** Representative images of immunofluorescent staining of brain sections from 7-month *App*$^{NL\text{-}G\text{-}F}$-*GS*^{WT} and *App*$^{NL\text{-}G\text{-}F}$-*GS*$^{i\Delta MG}$ mice. EYFP: microglia (green); 82E1: Aβ plaques (red). **I-K,** Quantitative analysis of microgliosis in the brain sections shown in **H**. Coverage of microglia (EYFP^{+}) area (**I**) and density of microglial puncta (**J**, EYFP^{+} puncta with diameter > 30 μm) per mm^2, and the ratio of overlapped microglia and plaque (EYFP^{+}82E1^{+}) area *vs.* total plaque (82E1^{+}) area (**K**) were quantified. **L,** Quantitative analysis of Aβ plaques in the brain sections shown in **H**. Ratio of Aβ plaques area per mm^2 was quantified. Data are shown as mean ± SEM. n = 5 animals in each condition. Each dot represents the average measurement value of 2 sections from an individual animal. P values are determined by two-tailed unpaired Student's t test (**I-L**).

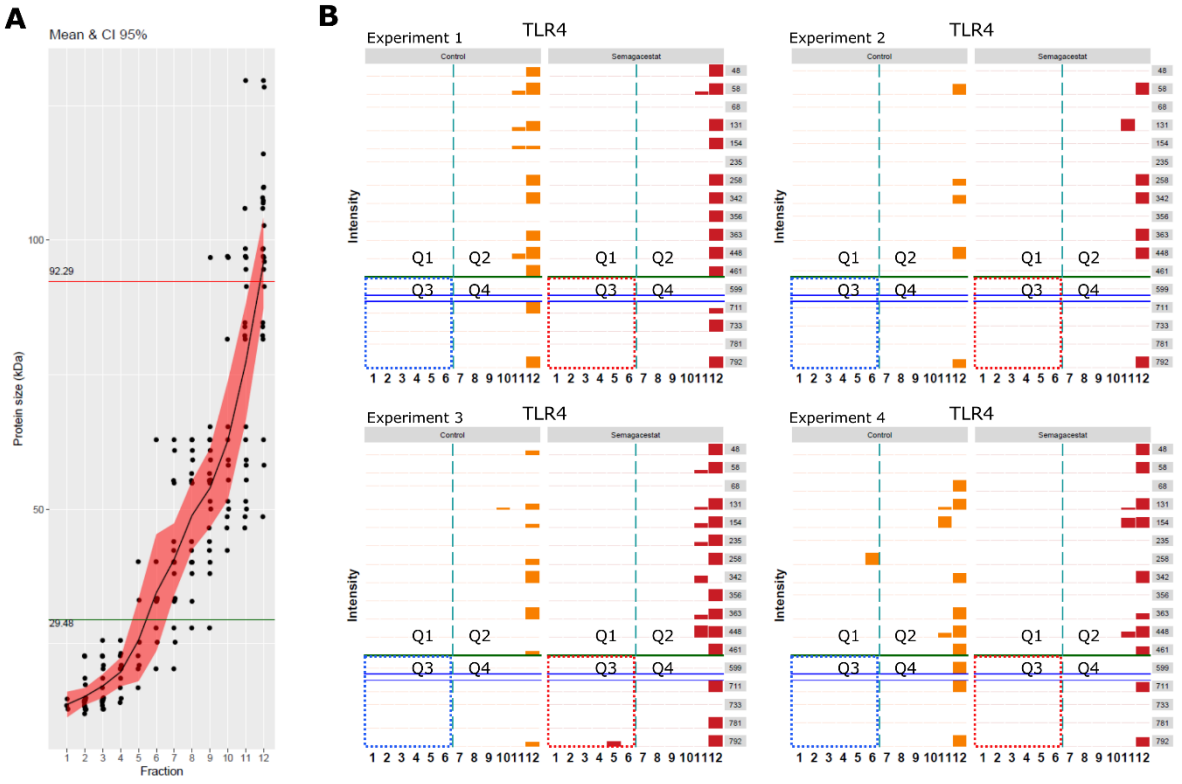


Figure S4. Faceted barplot of the non-substrate protein TLR4. A, Reference plot showing the mean and the 95% confidence interval of the protein size in each fraction. The predicted size of TLR4-FL (based on the number of aa) is 92.29 kDa and therefore TLR4-FL should distribute in fraction 11-12, and the predicted TLR4-CTF of 29.48 kDa should distribute in fraction 4-6. **B,** The faceted barplots show the relative abundance of each of the detected TLR4 peptides in the corresponding fractions in four independent experiments, control (left) and semagacestat treated sample (right). Q3 is the quadrant 3 region defined by the horizontal and vertical green lines and defines the area where TLR4-CTF derived peptides should distribute. The green horizontal line indicates the start of the TLR4-CTF. The blue double horizontal lines indicate the borders of the TLR4-TMD based on UniprotKB.[302] Here we show the results for TLR4 which is not a γ-secretase substrate.

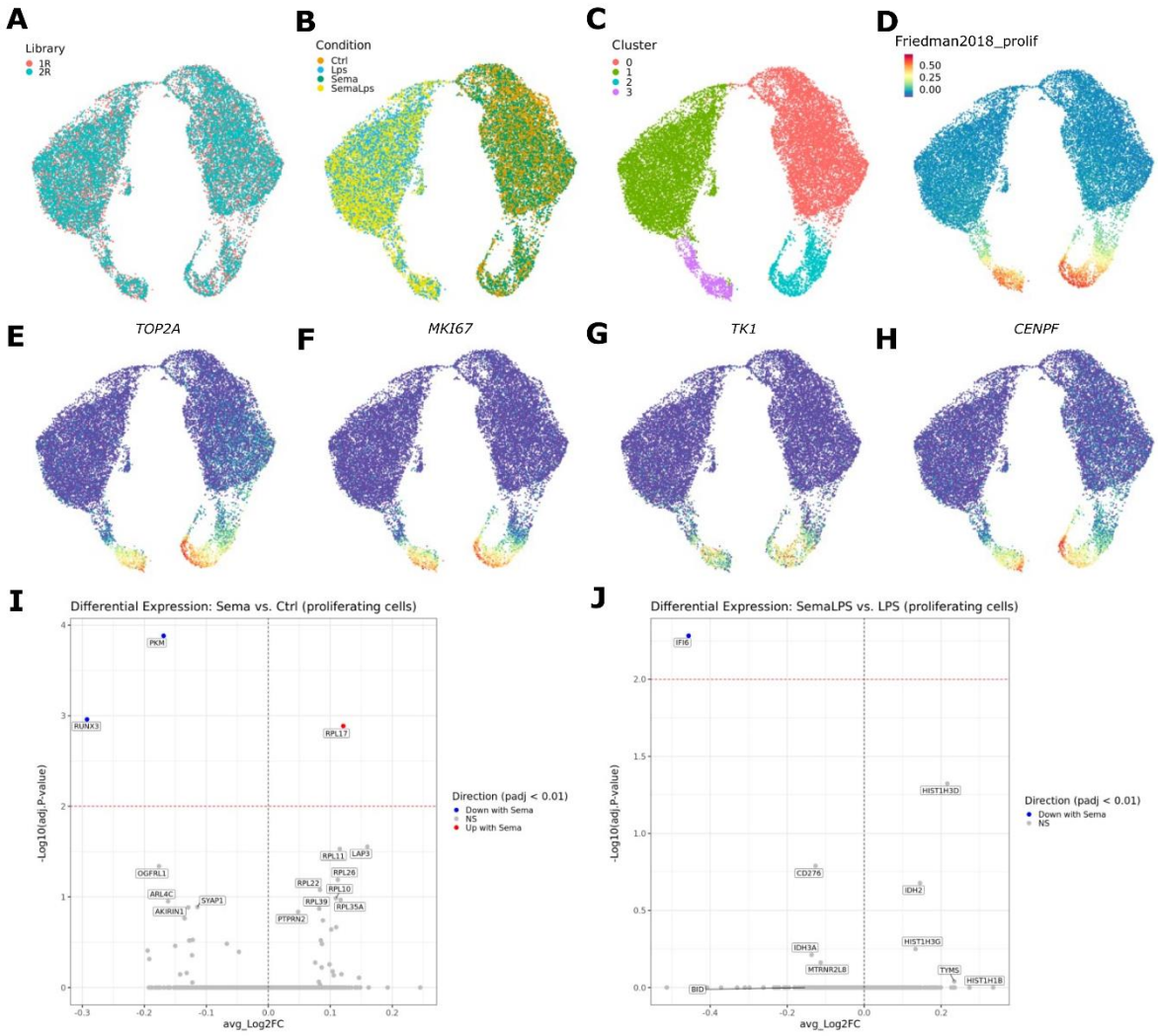
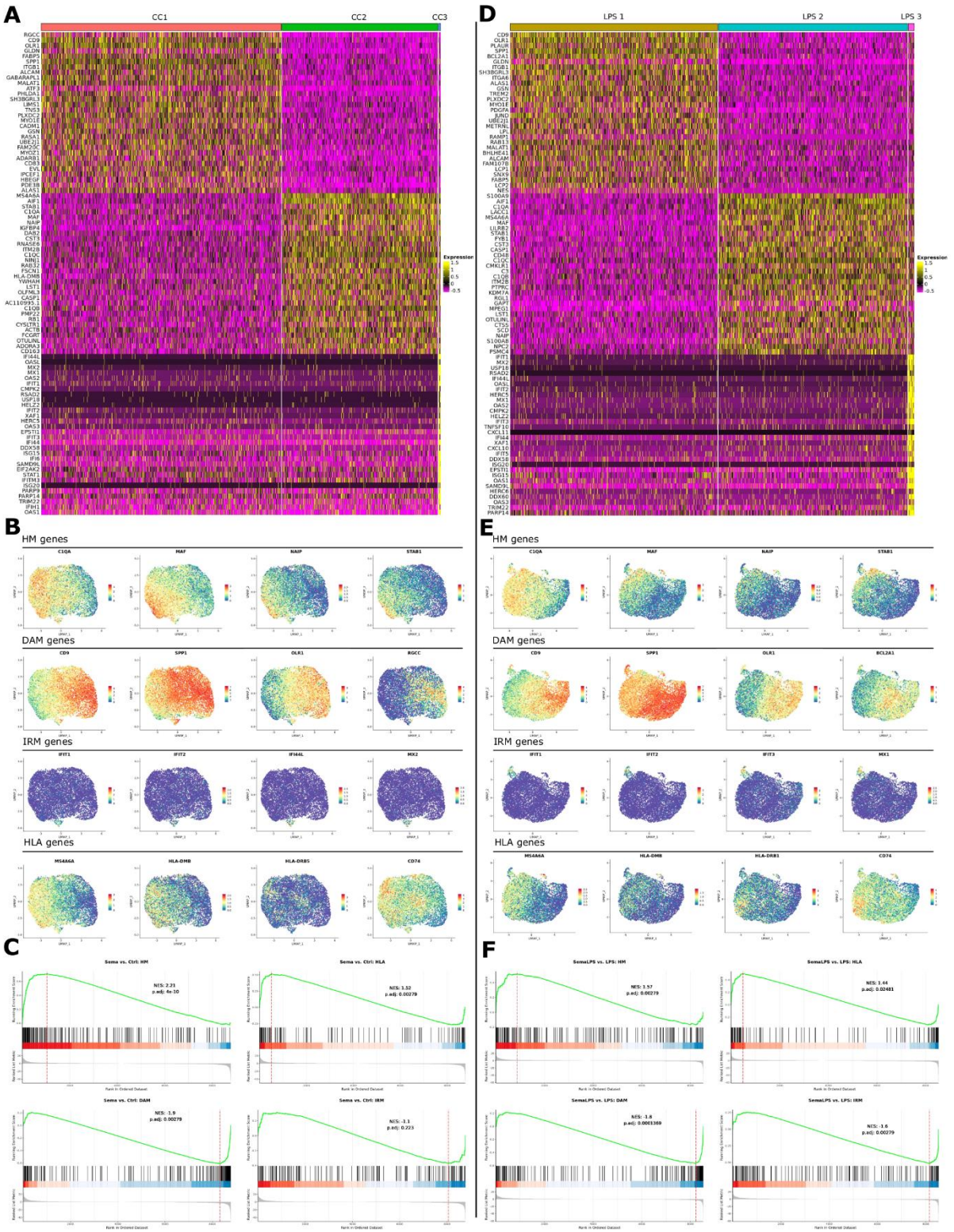


Figure S5. γ-Secretase inhibition mildly affects the proliferative population of H9MG, related to Figure 9. A-C, UMAP showing 19,421 single H9MG transcriptomes passing quality control and colored by libraries (**A**), conditions (**B**) and unbiased clusters using the Louvain algorithm (**C**). **D-H,** Cells annotated by the Friedman proliferating gene set[291] (**D**) and the top marker genes (**E-H**). **I-J**, Differential expression of Genes in the proliferative cells induced by Semagacestat in the normal condition (**I**) and in the LPS treated condition (**J**). Wilcoxon rank-sum test, P values adjusted with Bonferroni correction (P.adj < 0.01).



(Legend continued on next page)

Figure S6. Extended cell state annotations, related to Figure 9. A, Heatmap showing gene differential expression across all identified clusters in the normal condition. The top 30 genes in each cluster are represented. **B,** UMAP showing the relative expression levels of representative HM, DAM, IRM and HLA genes[150] in the normal condition. **C,** GSEA Enrichment Score curves. Gene set enrichment analysis (GSEA) for Semagecestat-treated vs. non-treated cells in the normal condition was performed using HM, DAM, IRM, HLA marker gene sets[150] as reference. Genes on the far left of the graph (red) represent those that are most up-regulated in Semagecestat-treated cells and genes on the far right (blue) are most down-regulated. The enrichment score (ES) curve is represented by the green curve. The ES of each gene set was normalized across all analyzed gene sets to obtain the normalized enrichment score (NES). The vertical red line denotes the maximum/minimal running enrichment score. The DAM gene set is significantly enriched in genes that are down-regulated in Semagecestat-treated cells, while the HM and HLA gene sets are significantly enriched in genes that are up-regulated in Semagecestat-treated cells. **D,** Heatmap showing gene differential expression across all identified clusters in the LPS stimulated condition. The top 30 genes in each cluster are represented. **E,** UMAP showing the relative expression levels of representative HM, DAM, IRM and HLA genes[150] in the LPS stimulated condition. **F,** GSEA Enrichment Score curves. Gene set enrichment analysis (GSEA) for Semagecestat-treated vs. non-treated cells in the LPS stimulated condition was performed using HM, DAM, IRM, HLA marker gene sets[150] as reference. The DAM and IRM gene set are significantly enriched in genes that are down-regulated in Semagecestat-treated cells, while the HM and HLA gene sets are significantly enriched in genes that are up-regulated in Semagecestat-treated cells.

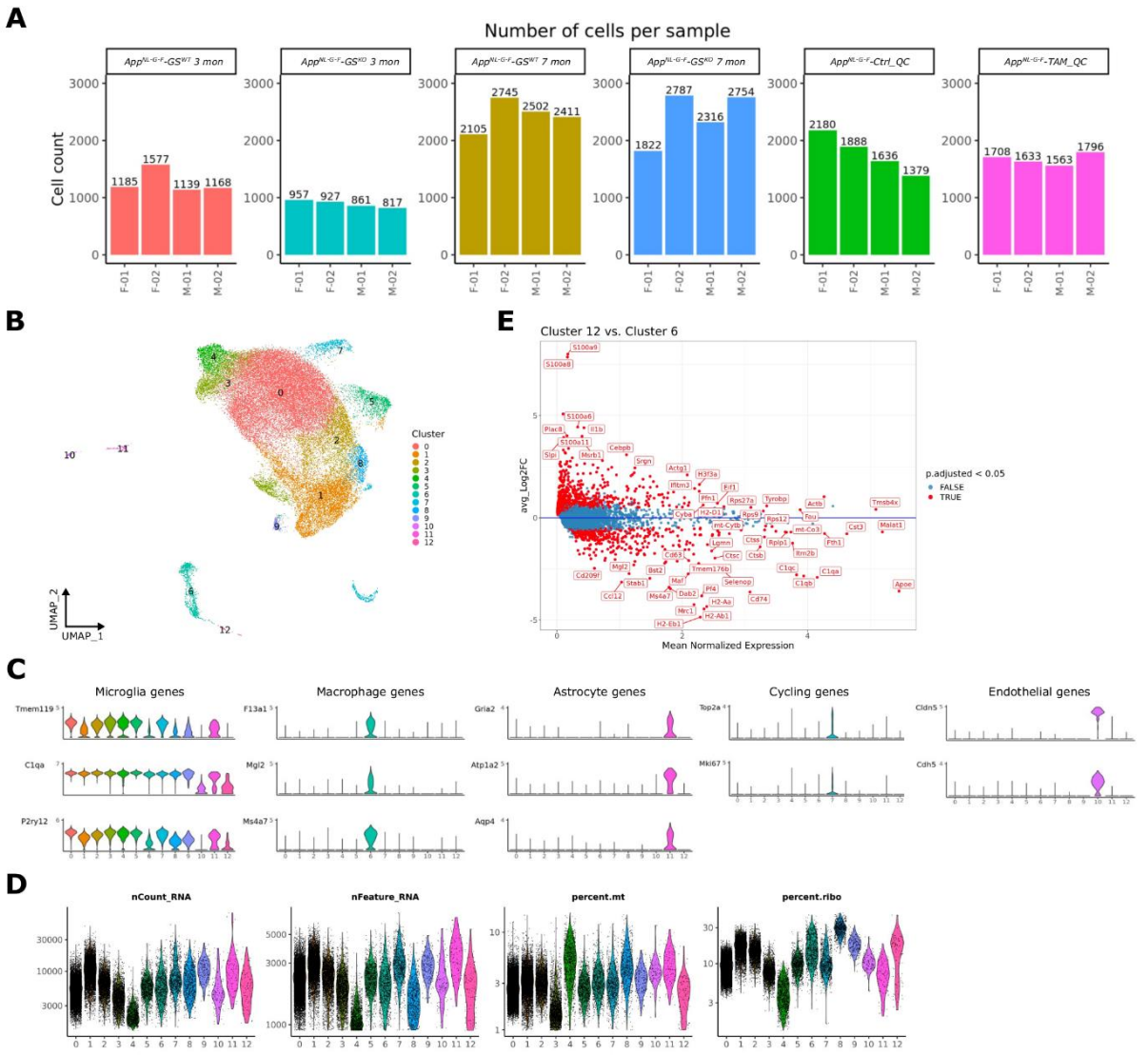
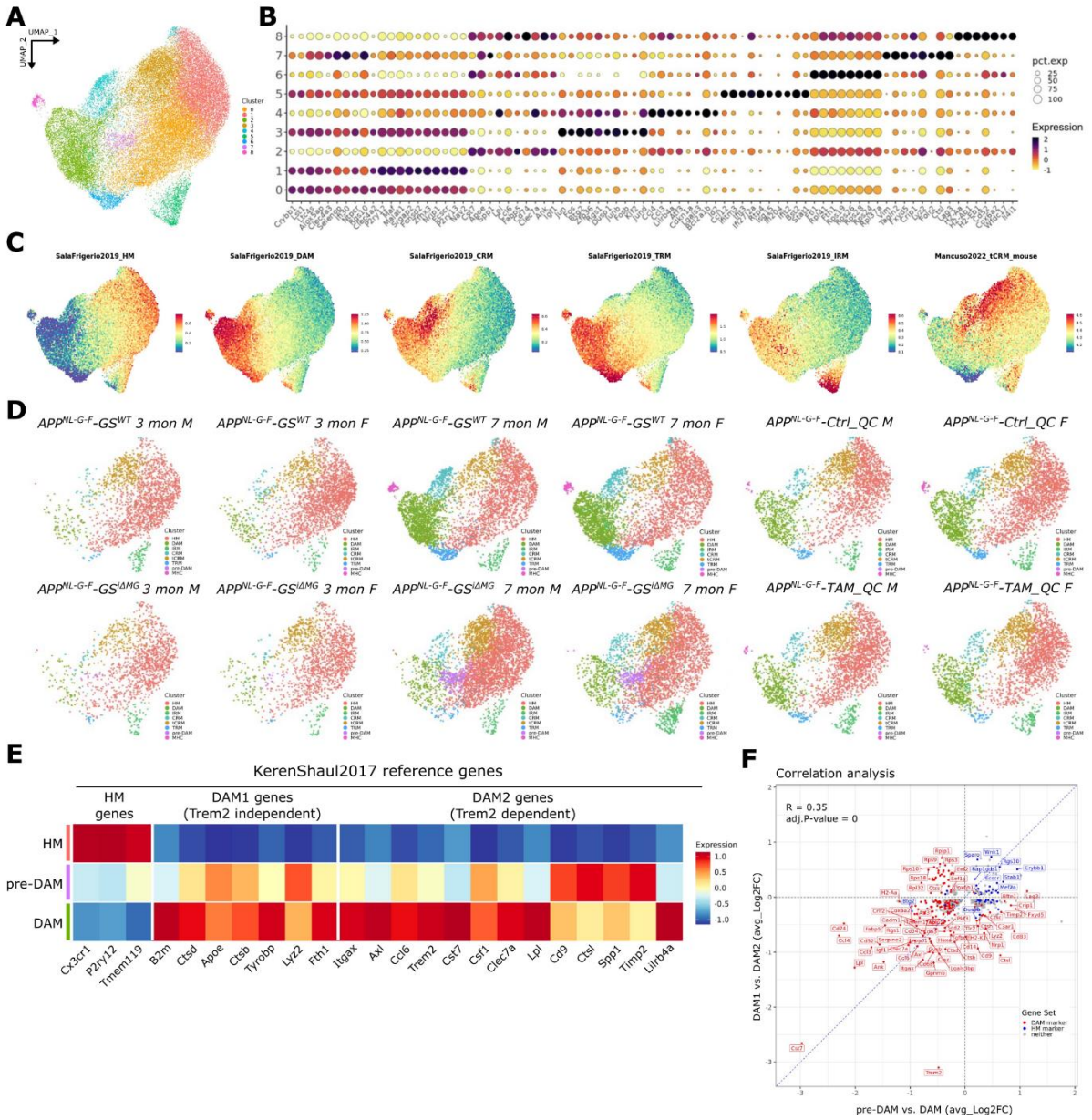


Figure S7. Summary of the datasets and identification of microglia clusters for single-cell data analysis related to Figure 11. A, An overview of the 41,856 single cell transcriptomes passing quality control and after removal of hashtag negative and doublet cells across 6 conditions: *App*$^{NL\text{-}G\text{-}F}$*-GS*^{WT} 3 month, *App*$^{NL\text{-}G\text{-}F}$*-GS*^{iΔMG} 3 month, *App*$^{NL\text{-}G\text{-}F}$*-GS*^{WT} 7 month, *App*$^{NL\text{-}G\text{-}F}$*-GS*^{iΔMG} 7 month, *App*$^{NL\text{-}G\text{-}F}$*-Ctrl_QC* and *App*$^{NL\text{-}G\text{-}F}$*-TAM_QC.* 2 female and 2 male animals were included in each condition. **B,** UMAP showing integrated 41,856 single cell trancriptomes (shown in **A**) in 13 unbiasedly identified clusters using the Louvain algorithm. **C,** Violin plots showing the expression of microglia, macrophage, astrocyte, cycling cell and endothelial cell marker genes across the 13 clusters (shown in **B**). **D,** Further quality control of cells from the 13 clusters (shown in **B**) by checking number of RNA counts, number of gene (feature) counts, percentage of mitochodria transcripts and percentage of ribosomal transcripts in each cluster. Cluster 4 is a group of low quality cells with low RNA and gene counts and a high percentage of mitochondria transcripts. **E**, Differential expression of genes in cluster 12 vs. cluster 6 suggesting that cluster 12 is a group of monocytic cells expressing *S100a8/9*. Wilcoxon rank-sum test, P values adjusted with Bonferroni correction (P.adj < 0.05).



(Legend continued on next page)

Figure S8. Extended cell state annotations related to Figure 11-12. A, UMAP showing retained 37,884 single mouse microglia after removal of cycling microglia, non-microglial and low-quality subpopulations. 9 clusters were unbiasedly identified using the Louvain algorithm. **B,** Top 10 differentially expressed genes in each identified cluster (as shown in **A**). The size of each dot represents the percentage of cells expressing the indicated gene within the cluster. The color of each dot represents the scaled and normalized average expression of the indicated gene. Note cluster 0 and 1 represent similar homeostatic microglia states and are therefore considered as one cell state in **Figure 11B**. **C,** UMAP plots colored by the relative expression levels of groups of genes that characterize distinct *in vivo* mouse microglial states previously reported by Sala Frigerio and Mancuso et al.[145,146,150] **D,** UMAP plots showing the distribution of microglia across the different clusters (shown in **Figure 11B**) in 12 conditions (from 6 conditions as shown in **Figure S7A** and further specified by gender). **E,** Heatmap showing the relative expression of the homeostatic, Trem2 independent (DAM1) and Trem2

dependent (DAM2) genes defined by Keren-Shaul et al. in the cells isolated and classified in this study. **F,** Pearson's correlation analysis of the Log2FC in pre-DAM vs. DAM clusters defined in this study (x-axis) with DAM1 vs. DAM2 clusters defined by Keren-Shaul et al. (y-axis). Differentially expressed genes were analyzed by Wilcoxon rank-sum test, P values adjusted with Bonferroni correction (P.adj < 0.05). The genes above the threshold and highly expressed in DAM and HM[145] are colored in red and blue, respectively.

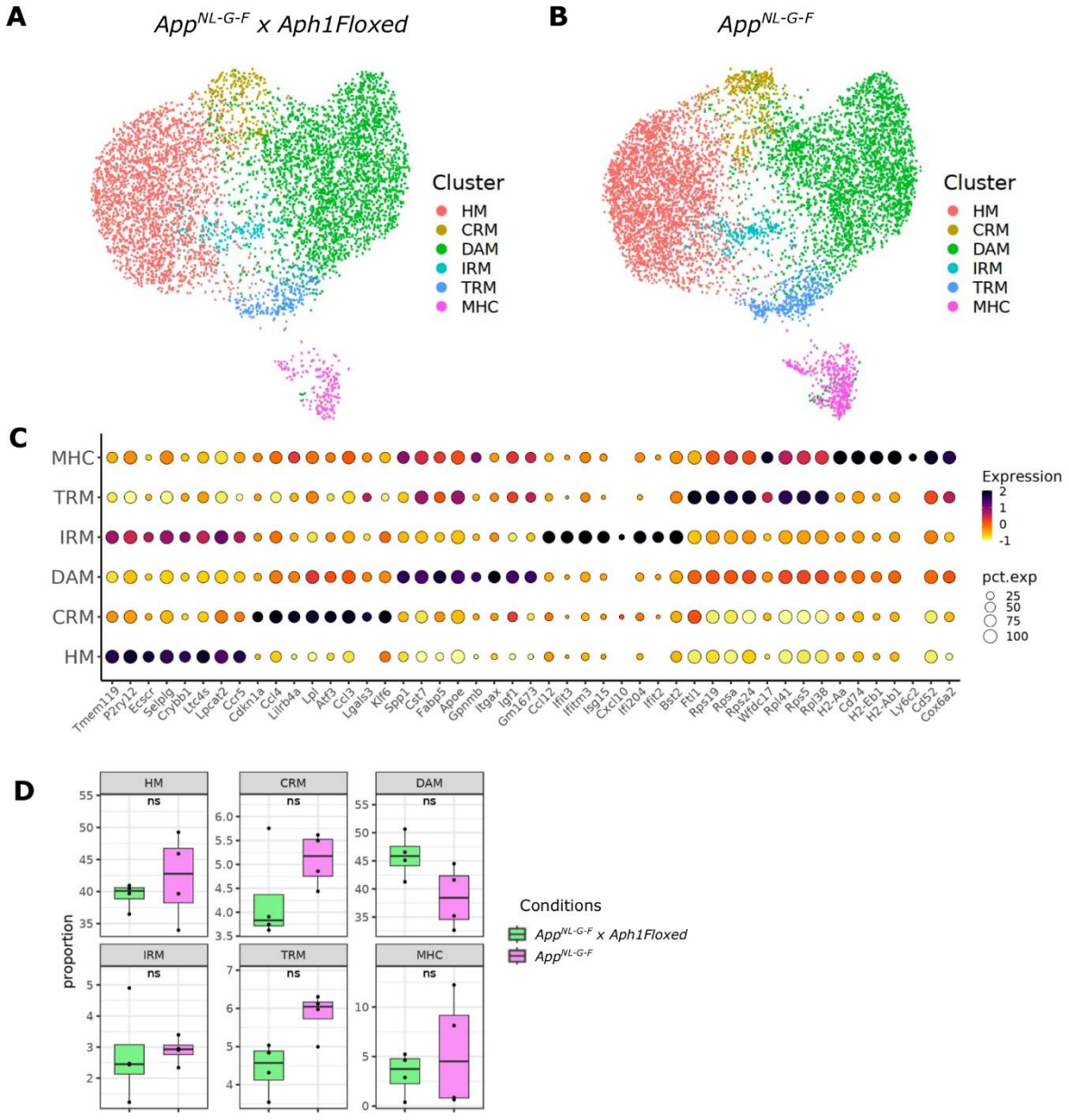


Figure S9. Comparison of microglia cell states between *App^{NL-G-F} x Aph1Floxed* (*App^{NL-G-F}-GS^{WT}*) mice and *App^{NL-G-F}* mice. A-B, UMAP plots showing 5,999 retained single mouse microglia from 12-month *App^{NL-G-F} x Aph1Floxed* (*App^{NL-G-F}-GS^{WT}*) mice (**A**) and 7,185 single mouse microglia from 12-month *App^{NL-G-F}* mice (**B**) after removal of cycling microglia, non-microglial and low-quality subpopulations. 6 clusters were unbiasedly identified using the Louvain algorithm. **C,** Top differentially expressed genes in each identified cluster (as shown in **A** and **B**). **D,** Box plots showing proportion of cells across all identified clusters in the different conditions. Statistical significance for each cluster was determined by multiple unpaired Student's t test corrected by Bonferroni method, n = 4 animals per condition. ns, not significant.

Chapter 5: General Discussion and Conclusions

Using the G-SECSI method to survey the membrane proteomes of H9 derived human microglia (H9MG) cells in the presence or absence of the γ-secretase inhibitor Semagacestat, we identify a remarkable large number of substrates (85), including 59 proteins hitherto unknown, that are processed by γ-secretase in steady state cell culture conditions. The only precedent study that tried to unbiasedly identify substrates by separating the CTF and FL proteins using conventional SDS-PAGE yielded 13 γ-secretase substrates in HELA cells.[82] Our method seems more precise and sensitive and brings home the message that even under normal cell culture conditions γ-secretase cleaves many substrates in parallel. Most are important signaling molecules, including tyrosine receptor kinases (AXL, CSF1R, EPHA2, EPHB2, EPHB3, MERTK), interleukin receptors (IL10RB, IL18R1, IL1RAP, IL6ST), tumor necrosis factor receptors (TNFRSF1A, TNFRSF1B, TNFRSF21), ITAM-receptors (GPNMB, FCGR2A, TYROBP), ITIM-receptors (CD300A, CD300IF, MILR1, LAIR1, PILRA) and so on (See Table S1-3). γ-Secretase activity thus appears in the center of a variety of crucial signaling pathways in microglia.

It is unexpected that so many substrates are processed by γ-secretase in parallel under, assumed, steady state conditions in cell culture. Indeed, γ-secretase cleavage is a highly regulated activity. Only a few substrates with natural short ectodomains can be cleaved directly,[77–80] while most need an activation step by another type of membrane anchored protease, for instance members of the “a disintegrin and metalloprotease” (ADAM) family.[308] This cleavage, which is also regulated, shortens the ectodomain of the candidate substrates so that they can be accommodated in the γ-secretase complex.[81] In addition, other proteins and lipids, for instance tetraspanin-enriched microdomains, regulate γ-secretase activity.[309] A more recent study demonstrated that interferon-induced transmembrane protein 3 (IFITM3) activates γ-secretase in the presence of inflammatory cytokines, which positively regulate Aβ generation.[310] Therefore, we hypothesize that γ-secretase serves as the converging point of many different upstream regulatory events, while the available γ-secretase substrate proteome reflects a series of cues present in the cell culture.

We analyzed the transcriptome of *in vitro* microglia in the presence and absence of the γ-secretase inhibitor Semagacestat to see how the inhibition of the processing of these proteins affects gene expression. The expression of 350 genes was altered (Figure

9H). We propose to extend the concept of “tonic signaling” to describe this effect on the expression of multiple genes in the absence of specific stimuli. The concept of “tonic signaling” was originally proposed in the field of lymphocyte biology and has been used to indicate the low-level constitutive signaling in resting B- and T-lymphocytes as a result of a dynamic equilibrium between positive and negative signals.[311–313]

We were surprised that the alteration in tonic signaling caused by γ-secretase inhibition did not initiate a dramatic shift in cell states, i.e. that the cells with γ-secretase deficiency do not cluster drastically differently in the UMAP plots (Figure 9E-F and J-K). Nevertheless, the tonic signaling defined as the change in gene expression brought on by blockage of γ-secretase is robust and remains discernible even in the background of a strong LPS-induced response (Figure 9H and M). Like the *in vitro* observations, genetic knockout of γ-secretase induced mild changes to the transcriptomic cell states of microglia in control mice (Figure 10). Nevertheless, again a consistent effect of γ-secretase inactivation on differential gene expression was observed with >900 genes altering their expression confirming that the enzyme regulates in a tonic way broadly gene expression. The observed lack of shift in cell states is somewhat puzzling. One possible explanation is that the differential gene expression induced by γ-secretase inhibition, despite encompassing hundreds of genes, may be not strong enough to drive affected cells into separate clusters. In agreement with this interpretation, the microglia showed a consistent upregulation of a group of genes (*e.g. Ctsl, Cd9, Timp2, Ctsb, Lyz2*) independent of their assigned cell states (Figure 10I). Interestingly, these genes are a subset of previously described DAM signatures.[144,145] Thus, our results suggest that normal γ-secretase activity promotes activating gene expression *in vitro* and homeostatic gene expression *in vivo*—the natural states of microglia in these two conditions.[314,315] We suggest that the main function of γ-secretase is the integration of a diverse array of extracellular signals provided by the cell’s environment, resulting in a basal signaling state onto which additional signals (via γ-secretase or other signaling mechanism) can be superimposed.

The altered expression of HM and DAM genes induced by γ-secretase deficiency in the *in vitro* (Figure 9) and *in vivo* (Figure 10) experiments made us wondering whether γ-secretase was involved in the regulation of microglia responses to amyloid pathology

in AD. We therefore generated a microglia specific γ-secretase knock out in the *App*$^{NL-G-F}$ mouse model. This experiment, in line with what we concluded above, demonstrated that γ-secretase deficiency mildly altered the microglia states in 3-month *App*$^{NL-G-F}$-*GS*^{iΔMG} mice, when amyloid pathology is mild, all the while inducing the same gene set that reflects dysregulated "tonic signaling" by γ-secretase as seen in the wild type condition (*Ctsl, Cd9, Timp2, Ctsb, Lyz2,* etc.). At 7 months however, the DAM response in *App*$^{NL-G-F}$-*GS*^{iΔMG} mice was severely attenuated compared to the control situation. Accordingly, γ-secretase deficient microglia showed abnormal phenotypic responses to the Aβ plaques in the brains of *App*$^{NL-G-F}$-*GS*^{iΔMG} mice (Figure 12H). Thus γ-secretase has a crucial role in the microglial transition from the homeostatic to the full DAM phenotype in AD. Apparently, in the context of the amyloid pathology, this effect is strong enough to affect the clustering of single cells into cell states.

The many subpopulations of microglia bearing distinct transcriptional signatures, i.e. HM, DAM, CRM, IRM, IAM and so on, have been described in AD,[144–146,307] demonstrating a high heterogeneity of microglia in the different conditions. However, what are the key regulators for the differentiation of this microglia diversity largely remains unclear. It is known that TREM2 is a crucial mediator for DAM formation in response to AD pathologies,[144,165] while other receptor proteins in the γ-secretase substrate proteome revealed in this study likely take part in the cell state regulation events as well. Using transcriptomic analyses, we show that this blockage induced by γ-secretase deficiency is not equivalent to the blockage previously observed in *Trem2*$^{-/-}$ *TgAD* mice reported by Keren-Shaul et al.[144] So, while it is likely that the blockage of γ-secretase cleavage on Trem2 contributes to the overall disturbance in the microglia, it is clear that other substrates also play a role in this phenomenon. The DAM phenotype is considered by some as a protective mechanism in AD.[148,316] Thus, indiscriminate inhibition of γ-secretase to lower Aβ production in AD will not only cause Notch signaling disturbances[27] but is also predicted to cause microglia dysfunction as demonstrated in this study. These may ultimately have contributed to the failure of the Semagacestat phase III clinical trial in 2013.[47,48]

The detailed mechanism by which γ-secretase regulates microglia state needs further investigations. It is known that γ-secretase has two physiological functions, including the degradation function by its "carboxypeptidase activity" and the signaling function

by its “ε-cleavage activity”. Here we speculate that γ-secretase deficiency might alter microglia biology by affecting both of these two γ-secretase physiological functions.

On the one hand, γ-secretase cleaves substrates into small fragments and releases them from the membrane for degradation and turnover in the cells.[317] When γ-secretase is inhibited, the increasing accumulation of CTFs on the membrane might cause alterations of microglia cell metabolism and hence might influence microglia states. It has been reported that the accumulation of β-CTF of APP induces Aβ-independent lysosomal-autophagic pathology in neurons,[319] while the accumulation of CTFs of other γ-secretase substrates might affect microglia as well. Moreover, the accumulated CTFs might competitively bind the adaptor proteins that are required for the signaling transduction by binding with the FL proteins. One functionally characterized example is TREM2, whose adaptor protein is TYROBP (DAP12).[162,167] It has been speculated that the TREM2-CTF accumulation interferes with TREM2 dependent signaling since TREM2-CTF still contains the motif for the electrostatic interaction with TYROBP.

On the other hand, γ-secretase ε-cleavage generates important intracellular signaling molecules, i.e. the released ICDs from the membrane.[55] One well-known example is γ-secretase mediated Notch signaling that plays a key role in cell fate decision.[27,321] Interestingly, we didn’t find the CTF accumulation of Notch in the Semagacestat treated H9MG in our study, suggesting that Notch signaling might be at a very low level in microglia and below the detection limit of our method. Another known example is SIRPa, whose ICD has been reported to be released by γ-secretase and functions as a pro-inflammatory intracellular molecule.[57] Therefore, we can deduce that the activating signaling through SIRPa-ICD is suppressed upon γ-secretase inhibition. Opposingly, LRP1-ICDs released by γ-secretase functions as an anti-inflammatory molecule,[56] and therefore γ-secretase inhibition might enhance cell activation. The “tonic signaling” function that we proposed here represents the integrated response on the activating and inhibiting signals regulated by γ-secretase in the cell in homeostatic conditions. Therefore, γ-secretase deficiency causes mild effects on microglia in physiological conditions, while γ-secretase deficiency causes profound effects on microglia in pathological conditions in which the activating signals overcome the original signaling balance. This is conceptually reminiscent to an action potential which is released only when the sum of the incoming signals surpass a certain threshold

intensity. So far all these functionally characterized examples are previously known γ-secretase substrates which account only for a small proportion of the microglia-specific γ-secretase substrate repertoires. Therefore, functional characterization of the many novel microglia-specific γ-secretase substrates as reported here is needed in the future to provide novel insights of γ-secretase activity in microglia cell biology.

Taken together, we investigate here in a systemic way the microglia-specific γ-secretase substrate proteome and provide evidence that γ-secretase regulates what we propose to call “tonic signaling” in microglia. The subset of proteins cleaved by γ-secretase activity at any moment reflects the cell state (which genes are expressed) and the cell environment (in this study: *in vitro* culture conditions or *in vivo* brain environment). This view substantially modifies the hypothesis that γ-secretase is merely responsible for clearing membranes from transmembrane domains of proteins (as proposed by the ‘proteasome of the membrane’ hypothesis)[59] and puts γ-secretase, at least in parallel to its degradation role, firmly as a central integrator of external cues into a consistent intracellular cell signal.

Limitations of the study

An important part of the γ-secretase cleavage occurring at any moment in time is regulated by the alpha-, beta- and potentially other proteolytic activities that process the ectodomains of the substrates.[318] These ectodomain shedding proteases contribute to the available protein substrate spectrum for γ-secretase processing depending on biological conditions or cell types and are an important part of the regulated intramembrane proteolysis cascade. This aspect was not investigated here. Although our study provides a powerful tool and a conceptual framework to investigate the role of γ-secretase herein, further studies are required to investigate the downstream signaling functions and how dysfunction in different cell types affects disease conditions. We have used for our *in vitro* experiments microglia derived from human embryonic stem cells. Microglia are very sensitive to culture conditions and therefore might only reflect partially *in vivo* microglia. In the *in vivo* studies we have focused on mouse microglia. Their response to amyloid plaques is different from the response of human microglia.

Perspectives

After more than a century since Alois Alzheimer first described AD, the etiology of this devastating disease remains still elusive.[320] In familial Alzheimer's disease (FAD), *PSEN* mutations alter the carboxypeptidase activity of γ-secretase and shift Aβ38/Aβ40 production to longer and aggregation-prone Aβ42/Aβ43.[69] However, it has been not fully investigated whether such *PSEN* mutations also affect the processing of other substrates besides APP and whether such alterations contribute to FAD beyond Aβ production. Indeed, while heterozygous carriers of *PSEN* mutations present with dominantly inherited early onset AD and display all cardinal features of sporadic AD, some patients present additional atypical clinical phenotypes such as myoclonus, seizures, pyramidal and extrapyramidal signs and atypical neuropathology, such as cotton wool amyloid plaques.[322,323] Furthermore, *PSEN1* mutation carriers present with a very early age of onset of AD, (mean age of onset: 43.6+/-7.2 years), which, in general, is 7 years earlier than patients with mutations in the *APP* gene.[322] Given our recent findings in the current project that loss of function of γ-secretase in microglia profoundly affects their capacity to respond to amyloid plaques and the clinical evidences that are described above, we hypothesize that, while the *PSEN* mutations cause aberrant proteolysis of APP in neurons, astroglia, and oligodendrocytes (the three major cell types producing Aβ in the brain), they also affect the cellular (DAM) response of microglia by affecting other substrates and therefore accelerate the pathology in AD. As *APP* is hardly expressed in microglia, APP misprocessing effects in microglia do not contribute to AD pathology in *APP* mutation carriers. Abundant evidence (including in house unpublished data) indicate however very strongly that microglia function indeed affects amyloid plaque seeding and condensation.

The key experiment to test this "dual-hits hypothesis of FAD" is the direct comparison of the γ-secretase substrate proteomes of microglia that express *PSEN*-mutant or *PSEN*-wild-type γ-secretases. Our G-SECSI method that surveys the whole γ-secretase substrate proteome under a specific cellular context provides a powerful solution to this end. Using G-SECSI, future work could identify the substrate proteins that are differentially cleaved by PSEN mutant γ-secretases by identifying and comparatively analyzing the γ-secretase substrate proteomes of human microglia-like cells (iMGLs) differentiated from FAD patient-derived PSEN mutant iPSC lines and their isogenic control lines.

Interestingly, pharmaceutic companies have developed over the last years several γ-secretase allosteric modulators (GAMs), which are thought to act in a reverse way of the *PSEN* mutations.[324] Unlike the non-selective γ-secretase inhibitors (GSIs) that directly bind the catalytic site of PSEN and indiscriminately block γ-secretase cleavage of all substrates, imidazole-based GAMs bind an allosteric site of PSEN (at an extracellular site, but not the intramembranous catalytic site), which enhances Aβ cleavage processivity by stabilizing the enzyme-substrate complex.[35] This leads to the generation of shorter Aβ peptides but no block of the initial ε-cleavage of substrates which releases the intracellular domains and is responsible for γ-secretase signaling functions.

Recently, Hofmann-La Roche has announced that they are starting phase II clinical trials with such a compound.[325] We believe that the novel evidence and the renewed interest from pharma in developing this type of medication, is a sufficient motivation to deeper investigate the critical question whether these novel drugs are indeed orders of magnitude safer than the classical GSIs used before. The G-SECSI protocol that we developed provides us with an unique tool to address the critical question of the mechanistic safety of the GAMs. For example, future work could examine whether the tested GAM candidate caused the accumulation of certain γ-secretase substrates or enhances the cleavage of certain γ-secretase substrates. Then functional characterization of the identified substrate needs to be performed to study the consequence of this alteration caused by the GAM candidate.

Scientific Acknowledgments, Personal Contributions and Conflict of Interests

Scientific Acknowledgments

This project received funding from the European Research Council (ERC) under the European Union's Horizon 2020 Research and Innovation Programme (grant agreement no. ERC-834682 CELLPHASE_AD). This work was also supported by UK Dementia Research Institute, the Flanders Institute for Biotechnology (VIB vzw), a Methusalem grant from KU Leuven and the Flemish Government, the Fonds voor Wetenschappelijk Onderzoek, KU Leuven, The Queen Elisabeth Medical Foundation for Neurosciences, the Opening the Future campaign of the Leuven Universitair Fonds, The Belgian Alzheimer Research Foundation (SAO-FRA) and the Alzheimer's Association USA. B.D.S. holds the Bax-Vanluffelen Chair for Alzheimer's Disease. B.D.S. receives funding from UKRI and the Medical Research Council (MR/Y014847/1) via the Dementia Research Institute. R.M. recieves funding from European Research Council (ERC) under the European Union's Horizon 2020 Research and Innovation Programme (project no. 101041867 - XenoMicrogliaAD), Fonds voor Wetenschappelijk Onderzoek (grants no. G0C9219N, G056022N and G0K9422N), BrightFocus Foundation (A2021034S), SAO-FRA (grant no. 2021/0021) and the University of Antwerp (BOF-TOP 2022-2025). We thank Véronique Hendrickx and Jonas Verwaeren for the animal husbandry. We thank Dr. Rajeshwar Narlawar, Dr. Francois Bischoff and Dr. Harrie M. Gijsen in Jassen Pharmaceuticals for the medicinal chemistry. P.H. is recipient of a PhD fellowship from China Scholarship Council (No. 201806170081). N.F. is recipient of a PhD fellowship from Fonds voor Wetenschappelijk Onderzoek (No. 1139520N). A.M.M. was supported by a fellowship from the FWO - Marie Skłodowska-Curie Actions - Seal of Excellence Postdoctoral Fellowship (No. 12ZX621N). Schematic figures in this article are created with BioRender.com.

Author Contributions

P.H. and B.D.S. conceived and designed the study with advices of L.S., A.M.M., M.F. and R.M.. P.H. and B.D.S. wrote the first versions of the manuscript. P.H. performed all experiments with help from L.S., A.M.M., L.W., D.T., S.B., R.M. and analyzed proteomics data with advices from L.S., M.F., R.M., A.J.M.H. and B.D.S.. M.Z. performed GO analysis and KEGG analysis of the proteomics data and analyzed all

single-cell transcriptomics data with advices from P.H., A.M.M., R.M., M.F. and B.D.S.. N.F. generated Figure 8 with advices from P.H.. L.W. prepared cDNA libraries for sequencing with assistance from S.P.. T.T. provided tissues for human primary microglia isolation. L.S. generated *Aph1a*$^{fl/fl}$*b*$^{-/-}$*c*$^{fl/fl}$ mouse strain (JAX stock #030985).[287] A.J.M.H. supervised all the MS sequencing related work and processed the raw proteomics data. L.S., R.M. and B.D.S. supervised all the experiments. All authors discussed the results and commented on the manuscript.

Declaration Of Interests

B.D.S. has been a consultant for Eli Lilly, Biogen, Janssen Pharmaceutica, Eisai, AbbVie and other companies and is now consultant to Eisai, Remynd and Muna therapeutics. B.D.S is a scientific founder of Augustine Therapeutics and a scientific founder and stockholder of Muna Therapeutics. R.M. has scientific collaborations with Alector, Nodthera and Alchemab, and has been consultant for Sanofi.

Supplemental table titles and legends

The supplemental tables can be found in the publication[326]: https://doi.org/10.1016/j.molcel.2023.10.029.

Table S1. Full list of identified γ-secretase substrates in H9MG related to Figure 7. The table displays 85 γ-secretase substrates identified in H9MG. Proteins listed in this table are single-pass type I/III membrane proteins. The following information for each protein are indicated accordingly: Uniprot ID, Protein name, Foldchange of CTF accumulation in Semagacestat vs. Control, P value, Protein type,if novel and if natural short ECD.

Table S2. Gene ontogeny enrichment analysis of the 85 identified γ-secretase substrates related to Figure 7. Gene ontogeny analysis showing the substrate-most-enriched biological processes (sheet 1) and molecular functions (sheet 2). Top 50 most significantly enriched terms of each category are grouped semantically into parent terms. See Method. 9 for details of the analysis.

Table S3. KEGG pathway enrichment analysis of the 85 identified γ-secretase substrates related to Figure 7. KEGG pathway analysis showing the substrate-most-enriched pathways. Top 50 most significantly enriched terms are grouped semantically into parent terms. See Method. 9 for details of the analysis.

Table S6. Size and location of fragments of known substrates related to Figure 6. Size and location information of fragments of known substrates used for the reference plot exemplified in Figure 1D.

Table S7. Sample metadata for single-cell experiments related to Figure 9-12.

References

1. Glenner, G.G., and Wong, C.W. (1984). Alzheimer's disease: Initial report of the purification and characterization of a novel cerebrovascular amyloid protein. Biochem. Biophys. Res. Commun. 10.1016/S0006-291X(84)80190-4.

2. Glenner, G.G., and Wong, C.W. (1984). Alzheimer's disease and Down's syndrome: Sharing of a unique cerebrovascular amyloid fibril protein. Biochem. Biophys. Res. Commun. 10.1016/0006-291X(84)91209-9.

3. Masters, C.L., Simms, G., Weinman, N.A., Multhaup, G., McDonald, B.L., and Beyreuther, K. (1985). Amyloid plaque core protein in Alzheimer disease and Down syndrome. Proc. Natl. Acad. Sci. U. S. A. 10.1073/pnas.82.12.4245.

4. Kang, J., Lemaire, H.G., Unterbeck, A., Salbaum, J.M., Masters, C.L., Grzeschik, K.H., Multhaup, G., Beyreuther, K., and Müller-Hill, B. (1987). The precursor of Alzheimer's disease amyloid A4 protein resembles a cell-surface receptor. Nature. 10.1038/325733a0.

5. Tanzi, R.E., Gusella, J.F., Watkins, P.C., Bruns, G.A.P., St. George-Hyslop, P., Van Keuren, M.L., Patterson, D., Pagan, S., Kurnit, D.M., and Neve, R.L. (1987). Amyloid β protein gene: CDNA, mRNA distribution, and genetic linkage near the Alzheimer locus. Science (80-.). 10.1126/science.2949367.

6. Goldgaber, D., Lerman, M.I., McBride, O.W., Saffiotti, U., and Gajdusek, D.C. (1987). Characterization and chromosomal localization of a cDNA encoding brain amyloid of Alzheimer's disease. Science (80-.). 10.1126/science.3810169.

7. St. George-Hyslop, P.H., Tanzi, R.E., Polinsky, R.J., Haines, J.L., Nee, L., Watkins, P.C., Myers, R.H., Feldman, R.G., Pollen, D., Drachman, D., et al. (1987). The genetic defect causing familial Alzheimer's disease maps on chromosome 21. Science (80-.). 10.1126/science.2880399.

8. Murrell, J., Farlow, M., Ghetti, B., and Benson, M.D. (1991). A mutation in the amyloid precursor protein associated with hereditary Alzheimer's disease. Science (80-.). 10.1126/science.1925564.

9. Goate, A., Chartier-Harlin, M.C., Mullan, M., Brown, J., Crawford, F., Fidani, L., Giuffra, L., Haynes, A., Irving, N., James, L., et al. (1991). Segregation of a missense mutation in the amyloid precursor protein gene with familial Alzheimer's disease. Nature. 10.1038/349704a0.

10. Chartier-Harlin, M.C., Crawford, F., Houlden, H., Warren, A., Hughes, D., Fidani, L., Goate, A., Rossor, M., Roques, P., Hardy, J., et al. (1991). Early-onset Alzheimer's disease caused by mutations at codon 717 of the β-amyloid precursor protein gene. Nature. 10.1038/353844a0.

11. Haass, C., and Selkoe, D.J. (1993). Cellular processing of β-amyloid precursor protein and the genesis of amyloid β-peptide. Cell. 10.1016/0092-8674(93)90312-E.

12. Selkoe, D.J. (1994). Cell biology of the amyloid β-protein precursor and the mechanism of Alzheimer's disease. Annu. Rev. Cell Biol. 10.1146/annurev.cb.10.110194.002105.

13. Simons, M., De Strooper, B., Multhaup, G., Tienari, P.J., Dotti, C.G., and Beyreuther, K. (1996). Amyloidogenic processing of the human amyloid precursor protein in primary cultures of rat hippocampal neurons. J. Neurosci. 10.1523/jneurosci.16-03-00899.1996.

14. Mills, J., and Reiner, P.B. (1999). Regulation of amyloid precursor protein cleavage. J. Neurochem. 10.1046/j.1471-4159.1999.0720443.x.

15. Rawson, R.B., Zelenski, N.G., Nijhawan, D., Ye, J., Sakai, J., Hasan, M.T., Chang, T.Y., Brown, M.S., and Goldstein, J.L. (1997). Complementation cloning of S2P, a gene encoding a putative metalloprotease required for intramembrane cleavage of SREBPs. Mol. Cell. 10.1016/S1097-2765(00)80006-4.

16. Duncan, E.A., Davé, U.P., Sakai, J., Goldstein, J.L., and Brown, M.S. (1998). Second-site cleavage in sterol regulatory element-binding protein occurs at transmembrane junction as determined by cysteine panning. J. Biol. Chem. 10.1074/jbc.273.28.17801.

17. Sherrington, R., Rogaev, E.I., Liang, Y., Rogaeva, E.A., Levesque, G., Ikeda, M., Chi, H., Lin, C., Li, G., Holman, K., et al. (1995). Cloning of a gene bearing missense mutations in early-onset familial Alzheimer's disease. Nature. 10.1038/375754a0.

18. Sherrington, R., Froelich, S., Sorbi, S., Campion, D., Chi, H., Rogaeva, E.A., Levesque, G., Rogaev, E.I., Lin, C., Liang, Y., et al. (1996). Alzheimer's disease associated with mutations in presenilin 2 is rare and variably penetrant. Hum. Mol. Genet. 10.1093/hmg/5.7.985.

19. Rogaev, E.I., Sherrington, R., Rogaeva, E.A., Levesque, G., Ikeda, M., Liang, Y., Chi, H., Lin, C., Holman, K., Tsuda, T., et al. (1995). Familial Alzheimer's disease in kindreds with missense mutations in a gene on chromosome 1 related to the Alzheimer's disease type 3 gene. Nature. 10.1038/376775a0.

20. Levy-Lahad, E., Wijsman, E.M., Nemens, E., Anderson, L., Goddard, K.A., Weber, J.L., Bird, T.D., and Schellenberg, G.D. (1995). A familial Alzheimer's disease locus on chromosome 1. Science *269*, 970–973. 10.1126/science.7638621.

21. Levy-Lahad, E., Wasco, W., Poorkaj, P., Romano, D.M., Oshima, J., Pettingell, W.H., Yu, C.E., Jondro, P.D., Schmidt, S.D., Wang, K., et al. (1995). Candidate gene for the chromosome 1 familial Alzheimer's disease locus. Science (80-.). 10.1126/science.7638622.

22. Scheuner, D., Eckman, C., Jensen, M., Song, X., Citron, M., Suzuki, N., Bird, T.D., Hardy, J., Hutton, M., Kukull, W., et al. (1996). Secreted amyloid β-protein similar to that in the senile plaques of Alzheimer's disease is increased in vivo by the presenilin 1 and 2 and APP mutations linked to familial Alzheimer's disease. Nat. Med. 10.1038/nm0896-864.

23. Borchelt, D.R., Thinakaran, G., Eckman, C.B., Lee, M.K., Davenport, F., Ratovitsky, T., Prada, C.M., Kim, G., Seekins, S., Yager, D., et al. (1996). Familial Alzheimer's disease-linked presenilin 1 variants elevate Abeta1-42/1-40 ratio in vitro and in vivo. Neuron *17*, 1005–1013. 10.1016/s0896-6273(00)80230-5.

24. De Strooper, B., Saftig, P., Craessaerts, K., Vanderstichele, H., Guhde, G., Annaert, W., Von Figura, K., and Van Leuven, F. (1998). Deficiency of presenilin-1 inhibits the normal cleavage of amyloid precursor protein. Nature. 10.1038/34910.

25. Herreman, A., Serneels, L., Annaert, W., Collen, D., Schoonjans, L., and De Strooper, B. (2000). Total inactivation of γ-secretase activity in presenilin-deficient embryonic stem cells. Nat. Cell Biol. 10.1038/35017105.

26. Wolfe, M.S., Xia, W., Ostaszewski, B.L., Diehl, T.S., Kimberly, W.T., and Selkoe, D.J. (1999). Two transmembrane aspartates in presenilin-1 required for presenilin endoproteolysis and γ-secretase activity. Nature. 10.1038/19077.

27. De Strooper, B., Annaert, W., Cupers, P., Saftig, P., Craessaerts, K., Mumm, J.S., Schroeter, E.H., Schrijvers, V., Wolfe, M.S., Ray, W.J., et al. (1999). A presenilin-1-

dependent γ-secretase-like protease mediates release of notch intracellular domain. Nature. 10.1038/19083.

28. Struhl, G., and Greenwald, I. (1999). Presenilin is required for activity and nuclear access of notch in drosophila. Nature. 10.1038/19091.

29. Esler, W.P., Kimberly, W.T., Ostaszewski, B.L., Diehl, T.S., Moore, C.L., Tsai, J.Y., Rahmati, T., Xia, W., Selkoe, D.J., and Wolfe, M.S. (2000). Transition-state analogue inhibitors of γ-secretase bind directly to presenilin-1. Nat. Cell Biol. 10.1038/35017062.

30. Li, Y.M., Xu, M., Lai, M.T., Huang, Q., Castro, J.L., DiMuzlo-Mower, J., Harrison, T., Lellis, C., Nadin, A., Neduvelli, J.G., et al. (2000). Photoactivated γ-secretase inhibitors directed to the active site covalently label presenilin 1. Nature. 10.1038/35015085.

31. Yu, G., Nishimura, M., Arawaka, S., Levitan, D., Zhang, L., Tandon, A., Song, Y.Q., Rogaeva, E., Chen, F., Kawarai, T., et al. (2000). Nicastrin modulates presenilin-mediated notch/glp-1 signal transduction and βAPP processing. Nature. 10.1038/35024009.

32. Goutte, C., Tsunozaki, M., Hale, V.A., and Priess, J.R. (2002). APH-1 is a multipass membrane protein essential for the Notch signaling pathway in Caenorhabditis elegans embryos. Proc. Natl. Acad. Sci. U. S. A. 10.1073/pnas.022523499.

33. Francis, R., McGrath, G., Zhang, J., and Ruddy, D. (2002). aph-1 and pen-2 are required for Notch pathway signaling, gamma-secretase cleavage of betaAPP, and presenilin protein accumulation. Dev Cell.

34. De Strooper, B. (2003). Aph-1, Pen-2, and Nicastrin with Presenilin generate an active γ-Secretase complex. Neuron. 10.1016/S0896-6273(03)00205-8.

35. Yang, G., Zhou, R., Guo, X., Yan, C., Lei, J., and Shi, Y. (2021). Structural basis of γ-secretase inhibition and modulation by small molecule drugs. Cell. 10.1016/j.cell.2020.11.049.

36. Sato, T., Diehl, T.S., Narayanan, S., Funamoto, S., Ihara, Y., De Strooper, B., Steiner, H., Haass, C., and Wolfe, M.S. (2007). Active γ-secretase complexes contain only one of each component. J. Biol. Chem. 10.1074/jbc.M705248200.

37. Hébert, S.S., Serneels, L., Dejaegere, T., Horré, K., Dabrowski, M., Baert, V., Annaert, W., Hartmann, D., and De Strooper, B. (2004). Coordinated and widespread expression of γ-secretase in vivo: Evidence for size and molecular heterogeneity. Neurobiol. Dis. 10.1016/j.nbd.2004.08.002.

38. Shirotani, K., Edbauer, D., Prokop, S., Haass, C., and Steiner, H. (2004). Identification of distinct γ-secretase complexes with different APH-1 variants. J. Biol. Chem. 10.1074/jbc.M405768200.

39. Clark, R.F., Hutton, M., Fuldner, M., Froelich, S., Karran, E., Talbot, C., Crook, R., Lendon, C., Prihar, G., He, C., et al. (1995). The structure of the presenilin 1 (S182) gene and identification of six novel mutations in early onset AD families. Nat. Genet. 10.1038/ng1095-219.

40. Anwar, R., Moynihan, T.P., Ardley, H., Brindle, N., Coletta, P.L., Cairns, N., Markham, A.F., and Robinson, P.A. (1996). Molecular analysis of the presenilin 1 (S182) gene in “sporadic” cases of Alzheimer’s disease: Identification and characterisation of unusual splice variants. J. Neurochem. 10.1046/j.1471-4159.1996.66041774.x.

41. Bresciani, L.G., Walsh, D.T., Gentleman, S.M., and Jen, L.S. (2002). Developmental regulation and possible alternative cleavage of presenilin 1 in the rat retina. Mol. Cell.

Neurosci. 10.1006/mcne.2002.1169.

42. Evin, G., Smith, M.J., Tziotis, A., McLean, C., Canterford, L., Sharples, R.A., Cappai, R., Weidemann, A., Beyreuther, K., Cotton, R.G.H., et al. (2002). Alternative transcripts of presenilin-1 associated with frontotemporal dementia. Neuroreport. 10.1097/00001756-200205070-00036.

43. Morihara, T., Katayama, T., Sato, N., Yoneda, T., Manabe, T., Hitomi, J., Abe, H., Imaizumi, K., and Tohyama, M. (2000). Absence of endoproteolysis but no effects on amyloid β production by alternative splicing forms of presenilin-1, which lack exon 8 and replace D257A. Mol. Brain Res. 10.1016/S0169-328X(00)00229-1.

44. Lee, S.F., Shah, S., Li, H., Yu, C., Han, W., and Yu, G. (2002). Mammalian APH-1 interacts with presenilin and nicastrin and is required for intramembrane proteolysis of amyloid-β precursor protein and Notch. J. Biol. Chem. 10.1074/jbc.M208164200.

45. Gu, Y., Chen, F., Sanjo, N., Kawarai, T., Hasegawa, H., Duthie, M., Li, W., Ruan, X., Luthra, A., Mount, H.T.J., et al. (2003). APH-1 interacts with mature and immature forms of presenilins and nicastrin and may play a role in maturation of presenilin·nicastrin complexes. J. Biol. Chem. 10.1074/jbc.M209499200.

46. Habets, R.A., De Bock, C.E., Serneels, L., Lodewijckx, I., Verbeke, D., Nittner, D., Narlawar, R., Demeyer, S., Dooley, J., Liston, A., et al. (2019). Safe targeting of T cell acute lymphoblastic leukemia by pathology-specific NOTCH inhibition. Sci. Transl. Med. 10.1126/scitranslmed.aau6246.

47. Doody, R.S., Raman, R., Farlow, M., Iwatsubo, T., Vellas, B., Joffe, S., Kieburtz, K., He, F., Sun, X., Thomas, R.G., et al. (2013). A phase 3 trial of semagacestat for treatment of Alzheimer's disease. N. Engl. J. Med. 10.1056/NEJMoa1210951.

48. De Strooper, B. (2014). Lessons from a failed γ-secretase Alzheimer trial. Cell. 10.1016/j.cell.2014.10.016.

49. Sannerud, R., Esselens, C., Ejsmont, P., Mattera, R., Rochin, L., Tharkeshwar, A.K., De Baets, G., De Wever, V., Habets, R., Baert, V., et al. (2016). Restricted Location of PSEN2/γ-Secretase Determines Substrate Specificity and Generates an Intracellular Aβ Pool. Cell. 10.1016/j.cell.2016.05.020.

50. Guo, X., Wang, Y., Zhou, J., Jin, C., Wang, J., Jia, B., Jing, D., Yan, C., Lei, J., Zhou, R., et al. (2022). Molecular basis for isoform-selective inhibition of presenilin-1 by MRK-560. Nat. Commun. 10.1038/s41467-022-33817-5.

51. Borgegård, T., Gustavsson, S., Nilsson, C., Parpal, S., Klintenberg, R., Berg, A.L., Rosqvist, S., Serneels, L., Svensson, S., Olsson, F., et al. (2012). Alzheimer's disease: Presenilin 2-sparing γ-secretase inhibition is a tolerable Aβ peptide-lowering strategy. J. Neurosci. 10.1523/JNEUROSCI.1451-12.2012.

52. Serneels, L., Van Biervliet, J., Craessaerts, K., Dejaegere, T., Horré, K., Van Houtvin, T., Esselmann, H., Paul, S., Schäfer, M.K., Berezovska, O., et al. (2009). γ-Secretase heterogeneity in the aph1 subunit: Relevance for alzheimer's disease. Science (80-.). 10.1126/science.1171176.

53. Serneels, L., Narlawar, R., Perez-Benito, L., Municoy, M., Guallar, V., T'Syen, D., Dewilde, M., Bischoff, F., Fraiponts, E., Tresadern, G., et al. (2023). Selective inhibitors of the PSEN1–gamma-secretase complex. J. Biol. Chem. 10.1016/j.jbc.2023.104794.

54. Güner, G., and Lichtenthaler, S.F. (2020). The substrate repertoire of γ-secretase/presenilin. Semin. Cell Dev. Biol. *105*, 27–42. 10.1016/j.semcdb.2020.05.019.

55. De Strooper, B., and Annaert, W. (2010). Novel research horizons for presenilins and γ-secretases in cell biology and disease. Annu. Rev. Cell Dev. Biol. 10.1146/annurev-cellbio-100109-104117.

56. Zurhove, K., Nakajima, C., Herz, J., Bock, H.H., and May, P. (2008). γ-secretase limits the inflammatory response through the processing of LRP1. Sci. Signal. *1*, 1–13. 10.1126/scisignal.1164263.

57. Londino, J.D., Gulick, D., Isenberg, J.S., and Mallampalli, R.K. (2015). Cleavage of signal regulatory protein α (sirpα) enhances inflammatory signaling. J. Biol. Chem. 10.1074/jbc.M115.682914.

58. Brown, M.S., Ye, J., Rawson, R.B., and Goldstein, J.L. (2000). Regulated intramembrane proteolysis: A control mechanism conserved from bacteria to humans. Cell. 10.1016/S0092-8674(00)80675-3.

59. Kopan, R., and Ilagan, M.X.G. (2004). γ-Secretase: Proteasome of the membrane? Nat. Rev. Mol. Cell Biol. 10.1038/nrm1406.

60. Takami, M., Nagashima, Y., Sano, Y., Ishihara, S., Morishima-Kawashima, M., Funamoto, S., and Ihara, Y. (2009). γ-Secretase: Successive tripeptide and tetrapeptide release from the transmembrane domain of β-carboxyl terminal fragment. J. Neurosci. 10.1523/JNEUROSCI.2362-09.2009.

61. Qi-Takahara, Y., Morishima-Kawashima, M., Tanimura, Y., Dolios, G., Hirotani, N., Horikoshi, Y., Kametani, F., Maeda, M., Saido, T.C., Wang, R., et al. (2005). Longer forms of amyloid β protein: Implications for the mechanism of intramembrane cleavage by γ-secretase. J. Neurosci. 10.1523/JNEUROSCI.1575-04.2005.

62. Weidemann, A., Eggert, S., Reinhard, F.B.M., Vogel, M., Paliga, K., Baier, G., Masters, C.L., Beyreuther, K., and Evin, G. (2002). A novel ε-cleavage within the transmembrane domain of the Alzheimer amyloid precursor protein demonstrates homology with notch processing. Biochemistry. 10.1021/bi015794o.

63. Petit, D., Fernández, S.G., Zoltowska, K.M., Enzlein, T., Ryan, N.S., O'Connor, A., Szaruga, M., Hill, E., Vandenberghe, R., Fox, N.C., et al. (2022). Aβ profiles generated by Alzheimer's disease causing PSEN1 variants determine the pathogenicity of the mutation and predict age at disease onset. Mol. Psychiatry. 10.1038/s41380-022-01518-6.

64. Saito, T., Suemoto, T., Brouwers, N., Sleegers, K., Funamoto, S., Mihira, N., Matsuba, Y., Yamada, K., Nilsson, P., Takano, J., et al. (2011). Potent amyloidogenicity and pathogenicity of Aβ 243. Nat. Neurosci. 10.1038/nn.2858.

65. Devkota, S., Williams, T.D., and Wolfe, M.S. (2021). Familial Alzheimer s disease mutations in amyloid protein precursor alter proteolysis by γ-secretase to increase amyloid β-peptides of ≥45 residues. J. Biol. Chem. 10.1016/j.jbc.2021.100281.

66. Duff, K., Eckman, C., Zehr, C., Yu, X., Prada, C.M., Perez-Tur, J., Hutton, M., Buee, L., Harigaya, Y., Yager, D., et al. (1996). Increased amyloid-β42(43) in brains of mice expressing mutant presenilin 1. Nature. 10.1038/383710a0.

67. Karran, E., Mercken, M., and Strooper, B. De (2011). The amyloid cascade hypothesis for Alzheimer's disease: An appraisal for the development of therapeutics. Nat. Rev. Drug Discov. 10.1038/nrd3505.

68. Lichtenthaler, S.F., Haass, C., and Steiner, H. (2011). Regulated intramembrane proteolysis - Lessons from amyloid precursor protein processing. J. Neurochem. 10.1111/j.1471-4159.2011.07248.x.

69. Szaruga, M., Munteanu, B., Lismont, S., Veugelen, S., Horré, K., Mercken, M., Saido, T.C., Ryan, N.S., De Vos, T., Savvides, S.N., et al. (2017). Alzheimer's-Causing Mutations Shift Aβ Length by Destabilizing γ-Secretase-Aβn Interactions. Cell. 10.1016/j.cell.2017.07.004.

70. Veugelen, S., Saito, T., Saido, T.C., Chávez-Gutiérrez, L., and De Strooper, B. (2016). Familial Alzheimer's Disease Mutations in Presenilin Generate Amyloidogenic Aβ Peptide Seeds. Neuron. 10.1016/j.neuron.2016.03.010.

71. Reiss, K., and Saftig, P. (2009). The "A Disintegrin And Metalloprotease" (ADAM) family of sheddases: Physiological and cellular functions. Semin. Cell Dev. Biol. 10.1016/j.semcdb.2008.11.002.

72. Bai, G., and Pfaff, S.L. (2011). Protease Regulation: The Yin and Yang of Neural Development and Disease. Neuron. 10.1016/j.neuron.2011.09.012.

73. Kuhn, P.H., Koroniak, K., Hogl, S., Colombo, A., Zeitschel, U., Willem, M., Volbracht, C., Schepers, U., Imhof, A., Hoffmeister, A., et al. (2012). Secretome protein enrichment identifies physiological BACE1 protease substrates in neurons. EMBO J. 10.1038/emboj.2012.173.

74. Serdaroglu, A., Müller, S.A., Schepers, U., Bräse, S., Weichert, W., Lichtenthaler, S.F., and Kuhn, P.H. (2017). An optimised version of the secretome protein enrichment with click sugars (SPECS) method leads to enhanced coverage of the secretome. Proteomics. 10.1002/pmic.201600423.

75. Kuhn, P.H., Voss, M., Haug-Kröper, M., Schröder, B., Scheperse, U., Bräse, S., Haass, C., Lichtenthaler, S.F., and Fluhrer, R. (2015). Secretome analysis identifies novel signal peptide peptidase-like 3 (Sppl3) substrates and reveals a role of Sppl3 in multiple golgi glycosylation pathways. Mol. Cell. Proteomics. 10.1074/mcp.M115.048298.

76. Kuhn, P.-H., Colombo, A.V., Schusser, B., Dreymueller, D., Wetzel, S., Schepers, U., Herber, J., Ludwig, A., Kremmer, E., Montag, D., et al. (2016). Systematic substrate identification indicates a central role for the metalloprotease ADAM10 in axon targeting and synapse function. Elife. 10.7554/elife.12748.

77. Laurent, S.A., Hoffmann, F.S., Kuhn, P.H., Cheng, Q., Chu, Y., Schmidt-Supprian, M., Hauck, S.M., Schuh, E., Krumbholz, M., Rübsamen, H., et al. (2015). γ-secretase directly sheds the survival receptor BCMA from plasma cells. Nat. Commun. 10.1038/ncomms8333.

78. Gowrishankar, K., Zeidler, M.G., and Vincenz, C. (2004). Release of a membrane-bound death domain by γ-secretase processing of the p75NTR homolog NRADD. J. Cell Sci. 10.1242/jcs.01263.

79. Vevea, J.D., Kusick, G.F., Courtney, K.C., Chen, E., Watanabe, S., and Chapman, E.R. (2021). Synaptotagmin 7 is targeted to the axonal plasma membrane through g-secretase processing to promote synaptic vesicle docking in mouse hippocampal neurons. Elife. 10.7554/eLife.67261.

80. Güner, G., Aßfalg, M., Zhao, K., Dreyer, T., Lahiri, S., Lo, Y., Slivinschi, B.I., Imhof, A., Jocher, G., Strohm, L., et al. (2022). Proteolytically generated soluble Tweak Receptor Fn14 is a blood biomarker for γ-secretase activity. EMBO Mol. Med. 10.15252/emmm.202216084.

81. Struhl, G., and Adachi, A. (2000). Requirements for Presenilin-dependent cleavage of notch and other transmembrane proteins. Mol. Cell. 10.1016/S1097-2765(00)00061-7.

82. Hemming, M.L., Elias, J.E., Gygi, S.P., and Selkoe, D.J. (2008). Proteomic profiling of

γ-secretase substrates and mapping of substrate requirements. PLoS Biol. 10.1371/journal.pbio.0060257.

83. Gulick, A.M. (2019). Enzymes engineered to trap reaction intermediates. Nature. 10.1038/d41586-018-07569-6.

84. Huguenin-Dezot, N., Alonzo, D.A., Heberlig, G.W., Mahesh, M., Nguyen, D.P., Dornan, M.H., Boddy, C.N., Schmeing, T.M., and Chin, J.W. (2019). Trapping biosynthetic acyl-enzyme intermediates with encoded 2,3-diaminopropionic acid. Nature. 10.1038/s41586-018-0781-z.

85. Tang, S., Beattie, A.T., Kafkova, L., Petris, G., Huguenin-Dezot, N., Fiedler, M., Freeman, M., and Chin, J.W. (2022). Mechanism-based traps enable protease and hydrolase substrate discovery. Nature. 10.1038/s41586-022-04414-9.

86. Wolfe, M.S. (2009). Intramembrane proteolysis. Chem. Rev. 10.1021/cr8004197.

87. Zanotti, A., Coelho, J.P.L., Kaylani, D., Singh, G., Tauber, M., Hitzenberger, M., Avci, D., Zacharias, M., Russell, R.B., Lemberg, M.K., et al. (2022). The human signal peptidase complex acts as a quality control enzyme for membrane proteins. Science (80-.). 10.1126/science.abo5672.

88. Blobel, G., and Dobberstein, B. (1975). Transfer of proteins across membranes: I. Presence of proteolytically processed and unprocessed nascent immunoglobulin light chains on membrane-bound ribosomes of murine myeloma. J. Cell Biol. 10.1083/jcb.67.3.835.

89. VON HEIJNE, G. (1983). Patterns of Amino Acids near Signal-Sequence Cleavage Sites. Eur. J. Biochem. 10.1111/j.1432-1033.1983.tb07424.x.

90. Petersen, T.N., Brunak, S., Von Heijne, G., and Nielsen, H. (2011). SignalP 4.0: Discriminating signal peptides from transmembrane regions. Nat. Methods. 10.1038/nmeth.1701.

91. Breimann, S., Kamp, F., Guner, G., Ortner, M., Lichtenthaler, S., Langosch, D., Frishman, D., and Steiner, H. (2022). Substrate-defining features of γ-secretase revealed by comparative physicochemical profiling and explainable AI. In 2nd International Meeting 2022 of the DFG-Research Unit 2290 “Understanding Intramembrane Proteolysis,” p. 20.

92. Kolodziejczyk, A.A., Kim, J.K., Svensson, V., Marioni, J.C., and Teichmann, S.A. (2015). The Technology and Biology of Single-Cell RNA Sequencing. Mol. Cell. 10.1016/j.molcel.2015.04.005.

93. Zeisel, A., M͡oz-Manchado, A.B., Codeluppi, S., Lönnerberg, P., Manno, G. La, Juréus, A., Marques, S., Munguba, H., He, L., Betsholtz, C., et al. (2015). Cell types in the mouse cortex and hippocampus revealed by single-cell RNA-seq. Science (80-.). 10.1126/science.aaa1934.

94. Nimmerjahn, A., Kirchhoff, F., and Helmchen, F. (2005). Resting microglial cells are highly dynamic surveillants of brain parenchyma in vivo. Science (80-.). 10.1126/science.1110647.

95. Li, Q., and Barres, B.A. (2018). Microglia and macrophages in brain homeostasis and disease. Nat. Rev. Immunol. 10.1038/nri.2017.125.

96. Ginhoux, F., Greter, M., Leboeuf, M., Nandi, S., See, P., Gokhan, S., Mehler, M.F., Conway, S.J., Ng, L.G., Stanley, E.R., et al. (2010). Fate mapping analysis reveals that adult microglia derive from primitive macrophages. Science (80-.). 10.1126/science.1194637.

97. Schulz, C., Perdiguero, E.G., Chorro, L., Szabo-Rogers, H., Cagnard, N., Kierdorf, K., Prinz, M., Wu, B., Jacobsen, S.E.W., Pollard, J.W., et al. (2012). A lineage of myeloid cells independent of myb and hematopoietic stem cells. Science (80-.). 10.1126/science.1219179.

98. Füger, P., Hefendehl, J.K., Veeraraghavalu, K., Wendeln, A.C., Schlosser, C., Obermüller, U., Wegenast-Braun, B.M., Neher, J.J., Martus, P., Kohsaka, S., et al. (2017). Microglia turnover with aging and in an Alzheimer's model via long-term in vivo single-cell imaging. Nat. Neurosci. 10.1038/nn.4631.

99. Réu, P., Khosravi, A., Bernard, S., Mold, J.E., Salehpour, M., Alkass, K., Perl, S., Tisdale, J., Possnert, G., Druid, H., et al. (2017). The Lifespan and Turnover of Microglia in the Human Brain. Cell Rep. 10.1016/j.celrep.2017.07.004.

100. Ajami, B., Bennett, J.L., Krieger, C., Tetzlaff, W., and Rossi, F.M.V. (2007). Local self-renewal can sustain CNS microglia maintenance and function throughout adult life. Nat. Neurosci. 10.1038/nn2014.

101. Askew, K., Li, K., Olmos-Alonso, A., Garcia-Moreno, F., Liang, Y., Richardson, P., Tipton, T., Chapman, M.A., Riecken, K., Beccari, S., et al. (2017). Coupled Proliferation and Apoptosis Maintain the Rapid Turnover of Microglia in the Adult Brain. Cell Rep. 10.1016/j.celrep.2016.12.041.

102. Davalos, D., Grutzendler, J., Yang, G., Kim, J. V., Zuo, Y., Jung, S., Littman, D.R., Dustin, M.L., and Gan, W.B. (2005). ATP mediates rapid microglial response to local brain injury in vivo. Nat. Neurosci. 10.1038/nn1472.

103. Colonna, M., and Butovsky, O. (2017). Microglia function in the central nervous system during health and neurodegeneration. Annu. Rev. Immunol. 10.1146/annurev-immunol-051116-052358.

104. Prinz, M., Jung, S., and Priller, J. (2019). Microglia Biology: One Century of Evolving Concepts. Cell. 10.1016/j.cell.2019.08.053.

105. Lemke, G. (2019). How macrophages deal with death. Nat. Rev. Immunol. 10.1038/s41577-019-0167-y.

106. Arandjelovic, S., and Ravichandran, K.S. (2015). Phagocytosis of apoptotic cells in homeostasis. Nat. Immunol. 10.1038/ni.3253.

107. Pluvinage, J. V., Haney, M.S., Smith, B.A.H., Sun, J., Iram, T., Bonanno, L., Li, L., Lee, D.P., Morgens, D.W., Yang, A.C., et al. (2019). CD22 blockade restores homeostatic microglial phagocytosis in ageing brains. Nature. 10.1038/s41586-019-1088-4.

108. Safaiyan, S., Kannaiyan, N., Snaidero, N., Brioschi, S., Biber, K., Yona, S., Edinger, A.L., Jung, S., Rossner, M.J., and Simons, M. (2016). Age-related myelin degradation burdens the clearance function of microglia during aging. Nat. Neurosci. 10.1038/nn.4325.

109. Mariani, M.M., and Kielian, T. (2009). Microglia in infectious diseases of the central nervous system. J. Neuroimmune Pharmacol. 10.1007/s11481-009-9170-6.

110. Giulian, D., Haverkamp, L.J., Yu, J.H., Karshin, W., Tom, D., Li, J., Kirkpatrick, J., Kuo, Y.M., and Roher, A.E. (1996). Specific domains of β-amyloid from Alzheimer plaque elicit neuron killing in human microglia. J. Neurosci. 10.1523/jneurosci.16-19-06021.1996.

111. Wyss-Coray, T. (2006). Inflammation in Alzheimer disease: Driving force, bystander or beneficial response? Nat. Med. 10.1038/nm1484.

112. Hanisch, U.K., and Kettenmann, H. (2007). Microglia: Active sensor and versatile effector cells in the normal and pathologic brain. Nat. Neurosci. 10.1038/nn1997.

113. Salter, M.W., and Stevens, B. (2017). Microglia emerge as central players in brain disease. Nat. Med. 10.1038/nm.4397.

114. Schafer, D.P., Lehrman, E.K., Kautzman, A.G., Koyama, R., Mardinly, A.R., Yamasaki, R., Ransohoff, R.M., Greenberg, M.E., Barres, B.A., and Stevens, B. (2012). Microglia Sculpt Postnatal Neural Circuits in an Activity and Complement-Dependent Manner. Neuron. 10.1016/j.neuron.2012.03.026.

115. Stevens, B., Allen, N.J., Vazquez, L.E., Howell, G.R., Christopherson, K.S., Nouri, N., Micheva, K.D., Mehalow, A.K., Huberman, A.D., Stafford, B., et al. (2007). The Classical Complement Cascade Mediates CNS Synapse Elimination. Cell. 10.1016/j.cell.2007.10.036.

116. Hong, S., Beja-Glasser, V.F., Nfonoyim, B.M., Frouin, A., Li, S., Ramakrishnan, S., Merry, K.M., Shi, Q., Rosenthal, A., Barres, B.A., et al. (2016). Complement and microglia mediate early synapse loss in Alzheimer mouse models. Science (80-.). *352*, 712–716. 10.1126/science.aad8373.

117. Dejanovic, B., Huntley, M.A., De Mazière, A., Meilandt, W.J., Wu, T., Srinivasan, K., Jiang, Z., Gandham, V., Friedman, B.A., Ngu, H., et al. (2018). Changes in the Synaptic Proteome in Tauopathy and Rescue of Tau-Induced Synapse Loss by C1q Antibodies. Neuron. 10.1016/j.neuron.2018.10.014.

118. DeKosky, S.T., and Scheff, S.W. (1990). Synapse loss in frontal cortex biopsies in Alzheimer's disease: Correlation with cognitive severity. Ann. Neurol. 10.1002/ana.410270502.

119. Terry, R.D., Masliah, E., Salmon, D.P., Butters, N., DeTeresa, R., Hill, R., Hansen, L.A., and Katzman, R. (1991). Physical basis of cognitive alterations in alzheimer's disease: Synapse loss is the major correlate of cognitive impairment. Ann. Neurol. 10.1002/ana.410300410.

120. Mucke, L., and Selkoe, D.J. (2012). Neurotoxicity of amyloid β-protein: Synaptic and network dysfunction. Cold Spring Harb. Perspect. Med. 10.1101/cshperspect.a006338.

121. De Schepper, S., Ge, J.Z., Crowley, G., Ferreira, L.S.S., Garceau, D., Toomey, C.E., Sokolova, D., Rueda-Carrasco, J., Shin, S.H., Kim, J.S., et al. (2023). Perivascular cells induce microglial phagocytic states and synaptic engulfment via SPP1 in mouse models of Alzheimer's disease. Nat. Neurosci. 10.1038/s41593-023-01257-z.

122. Rueda-Carrasco, J., Sokolova, D., Lee, S., Childs, T., Jurčáková, N., Crowley, G., De Schepper, S., Ge, J.Z., Lachica, J.I., Toomey, C.E., et al. (2023). Microglia-synapse engulfment via PtdSer-TREM2 ameliorates neuronal hyperactivity in Alzheimer's disease models. EMBO J. 10.15252/embj.2022113246.

123. Grathwohl, S.A., Kälin, R.E., Bolmont, T., Prokop, S., Winkelmann, G., Kaeser, S.A., Odenthal, J., Radde, R., Eldh, T., Gandy, S., et al. (2009). Formation and maintenance of Alzheimer's disease β-amyloid plaques in the absence of microglia. Nat. Neurosci. 10.1038/nn.2432.

124. Kiani Shabestari, S., Morabito, S., Danhash, E.P., McQuade, A., Sanchez, J.R., Miyoshi, E., Chadarevian, J.P., Claes, C., Coburn, M.A., Hasselmann, J., et al. (2022). Absence of microglia promotes diverse pathologies and early lethality in Alzheimer's disease mice. Cell Rep. 10.1016/j.celrep.2022.110961.

125. Rock, R.B., Gekker, G., Hu, S., Sheng, W.S., Cheeran, M., Lokensgard, J.R., and

Peterson, P.K. (2004). Role of microglia in central nervous system infections. Clin. Microbiol. Rev. 10.1128/CMR.17.4.942-964.2004.

126. Nau, R., and Brück, W. (2002). Neuronal injury in bacterial meningitis: Mechanisms and implications for therapy. Trends Neurosci. 10.1016/S0166-2236(00)02024-5.

127. Hardy, J., and Selkoe, D.J. (2002). The amyloid hypothesis of Alzheimer's disease: Progress and problems on the road to therapeutics. Science (80-.). 10.1126/science.1072994.

128. Hardy, J.A., and Higgins, G.A. (1992). Alzheimer's disease: The amyloid cascade hypothesis. Science (80-.). 10.1126/science.1566067.

129. Kunkle, B.W., Grenier-Boley, B., Sims, R., Bis, J.C., Damotte, V., Naj, A.C., Boland, A., Vronskaya, M., van der Lee, S.J., Amlie-Wolf, A., et al. (2019). Genetic meta-analysis of diagnosed Alzheimer's disease identifies new risk loci and implicates Aβ, tau, immunity and lipid processing. Nat. Genet. 10.1038/s41588-019-0358-2.

130. Nott, A., Holtman, I.R., Coufal, N.G., Schlachetzki, J.C.M., Yu, M., Hu, R., Han, C.Z., Pena, M., Xiao, J., Wu, Y., et al. (2019). Brain cell type–specific enhancer–promoter interactome maps and disease-risk association. Science (80-.). 10.1126/science.aay0793.

131. Guerreiro, R., Wojtas, A., Bras, J., Carrasquillo, M., Rogaeva, E., Majounie, E., Cruchaga, C., Sassi, C., Kauwe, J.S.K., Younkin, S., et al. (2013). TREM2 variants in Alzheimer's disease. N. Engl. J. Med. 10.1056/NEJMoa1211851.

132. Lambert, J.C., Ibrahim-Verbaas, C.A., Harold, D., Naj, A.C., Sims, R., Bellenguez, C., Jun, G., DeStefano, A.L., Bis, J.C., Beecham, G.W., et al. (2013). Meta-analysis of 74,046 individuals identifies 11 new susceptibility loci for Alzheimer's disease. Nat. Genet. 10.1038/ng.2802.

133. Marioni, R.E., Harris, S.E., Zhang, Q., McRae, A.F., Hagenaars, S.P., Hill, W.D., Davies, G., Ritchie, C.W., Gale, C.R., Starr, J.M., et al. (2018). GWAS on family history of Alzheimer's disease. Transl. Psychiatry. 10.1038/s41398-018-0150-6.

134. Sims, R., Van Der Lee, S.J., Naj, A.C., Bellenguez, C., Badarinarayan, N., Jakobsdottir, J., Kunkle, B.W., Boland, A., Raybould, R., Bis, J.C., et al. (2017). Rare coding variants in PLCG2, ABI3, and TREM2 implicate microglial-mediated innate immunity in Alzheimer's disease. Nat. Genet. 10.1038/ng.3916.

135. Villegas-Llerena, C., Phillips, A., Reitboeck, P.G., Hardy, J., and Pocock, J.M. (2016). Microglial genes regulating neuroinflammation in the progression of Alzheimer's disease. Curr. Opin. Neurobiol. 10.1016/j.conb.2015.10.004.

136. Verheijen, J., and Sleegers, K. (2018). Understanding Alzheimer Disease at the Interface between Genetics and Transcriptomics. Trends Genet. 10.1016/j.tig.2018.02.007.

137. Wightman, D.P., Jansen, I.E., Savage, J.E., Shadrin, A.A., Bahrami, S., Holland, D., Rongve, A., Børte, S., Winsvold, B.S., Drange, O.K., et al. (2021). A genome-wide association study with 1,126,563 individuals identifies new risk loci for Alzheimer's disease. Nat. Genet. 10.1038/s41588-021-00921-z.

138. De Strooper, B., and Karran, E. (2016). The Cellular Phase of Alzheimer's Disease. Cell. 10.1016/j.cell.2015.12.056.

139. Leng, F., and Edison, P. (2021). Neuroinflammation and microglial activation in Alzheimer disease: where do we go from here? Nat. Rev. Neurol. 10.1038/s41582-020-00435-y.

140. Chen, W.T., Lu, A., Craessaerts, K., Pavie, B., Sala Frigerio, C., Corthout, N., Qian, X., Laláková, J., Kühnemund, M., Voytyuk, I., et al. (2020). Spatial Transcriptomics and In Situ Sequencing to Study Alzheimer's Disease. Cell. 10.1016/j.cell.2020.06.038.

141. Wang, S., and Colonna, M. (2019). Microglia in Alzheimer's disease: A target for immunotherapy. J. Leukoc. Biol. 10.1002/JLB.MR0818-319R.

142. Deczkowska, A., Weiner, A., and Amit, I. (2020). The Physiology, Pathology, and Potential Therapeutic Applications of the TREM2 Signaling Pathway. Cell. 10.1016/j.cell.2020.05.003.

143. Lewcock, J.W., Schlepckow, K., Di Paolo, G., Tahirovic, S., Monroe, K.M., and Haass, C. (2020). Emerging Microglia Biology Defines Novel Therapeutic Approaches for Alzheimer's Disease. Neuron. 10.1016/j.neuron.2020.09.029.

144. Keren-Shaul, H., Spinrad, A., Weiner, A., Matcovitch-Natan, O., Dvir-Szternfeld, R., Ulland, T.K., David, E., Baruch, K., Lara-Astaiso, D., Toth, B., et al. (2017). A Unique Microglia Type Associated with Restricting Development of Alzheimer's Disease. Cell. 10.1016/j.cell.2017.05.018.

145. Sala Frigerio, C., Wolfs, L., Fattorelli, N., Thrupp, N., Voytyuk, I., Schmidt, I., Mancuso, R., Chen, W.T., Woodbury, M.E., Srivastava, G., et al. (2019). The Major Risk Factors for Alzheimer's Disease: Age, Sex, and Genes Modulate the Microglia Response to Aβ Plaques. Cell Rep. 10.1016/j.celrep.2019.03.099.

146. Mancuso, R., Van Den Daele, J., Fattorelli, N., Wolfs, L., Balusu, S., Burton, O., Liston, A., Sierksma, A., Fourne, Y., Poovathingal, S., et al. (2019). Stem-cell-derived human microglia transplanted in mouse brain to study human disease. Nat. Neurosci. 10.1038/s41593-019-0525-x.

147. Hasselmann, J., Coburn, M.A., England, W., Figueroa Velez, D.X., Kiani Shabestari, S., Tu, C.H., McQuade, A., Kolahdouzan, M., Echeverria, K., Claes, C., et al. (2019). Development of a Chimeric Model to Study and Manipulate Human Microglia In Vivo. Neuron. 10.1016/j.neuron.2019.07.002.

148. Schlepckow, K., Monroe, K.M., Kleinberger, G., Cantuti-Castelvetri, L., Parhizkar, S., Xia, D., Willem, M., Werner, G., Pettkus, N., Brunner, B., et al. (2020). Enhancing protective microglial activities with a dual function TREM 2 antibody to the stalk region . EMBO Mol. Med. 10.15252/emmm.201911227.

149. Wang, S., Sudan, R., Peng, V., Zhou, Y., Du, S., Yuede, C.M., Lei, T., Hou, J., Cai, Z., Cella, M., et al. (2022). TREM2 drives microglia response to amyloid-β via SYK-dependent and -independent pathways. Cell. 10.1016/j.cell.2022.09.033.

150. Mancuso, R., Fattorelli, N., Martinez-Muriana, A., Davis, E., Wolfs, L., Van den Daele, J., Geric, I., Preman, P., Serneels, L., and Poovathingal, S. (2022). A multi-pronged human microglia response to Alzheimer's disease Aβ pathology. bioRxiv.

151. Spangenberg, E., Severson, P.L., Hohsfield, L.A., Crapser, J., Zhang, J., Burton, E.A., Zhang, Y., Spevak, W., Lin, J., Phan, N.Y., et al. (2019). Sustained microglial depletion with CSF1R inhibitor impairs parenchymal plaque development in an Alzheimer's disease model. Nat. Commun. 10.1038/s41467-019-11674-z.

152. Sosna, J., Philipp, S., Albay, R.I., Reyes-Ruiz, J.M., Baglietto-Vargas, D., LaFerla, F.M., and Glabe, C.G. (2018). Early long-term administration of the CSF1R inhibitor PLX3397 ablates microglia and reduces accumulation of intraneuronal amyloid, neuritic plaque deposition and pre-fibrillar oligomers in 5XFAD mouse model of Alzheimer's disease. Mol. Neurodegener. 10.1186/s13024-018-0244-x.

153. Mancuso, R., Fryatt, G., Cleal, M., Obst, J., Pipi, E., Monzón-Sandoval, J., Ribe, E., Winchester, L., Webber, C., Nevado, A., et al. (2019). CSF1R inhibitor JNJ-40346527 attenuates microglial proliferation and neurodegeneration in P301S mice. Brain. 10.1093/brain/awz241.

154. Glenn, G., and van der Geer, P. (2008). Toll-like receptors stimulate regulated intramembrane proteolysis of the CSF-1 receptor through Erk activation. FEBS Lett. 10.1016/j.febslet.2008.02.029.

155. Merilahti, J.A.M., and Elenius, K. (2019). Gamma-secretase-dependent signaling of receptor tyrosine kinases. Oncogene. 10.1038/s41388-018-0465-z.

156. Merilahti, J.A.M., Ojala, V.K., Knittle, A.M., Pulliainen, A.T., and Elenius, K. (2017). Genome-wide screen of gamma-secretase-mediated intramembrane cleavage of receptor tyrosine kinases. Mol. Biol. Cell. 10.1091/mbc.E17-04-0261.

157. Huang, Y., Happonen, K.E., Burrola, P.G., O'Connor, C., Hah, N., Huang, L., Nimmerjahn, A., and Lemke, G. (2021). Microglia use TAM receptors to detect and engulf amyloid β plaques. Nat. Immunol. 10.1038/s41590-021-00913-5.

158. Adams, S., van der Laan, L.J.W., Vernon-Wilson, E., Renardel de Lavalette, C., Döpp, E.A., Dijkstra, C.D., Simmons, D.L., and van den Berg, T.K. (1998). Signal-Regulatory Protein Is Selectively Expressed by Myeloid and Neuronal Cells. J. Immunol. 10.4049/jimmunol.161.4.1853.

159. Neznanov, N., Neznanova, L., Kondratov, R. V., Burdelya, L., Kandel, E.S., O'Rourke, D.M., Ullrich, A., and Gudkov, A. V. (2003). Dominant negative form of signal-regulatory protein-α (SIRPα/SHPS-1) inhibits tumor necrosis factor-mediated apoptosis by activation of NF-κB. J. Biol. Chem. 10.1074/jbc.M210698200.

160. Oldenborg, P.A., Zheleznyak, A., Fang, Y.F., Lagenaur, C.F., Gresham, H.D., and Lindberg, F.P. (2000). Role of CD47 as a marker of self on red blood cells. Science (80-.). 10.1126/science.288.5473.2051.

161. Zheng, Q., Van Die, I., and Cummings, R.D. (2002). Negative regulation of platelet clearance and of the macrophage phagocytic response by the transmembrane glycoprotein SHPS-1. J. Biol. Chem. 10.1074/jbc.M203287200.

162. Wunderlich, P., Glebov, K., Kemmerling, N., Tien, N.T., Neumann, H., and Walter, J. (2013). Sequential proteolytic processing of the triggering receptor expressed on myeloid cells-2 (TREM2) protein by ectodomain shedding and γ-secretase- dependent intramembranous cleavage. J. Biol. Chem. 10.1074/jbc.M113.517540.

163. Jonsson, T., Stefansson, H., Steinberg, S., Jonsdottir, I., Jonsson, P. V., Snaedal, J., Bjornsson, S., Huttenlocher, J., Levey, A.I., Lah, J.J., et al. (2013). Variant of TREM2 associated with the risk of Alzheimer's disease. N. Engl. J. Med. 10.1056/NEJMoa1211103.

164. Parhizkar, S., Arzberger, T., Brendel, M., Kleinberger, G., Deussing, M., Focke, C., Nuscher, B., Xiong, M., Ghasemigharagoz, A., Katzmarski, N., et al. (2019). Loss of TREM2 function increases amyloid seeding but reduces plaque-associated ApoE. Nat. Neurosci. 10.1038/s41593-018-0296-9.

165. Krasemann, S., Madore, C., Cialic, R., Baufeld, C., Calcagno, N., El Fatimy, R., Beckers, L., O'Loughlin, E., Xu, Y., Fanek, Z., et al. (2017). The TREM2-APOE Pathway Drives the Transcriptional Phenotype of Dysfunctional Microglia in Neurodegenerative Diseases. Immunity. 10.1016/j.immuni.2017.08.008.

166. Lowell, C.A. (2011). Src-family and Syk kinases in activating and inhibitory pathways in innate immune cells: Signaling cross talk. Cold Spring Harb. Perspect. Biol.

10.1101/cshperspect.a002352.

167. Glebov, K., Wunderlich, P., Karaca, I., and Walter, J. (2016). Functional involvement of γ-secretase in signaling of the triggering receptor expressed on myeloid cells-2 (TREM2). J. Neuroinflammation. 10.1186/s12974-016-0479-9.

168. Theos, A.C., Watt, B., Harper, D.C., Janczura, K.J., Theos, S.C., Herman, K.E., and Marks, M.S. (2013). The PKD domain distinguishes the trafficking and amyloidogenic properties of the pigment cell protein PMEL and its homologue GPNMB. Pigment Cell Melanoma Res. 10.1111/pcmr.12084.

169. Kummer, M.P., Maruyama, H., Huelsmann, C., Baches, S., Weggen, S., and Koo, E.H. (2009). Formation of Pmel17 amyloid is regulated by juxtamembrane metalloproteinase cleavage, and the resulting C-terminal fragment is a substrate for γ-secretase. J. Biol. Chem. 10.1074/jbc.M808904200.

170. Hüttenrauch, M., Ogorek, I., Klafki, H., Otto, M., Stadelmann, C., Weggen, S., Wiltfang, J., and Wirths, O. (2018). Glycoprotein NMB: a novel Alzheimer's disease associated marker expressed in a subset of activated microglia. Acta Neuropathol. Commun. 10.1186/s40478-018-0612-3.

171. Satoh, J. ichi, Kino, Y., Yanaizu, M., Ishida, T., and Saito, Y. (2019). Microglia express GPNMB in the brains of Alzheimer's disease and Nasu-Hakola disease. Intractable Rare Dis. Res. 10.5582/irdr.2019.01049.

172. Diaz-Ortiz, M.E., Seo, Y., Posavi, M., Cordon, M.C., Clark, E., Jain, N., Charan, R., Gallagher, M.D., Unger, T.L., Amari, N., et al. (2022). GPNMB confers risk for Parkinson's disease through interaction with α-synuclein. Science (80-.). 10.1126/science.abk0637.

173. Watt, B., Van Niel, G., Raposo, G., and Marks, M.S. (2013). PMEL: A pigment cell-specific model for functional amyloid formation. Pigment Cell Melanoma Res. 10.1111/pcmr.12067.

174. Rochin, L., Hurbain, I., Serneels, L., Fort, C., Watt, B., Leblanc, P., Marks, M.S., De Strooper, B., Raposo, G., and Van Niel, G. (2013). BACE2 processes PMEL to form the melanosome amyloid matrix in pigment cells. Proc. Natl. Acad. Sci. U. S. A. 10.1073/pnas.1220748110.

175. Watt, B., Tenza, D., Lemmon, M.A., Kerje, S., Raposo, G., Andersson, L., and Marks, M.S. (2011). Mutations in or near the transmembrane domain alter PMEL amyloid formation from functional to pathogenic. PLoS Genet. 10.1371/journal.pgen.1002286.

176. Bult, C.J., Blake, J.A., Smith, C.L., Kadin, J.A., Richardson, J.E., Anagnostopoulos, A., Asabor, R., Baldarelli, R.M., Beal, J.S., Bello, S.M., et al. (2019). Mouse Genome Database (MGD) 2019. Nucleic Acids Res. 10.1093/nar/gky1056.

177. Stützer, I., Selevsek, N., Esterházy, D., Schmidt, A., Aebersold, R., and Stoffel, M. (2013). Systematic proteomic analysis identifies β-site amyloid precursor protein cleaving enzyme 2 and 1 (BACE2 and BACE1) substrates in pancreatic β-cells. J. Biol. Chem. 10.1074/jbc.M112.444703.

178. Bartolomé, A., Liang, J., Wang, P., Ho, D.D., and Pajvani, U.B. (2021). Angiotensin converting enzyme 2 is a novel target of the γ-secretase complex. Sci. Rep. 10.1038/s41598-021-89379-x.

179. Tousseyn, T., Thathiah, A., Jorissen, E., Raemaekers, T., Konietzko, U., Reiss, K., Maes, E., Snellinx, A., Serneels, L., Nyabi, O., et al. (2009). ADAM10, the rate-limiting protease of regulated intramembrane proteolysis of notch and other proteins, is processed by ADAMS-9, ADAMS-15, and the γ-secretase. J. Biol. Chem.

10.1074/jbc.M805894200.

180. Araki, Y., Miyagi, N., Kato, N., Yoshida, T., Wada, S., Nishimura, M., Komano, H., Yamamoto, T., De Strooper, B., Yamamoto, K., et al. (2004). Coordinated metabolism of Alcadein and amyloid β-protein precursor regulates FE65-dependent gene transactivation. J. Biol. Chem. 10.1074/jbc.M401925200.

181. Scheinfeld, M.H., Ghersi, E., Laky, K., Fowlkes, B.J., and D'Adamio, L. (2002). Processing of β-amyloid precursor-like protein-1 and -2 by γ-secretase regulates transcription. J. Biol. Chem. 10.1074/jbc.M208110200.

182. May, P., Bock, H.H., Nimpf, J., and Herz, J. (2003). Differential glycosylation regulates processing of lipoprotein receptors by γ-secretase. J. Biol. Chem. 10.1074/jbc.M305858200.

183. Lu, Y., Wan, J., Yang, Z., Lei, X., Niu, Q., Jiang, L., Passtoors, W.M., Zang, A., Fraering, P.C., and Wu, F. (2017). Regulated intramembrane proteolysis of the AXL receptor kinase generates an intracellular domain that localizes in the nucleus of cancer cells. FASEB J. 10.1096/fj.201600702R.

184. Stoeck, A., Shang, L., and Dempsey, P.J. (2010). Sequential and γ-secretase-dependent processing of the betacellulin precursor generates a palmitoylated intracellular-domain fragment that inhibits cell growth. J. Cell Sci. 10.1242/jcs.060830.

185. Blair, C.R., Stone, J.B., and Wells, R.G. (2011). The type III TGF-β receptor betaglycan transmembrane-cytoplasmic domain fragment is stable after ectodomain cleavage and is a substrate of the intramembrane protease β-secretase. Biochim. Biophys. Acta - Mol. Cell Res. 10.1016/j.bbamcr.2010.12.005.

186. Rudan Njavro, J., Klotz, J., Dislich, B., Wanngren, J., Shmueli, M.D., Herber, J., Kuhn, P.H., Kumar, R., Koeglsperger, T., Conrad, M., et al. (2020). Mouse brain proteomics establishes MDGA1 and CACHD1 as in vivo substrates of the Alzheimer protease BACE1. FASEB J. 10.1096/fj.201902347R.

187. Schiffmacher, A.T., Padmanabhan, R., Jhingory, S., and Taneyhill, L.A. (2014). Cadherin-6B is proteolytically processed during epithelial-to-mesenchymal transitions of the cranial neural crest. Mol. Biol. Cell. 10.1091/mbc.E13-08-0459.

188. Nagara, Y., Hagiyama, M., Hatano, N., Futai, E., Suo, S., Takaoka, Y., Murakami, Y., Ito, A., and Ishiura, S. (2012). Tumor suppressor cell adhesion molecule 1 (CADM1) is cleaved by a disintegrin and metalloprotease 10 (ADAM10) and subsequently cleaved by γ-secretase complex. Biochem. Biophys. Res. Commun. 10.1016/j.bbrc.2011.11.140.

189. Houri, N., Huang, K.C., and Nalbantoglu, J. (2013). The Coxsackievirus and Adenovirus Receptor (CAR) Undergoes Ectodomain Shedding and Regulated Intramembrane Proteolysis (RIP). PLoS One. 10.1371/journal.pone.0073296.

190. Yong, Y. Le, Zhang, R.Y., Liu, Z.K., Wei, D., Shang, Y.K., Wu, J., Zhang, Z.Y., Li, C., Chen, Z.N., and Bian, H. (2019). Gamma-secretase complex-dependent intramembrane proteolysis of CD147 regulates the Notch1 signaling pathway in hepatocellular carcinoma. J. Pathol. 10.1002/path.5316.

191. Chen, Z., Kapus, A., Khatri, I., Kos, O., Zhu, F., and Gorczynski, R.M. (2018). Cell membrane-bound CD200 signals both via an extracellular domain and following nuclear translocation of a cytoplasmic fragment. Leuk. Res. 10.1016/j.leukres.2018.04.007.

192. Andersson, C.X., Fernandez-Rodriguez, J., Laos, S., Baeckström, D., Haass, C., and Hansson, G.C. (2005). Shedding and γ-secretase-mediated intramembrane

proteolysis of the mucin-type molecule CD43. Biochem. J. 10.1042/BJ20041387.

193. Murakami, D., Okamoto, I., Nagano, O., Kawano, Y., Tomita, T., Iwatsubo, T., De Strooper, B., Yumoto, E., and Saya, H. (2003). Presenilin-dependent γ-secretase activity mediates the intramembranous cleavage of CD44. Oncogene. 10.1038/sj.onc.1206298.

194. Bedau, T., Peters, F., Prox, J., Arnold, P., Schmidt, F., Finkernagel, M., Köllmann, S., Wichert, R., Otte, A., Ohler, A., et al. (2017). Ectodomain shedding of CD99 within highly conserved regions is mediated by the metalloprotease meprin β and promotes transendothelial cell migration. FASEB J. 10.1096/fj.201601113R.

195. Wilhelmsen, K., and van der Geer, P. (2004). Phorbol 12-Myristate 13-Acetate-Induced Release of the Colony-Stimulating Factor 1 Receptor Cytoplasmic Domain into the Cytosol Involves Two Separate Cleavage Events. Mol. Cell. Biol. 10.1128/mcb.24.1.454-464.2004.

196. Schulte, A., Schulz, B., Andrzejewski, M.G., Hundhausen, C., Mletzko, S., Achilles, J., Reiss, K., Paliga, K., Weber, C., Rose John, S., et al. (2007). Sequential processing of the transmembrane chemokines CX3CL1 and CXCL16 by α- and γ-secretases. Biochem. Biophys. Res. Commun. 10.1016/j.bbrc.2007.04.100.

197. Taniguchi, Y., Kim, S.H., and Sisodia, S.S. (2003). Presenilin-dependent "γ-secretase" processing of deleted in colorectal cancer (DCC). J. Biol. Chem. 10.1074/jbc.C300239200.

198. Ikeuchi, T., and Sisodia, S.S. (2003). The Notch ligands, Delta1 and Jagged2, are substrates for presenilin-dependent "γ-secretase" cleavage. J. Biol. Chem. 10.1074/jbc.C200711200.

199. Six, E., Ndiaye, D., Laâbi, Y., Brou, C., Gupta-Rossi, N., Israël, A., and Logeat, F. (2003). The Notch ligand Delta1 is sequentially cleaved by an ADAM protease and γ-secretase. Proc. Natl. Acad. Sci. U. S. A. 10.1073/pnas.1230693100.

200. LaVoie, M.J., and Selkoe, D.J. (2003). The Notch Ligands, Jagged and Delta, Are Sequentially Processed by α-Secretase and Presenilin/γ-Secretase and Release Signaling Fragments. J. Biol. Chem. 10.1074/jbc.M302659200.

201. Colombo, A., Hsia, H., Wang, M., Kuhn, P., Brill, M.S., Canevazzi, P., Feederle, R., Taveggia, C., Misgeld, T., and Lichtenthaler, S.F. (2018). Non-cell-autonomous function of DR6 in Schwann cell proliferation. EMBO J. 10.15252/embj.201797390.

202. Sachse, S.M., Lievens, S., Ribeiro, L.F., Dascenco, D., Masschaele, D., Horré, K., Misbaer, A., Vanderroost, N., De Smet, A.S., Salta, E., et al. (2019). Nuclear import of the DSCAM -cytoplasmic domain drives signaling capable of inhibiting synapse formation . EMBO J. 10.15252/embj.201899669.

203. Marambaud, P., Shioi, J., Serban, G., Georgakopoulos, A., Sarner, S., Nagy, V., Baki, L., Wen, P., Efthimiopoulos, S., Shao, Z., et al. (2002). A presenilin-1/γ-secretase cleavage releases the E-cadherin intracellular domain and regulates disassembly of adherens junctions. EMBO J. 10.1093/emboj/21.8.1948.

204. Maetzel, D., Denzel, S., Mack, B., Canis, M., Went, P., Benk, M., Kieu, C., Papior, P., Baeuerle, P.A., Munz, M., et al. (2009). Nuclear signalling by tumour-associated antigen EpCAM. Nat. Cell Biol. 10.1038/ncb1824.

205. Javier-Torrent, M., Marco, S., Rocandio, D., Pons-Vizcarra, M., Janes, P.W., Lackmann, M., Egea, J., and Saura, C.A. (2019). Presenilin/γ-secretase-dependent epha3 processing mediates axon elongation through non-muscle myosin IIA. Elife. 10.7554/eLife.43646.

206. Inoue, E., Deguchi-Tawarada, M., Togawa, A., Matsui, C., Arita, K., Katahira-Tayama, S., Sato, T., Yamauchi, E., Oda, Y., and Takai, Y. (2009). Synaptic activity prompts γ-secretase-mediated cleavage of EphA4 and dendritic spine formation. J. Cell Biol. 10.1083/jcb.200809151.

207. Litterst, C., Georgakopoulos, A., Shioi, J., Ghersi, E., Wisniewski, T., Wang, R., Ludwig, A., and Robakis, N.K. (2007). Ligand binding and calcium influx induce distinct ectodomain/γ- secretase-processing pathways of EphB2 receptor. J. Biol. Chem. 10.1074/jbc.M611449200.

208. Tomita, T., Tanaka, S., Morohashi, Y., and Iwatsubo, T. (2006). Presenilin-dependent intramembrane cleavage of ephrin-BI. Mol. Neurodegener. 10.1186/1750-1326-1-2.

209. Georgakopoulos, A., Litterst, C., Ghersi, E., Baki, L., Xu, C.J., Serban, G., and Robakis, N.K. (2006). Metalloproteinase/Presenilin1 processing of ephrinB regulates EphB-induced Src phosphorylation and signaling. EMBO J. 10.1038/sj.emboj.7601031.

210. Ni, C.Y., Murphy, M.P., Golde, T.E., and Carpenter, G. (2001). γ-secretase cleavage and nuclear locatization of ErbB-4 receptor tyrosine kinase. Science (80-.). 10.1126/science.1065412.

211. Degnin, C.R., Laederich, M.B., and Horton, W.A. (2011). Ligand activation leads to regulated intramembrane proteolysis of fibroblast growth factor receptor 3. Mol. Biol. Cell. 10.1091/mbc.E11-01-0080.

212. Cai, J., Jiang, W.G., Grant, M.B., and Boulton, M. (2006). Pigment epithelium-derived factor inhibits angiogenesis via regulated intracellular proteolysis of vascular endothelial growth factor receptor 1. J. Biol. Chem. 10.1074/jbc.M507401200.

213. Restrepo, L.J., DePew, A.T., Moese, E.R., Tymanskyj, S.R., Parisi, M.J., Aimino, M.A., Duhart, J.C., Fei, H., and Mosca, T.J. (2022). γ-secretase promotes Drosophila postsynaptic development through the cleavage of a Wnt receptor. Dev. Cell. 10.1016/j.devcel.2022.05.006.

214. Cowan, J.W., Wang, X., Guan, R., He, K., Jiang, J., Baumann, G., Black, R.A., Wolfe, M.S., and Frank, S.J. (2005). Growth hormone receptor is a target for presenilin-dependent γ-secretase cleavage. J. Biol. Chem. 10.1074/jbc.M500621200.

215. Meyer, E.L., Strutz, N., Gahring, L.C., and Rogers, S.W. (2003). Glutamate receptor subunit 3 is modified by site-specific limited proteolysis including cleavage by γ-secretase. J. Biol. Chem. 10.1074/jbc.M301360200.

216. Nakahara, S., Saito, T., Kondo, N., Moriwaki, K., Noda, K., Ihara, S., Takahashi, M., Ide, Y., Gu, J., Inohara, H., et al. (2006). A secreted type of β1,6 N-acetylglucosaminyltransferase V (GnT-V), a novel angiogenesis inducer, is regulated by γ-secretase. FASEB J. 10.1096/fj.05-5066com.

217. Liu, D., Zha, L., Liu, Y., Zhao, X., Xu, X., Liu, S., Ma, W., Zheng, J., and Shi, M. (2020). β2-AR activation promotes cleavage and nuclear translocation of Her2 and metastatic potential of cancer cells. Cancer Sci. 10.1111/cas.14676.

218. Carey, B.W., Kim, D.Y., and Kovacs, D.M. (2007). Presenilin/γ-secretase and α-secretase-like peptidases cleave human MHC Class I proteins. Biochem. J. 10.1042/BJ20060847.

219. Saleh, A.Z.M., Fang, A.T., Arch, A.E., Neupane, D., El Fiky, A., and Krolewski, J.J. (2004). Regulated proteolysis of the IFNaR2 subunit of the interferon-alpha receptor. Oncogene. 10.1038/sj.onc.1207955.

220. McElroy, B., Powell, J.C., and McCarthy, J. V. (2007). The insulin-like growth factor 1 (IGF-1) receptor is a substrate for γ-secretase-mediated intramembrane proteolysis. Biochem. Biophys. Res. Commun. 10.1016/j.bbrc.2007.05.062.

221. Lokau, J., Flynn, C.M., and Garbers, C. (2017). Cleavage of the Interleukin-11 receptor induces processing of its C-terminal fragments by the gamma-secretase and the proteasome. Biochem. Biophys. Res. Commun. 10.1016/j.bbrc.2017.07.106.

222. Elzinga, B.M., Twomey, C., Powell, J.C., Harte, F., and McCarthy, J. V. (2009). Interleukin-1 receptor type 1 is a substrate for γ-secretase- dependent regulated intramembrane proteolysis. J. Biol. Chem. 10.1074/jbc.M803108200.

223. Kuhn, P.H., Marjaux, E., Imhof, A., De Strooper, B., Haass, C., and Lichtenthaler, S.F. (2007). Regulated intramembrane proteolysis of the interleukin-1 receptor II by α-, β-, and γ-secretase. J. Biol. Chem. 10.1074/jbc.M700356200.

224. Chalaris, A., Gewiese, J., Paliga, K., Fleig, L., Schneede, A., Krieger, K., Rose-John, S., and Scheller, J. (2010). ADAM17-mediated shedding of the IL6R induces cleavage of the membrane stub by γ-secretase. Biochim. Biophys. Acta - Mol. Cell Res. 10.1016/j.bbamcr.2009.12.001.

225. Kasuga, K., Kaneko, H., Nishizawa, M., Onodera, O., and Ikeuchi, T. (2007). Generation of intracellular domain of insulin receptor tyrosine kinase by γ-secretase. Biochem. Biophys. Res. Commun. 10.1016/j.bbrc.2007.06.022.

226. Niwa, M., Sidrauski, C., Kaufman, R.J., and Walter, P. (1999). A role for presenilin-1 in nuclear accumulation of Ire1 fragments and induction of the mammalian unfolded protein response. Cell. 10.1016/S0092-8674(00)81667-0.

227. Sachse, C.C., Kim, Y.H., Agsten, M., Huth, T., Alzheimer, C., Kovacs, D.M., and Kim, D.Y. (2013). BACE1 and presenilin/γ-secretase regulate proteolytic processing of KCNE1 and 2, auxiliary subunits of voltage-gated potassium channels. FASEB J. 10.1096/fj.12-214056.

228. Bloch, L., Sineshchekova, O., Reichenbach, D., Reiss, K., Saftig, P., Kuro-o, M., and Kaether, C. (2009). Klotho is a substrate for α-, β- and γ-secretase. FEBS Lett. 10.1016/j.febslet.2009.09.009.

229. Maretzky, T., Schulte, M., Ludwig, A., Rose-John, S., Blobel, C., Hartmann, D., Altevogt, P., Saftig, P., and Reiss, K. (2005). L1 Is Sequentially Processed by Two Differently Activated Metalloproteases and Presenilin/γ-Secretase and Regulates Neural Cell Adhesion, Cell Migration, and Neurite Outgrowth. Mol. Cell. Biol. 10.1128/mcb.25.20.9040-9053.2005.

230. Haapasalo, A., Doo, Y.K., Carey, B.W., Turunen, M.K., Pettingell, W.H., and Kovacs, D.M. (2007). Presenilin/γ-secretase-mediated cleavage regulates association of Leukocyte-common Antigen-related (LAR) receptor tyrosine phosphatase with β-catenin. J. Biol. Chem. 10.1074/jbc.M611324200.

231. May, P., Krishna Reddy, Y., and Herz, J. (2002). Proteolytic processing of low density lipoprotein receptor-related protein mediates regulated release of its intracellular domain. J. Biol. Chem. 10.1074/jbc.M201979200.

232. Liu, C.X., Ranganathan, S., Robinson, S., and Strickland, D.K. (2007). γ-secretase-mediated release of the low density lipoprotein receptor-related protein 1B intracellular domain suppresses anchorage- independent growth of neuroglioma cells. J. Biol. Chem. 10.1074/jbc.M608088200.

233. Mi, K., and Johnson, G.V.W. (2007). Regulated proteolytic processing of LRP6 results in release of its intracellular domain. J. Neurochem. 10.1111/j.1471-

4159.2007.04447.x.

234. Zou, Z., Chung, B., Nguyen, T., Mentone, S., Thomson, B., and Biemesderfer, D. (2004). Linking receptor-mediated endocytosis and cell signaling: Evidence for regulated intramembrane proteolysis of megalin in proximal tubule. J. Biol. Chem. 10.1074/jbc.M405608200.

235. Foveau, B., Ancot, F., Leroy, C., Petrelli, A., Reiss, K., Vingtdeux, V., Giordano, S., Fafeur, V., and Tulasne, D. (2009). Down-regulation of the met receptor tyrosine kinase by presenilin-dependent regulated intramembrane proteolysis. Mol. Biol. Cell. 10.1091/mbc.E08-09-0969.

236. Julian, J.A., Dharmaraj, N., and Carson, D.D. (2009). MUC1 is a substrate for γ-secretase. J. Cell. Biochem. 10.1002/jcb.22292.

237. Marambaud, P., Wen, P.H., Dutt, A., Shioi, J., Takashima, A., Siman, R., and Robakis, N.K. (2003). A CBP binding transcriptional repressor produced by the PS1/ ε-cleavage of N-Cadherin is inhibited by PS1 FAD mutations. Cell. 10.1016/j.cell.2003.08.008.

238. Kim, D.Y., Ingano, L.A.M.K., and Kovacs, D.M. (2002). Nectin-1α, an immunoglobulin-like receptor involved in the formation of synapses, is a substrate for presenilin/γ-secretase-like cleavage. J. Biol. Chem. 10.1074/jbc.M210179200.

239. Kim, J., Chang, A., Dudak, A., Federoff, H.J., and Lim, S.T. (2011). Characterization of nectin processing mediated by presenilin-dependent gamma-secretase. J. Neurochem. 10.1111/j.1471-4159.2011.07479.x.

240. Goldschneider, D., Rama, N., Guix, C., and Mehlen, P. (2008). The Neogenin Intracellular Domain Regulates Gene Transcription via Nuclear Translocation. Mol. Cell. Biol. 10.1128/mcb.02114-07.

241. Bao, J., Wolpowitz, D., Role, L.W., and Talmage, D.A. (2003). Back signaling by the Nrg-1 intracellular domain. J. Cell Biol. 10.1083/jcb.200212085.

242. Czarnek, M., and Bereta, J. (2020). Proteolytic Processing of Neuregulin 2. Mol. Neurobiol. 10.1007/s12035-019-01846-9.

243. Saura, C.A., Servián-Morilla, E., and Scholl, F.G. (2011). Presenilin/γ-secretase regulates neurexin processing at synapses. PLoS One. 10.1371/journal.pone.0019430.

244. Bot, N., Schweizer, C., Halima, S. Ben, and Fraering, P.C. (2011). Processing of the synaptic cell adhesion molecule neurexin-3β by Alzheimer disease α- and γ-secretases. J. Biol. Chem. 10.1074/jbc.M110.142521.

245. Suzuki, K., Hayashi, Y., Nakahara, S., Kumazaki, H., Prox, J., Horiuchi, K., Zeng, M., Tanimura, S., Nishiyama, Y., Osawa, S., et al. (2012). Activity-Dependent Proteolytic Cleavage of Neuroligin-1. Neuron. 10.1016/j.neuron.2012.10.003.

246. Peixoto, R.T., Kunz, P.A., Kwon, H., Mabb, A.M., Sabatini, B.L., Philpot, B.D., and Ehlers, M.D. (2012). Transsynaptic Signaling by Activity-Dependent Cleavage of Neuroligin-1. Neuron. 10.1016/j.neuron.2012.07.006.

247. Dominik, S., Angela, N., Jeet, S., Renato, F., Daniele, M., Fabien, B., S, P.S., Kristina, E., Beat, L., Konstantin, R., et al. (2014). Oligodendrocyte precursor cells modulate the neuronal network by activity-dependent ectodomain cleavage of glial NG2. PLoS Biol.

248. Lee, H., Lee, E.J., Song, Y.S., and Kim, E. (2014). Long-term depression-inducing stimuli promote cleavage of the synaptic adhesion molecule NGL-3 through NMDA

receptors, matrix metalloproteinases and presenilin/γ-secretase. Philos. Trans. R. Soc. B Biol. Sci. 10.1098/rstb.2013.0158.

249. Akter, J., Takatori, A., Islam, M.S., Nakazawa, A., Ozaki, T., Nagase, H., and Nakagawara, A. (2014). Intracellular fragment of NLRR3 (NLRR3-ICD) stimulates ATRA-dependent neuroblastoma differentiation. Biochem. Biophys. Res. Commun. 10.1016/j.bbrc.2014.09.065.

250. Saxena, M.T., Schroeter, E.H., Mumm, J.S., and Kopan, R. (2001). Murine Notch Homologs (N1-4) Undergo Presenilin-dependent Proteolysis. J. Biol. Chem. 10.1074/jbc.M107234200.

251. Kanning, K.C., Hudson, M., Amieux, P.S., Wiley, J.C., Bothwell, M., and Schecterson, L.C. (2003). Proteolytic processing of the p75 neurotrophin receptor and two homologs generates C-terminal fragments with signaling capability. J. Neurosci. 10.1523/jneurosci.23-13-05425.2003.

252. Rajagopal, C., Stone, K.L., Mains, R.E., and Eipper, B.A. (2010). Secretion stimulates intramembrane proteolysis of a secretory granule membrane enzyme. J. Biol. Chem. 10.1074/jbc.M110.145334.

253. Yurrita, M.M., Fernández-Muñoz, B., Del Castillo, G., Martín-Villar, E., Renart, J., and Quintanilla, M. (2014). Podoplanin is a substrate of presenilin-1/γ-secretase. Int. J. Biochem. Cell Biol. 10.1016/j.biocel.2013.11.016.

254. Biswas, S., Adrian, M., Weber, J., Evdokimov, K., Winkler, M., and Géraud, C. (2016). Posttranslational proteolytic processing of Leda-1/Pianp involves cleavage by MMPs, ADAM10/17 and gamma-secretase. Biochem. Biophys. Res. Commun. 10.1016/j.bbrc.2016.06.116.

255. Merrick, D., Chapin, H., Baggs, J.E., Yu, Z., Somlo, S., Sun, Z., Hogenesch, J.B., and Caplan, M.J. (2012). The γ-Secretase Cleavage Product of Polycystin-1 Regulates TCF and CHOP-Mediated Transcriptional Activation through a p300-Dependent Mechanism. Dev. Cell. 10.1016/j.devcel.2011.10.028.

256. Kaimori, J. ya, Nagasawa, Y., Menezes, L.F., Garcia-Gonzalez, M.A., Deng, J., Imai, E., Onuchic, L.F., Guay-Woodford, L.M., and Germino, G.G. (2007). Polyductin undergoes notch-like processing and regulated release from primary cilia. Hum. Mol. Genet. 10.1093/hmg/ddm039.

257. García-Ayllón, M.S., Campanari, M.L., Montenegro, M.F., Cuchillo-Ibáñez, I., Belbin, O., Lleó, A., Tsim, K., Vidal, C.J., and Sáez-Valero, J. (2014). Presenilin-1 influences processing of the acetylcholinesterase membrane anchor PRiMA. Neurobiol. Aging. 10.1016/j.neurobiolaging.2014.01.147.

258. Bouillot, S., Tillet, E., Carmona, G., Prandini, M.H., Gauchez, A.S., Hoffmann, P., Alfaidy, N., Cand, F., and Huber, P. (2011). Protocadherin-12 cleavage is a regulated process mediated by ADAM10 protein: Evidence of shedding up-regulation in pre-eclampsia. J. Biol. Chem. 10.1074/jbc.M111.230045.

259. Bonn, S., Seeburg, P.H., and Schwarz, M.K. (2007). Combinatorial Expression of α- and γ-Protocadherins Alters Their Presenilin-Dependent Processing. Mol. Cell. Biol. 10.1128/mcb.01708-06.

260. Haas, I.G., Frank, M., Véron, N., and Kemler, R. (2005). Presenilin-dependent processing and nuclear function of γ-protocadherins. J. Biol. Chem. 10.1074/jbc.M412909200.

261. Watanabe, Y., and Nakamura, H. (2012). Nuclear translocation of intracellular domain of Protogenin by proteolytic cleavage. Dev. Growth Differ. 10.1111/j.1440-

169X.2011.01315.x.

262. Na, H.W., Shin, W.S., Ludwig, A., and Lee, S.T. (2012). The cytosolic domain of protein-tyrosine kinase 7 (PTK7), generated from sequential cleavage by a disintegrin and metalloprotease 17 (ADAM17) and γ-secretase, enhances cell proliferation and migration in colon cancer cells. J. Biol. Chem. 10.1074/jbc.M112.348904.

263. Liu, S., Zhang, Z., Li, L., Yao, L., Ma, Z., and Li, J. (2023). ADAM10- and γ-secretase-dependent cleavage of the transmembrane protein PTPRT attenuates neurodegeneration in the mouse model of Alzheimer's disease. FASEB J. 10.1096/fj.202201396R.

264. Chow, J.P.H., Fujikawa, A., Shimizu, H., Suzuki, R., and Noda, M. (2008). Metalloproteinase- and γ-secretase-mediated cleavage of protein-tyrosine phosphatase receptor type Z. J. Biol. Chem. 10.1074/jbc.M802976200.

265. Galichet, A., Weibel, M., and Heizmann, C.W. (2008). Calcium-regulated intramembrane proteolysis of the RAGE receptor. Biochem. Biophys. Res. Commun. 10.1016/j.bbrc.2008.02.163.

266. Seki, M., Watanabe, A., Enomoto, S., Kawamura, T., Ito, H., Kodama, T., Hamakubo, T., and Aburatani, H. (2010). Human ROBO1 is cleaved by metalloproteinases and γ-secretase and migrates to the nucleus in cancer cells. FEBS Lett. 10.1016/j.febslet.2010.05.009.

267. Anders, L., Mertins, P., Lammich, S., Murgia, M., Hartmann, D., Saftig, P., Haass, C., and Ullrich, A. (2006). Furin-, ADAM 10-, and γ-Secretase-Mediated Cleavage of a Receptor Tyrosine Phosphatase and Regulation of β-Catenin's Transcriptional Activity. Mol. Cell. Biol. 10.1128/mcb.26.10.3917-3934.2006.

268. Lyu, J., Yamamoto, V., and Lu, W. (2008). Cleavage of the Wnt Receptor Ryk Regulates Neuronal Differentiation during Cortical Neurogenesis. Dev. Cell. 10.1016/j.devcel.2008.10.004.

269. Pigoni, M., Wanngren, J., Kuhn, P.H., Munro, K.M., Gunnersen, J.M., Takeshima, H., Feederle, R., Voytyuk, I., De Strooper, B., Levasseur, M.D., et al. (2016). Seizure protein 6 and its homolog seizure 6-like protein are physiological substrates of BACE1 in neurons. Mol. Neurodegener. 10.1186/s13024-016-0134-z.

270. Nyborg, Andrew C., et al. (2006). Sortilin, SorCS1b, and SorLA Vps10p sorting receptors, are novel gamma-secretase substrates. Mol Neurodegener.

271. Hermey, G., Sjøgaard, S.S., Petersen, C.M., Nykjær, A., and Gliemann, J. (2006). Tumour necrosis factor α-converting enzyme mediates ectodomain shedding of Vps10p-domain receptor family members. Biochem. J. 10.1042/BJ20051364.

272. Böhm, C., Seibel, N.M., Henkel, B., Steiner, H., Haass, C., and Hampe, W. (2006). SorLA signaling by regulated intramembrane proteolysis. J. Biol. Chem. 10.1074/jbc.M601660200.

273. Schulz, J.G., Annaert, W., Vandekerckhove, J., Zimmermann, P., De Strooper, B., and David, G. (2003). Syndecan 3 intramembrane proteolysis is presenilin/γ-secretase-dependent and modulates cytosolic signaling. J. Biol. Chem. 10.1074/jbc.M308424200.

274. Marron, M.B., Singh, H., Tahir, T.A., Kavumkal, J., Kim, H.Z., Gou, Y.K., and Brindle, N.P.J. (2007). Regulated proteolytic processing of Tie1 modulates ligand responsiveness of the receptor-tyrosine kinase Tie2. J. Biol. Chem. 10.1074/jbc.M702535200.

275. Ali, N., and Knäuper, V. (2007). Phorbol ester-induced shedding of the prostate cancer marker transmembrane protein with epidermal growth factor and two follistatin motifs 2 is mediated by the disintegrin and metalloproteinase-17. J. Biol. Chem. 10.1074/jbc.M702170200.

276. Harte, F.M., Elzinga, B.M., and McCarthy, J. V. (2008). P4-217: Regulated intramembrane proteolysis of tumour necrosis factor receptor 1 (TNFR 1). Alzheimer's Dement. 10.1016/j.jalz.2008.05.2285.

277. Tejeda, G.S., Ayuso-Dolado, S., Arbeteta, R., Esteban-Ortega, G.M., Vidaurre, O.G., and Díaz-Guerra, M. (2016). Brain ischaemia induces shedding of a BDNF-scavenger ectodomain from TrkB receptors by excitotoxicity activation of metalloproteinases and γ-secretases. J. Pathol. 10.1002/path.4684.

278. Stoyanova, T., Goldstein, A.S., Cai, H., Drake, J.M., Huang, J., and Witte, O.N. (2012). Regulated proteolysis of Trop2 drives epithelial hyperplasia and stem cell self-renewal via β-catenin signaling. Genes Dev. 10.1101/gad.196451.112.

279. Wang, R., Tang, P., Wang, P., Boissy, R.E., and Zheng, H. (2006). Regulation of tyrosinase trafficking and processing by presenilins: Partial loss of function by familial Alzheimer's disease mutation. Proc. Natl. Acad. Sci. U. S. A. 10.1073/pnas.0509822102.

280. Schulz, B., Pruessmeyer, J., Maretzky, T., Ludwig, A., Blobel, C.P., Saftig, P., and Reiss, K. (2008). ADAMIO regulates endothelial permeability and T-cell transmigration by proteolysis of vascular endothelial cadherin. Circ. Res. 10.1161/CIRCRESAHA.107.169805.

281. Ablonczy, Z., Prakasam, A., Fant, J., Fauq, A., Crosson, C., and Sambamurti, K. (2009). Pigment epithelium-derived factor maintains retinal pigment epithelium function by inhibiting vascular endothelial growth factor-R2 signaling through γ-secretase. J. Biol. Chem. 10.1074/jbc.M109.032391.

282. Wong, H.K., Sakurai, T., Oyama, F., Kaneko, K., Wada, K., Miyazaki, H., Kurosawa, M., De Strooper, B., Saftig, P., and Nukina, N. (2005). β subunits of voltage-gated sodium channels are novel substrates of β-site amyloid precursor protein-cleaving enzyme (BACE1) and γ-secretase. J. Biol. Chem. 10.1074/jbc.M414648200.

283. Kim, D.Y., Ingano, L.A.M.K., Carey, B.W., Pettingell, W.H., and Kovacs, D.M. (2005). Presenilin/γ-secretase-mediated cleavage of the voltage-gated sodium channel β2-subunit regulates cell adhesion and migration. J. Biol. Chem. 10.1074/jbc.M412938200.

284. Hoe, H.S., and Rebeck, G.W. (2005). Regulation of ApoE receptor proteolysis by ligand binding. Mol. Brain Res. 10.1016/j.molbrainres.2005.02.013.

285. Esselens, G., Oorschot, V., Baert, V., Raemaekers, T., Spittaels, K., Serneels, L., Zheng, H., Saftig, P., De Strooper, B., Klumperman, J., et al. (2004). Presenilin 1 mediates the turnover of telencephalin in hippocampal neurons via an autophagic degradative pathway. J. Cell Biol. 10.1083/jcb.200406060.

286. Annaert, W.G., Esselens, C., Baert, V., Boeve, C., Snellings, G., Cupers, P., Craessaerts, K., and De Strooper, B. (2001). Interaction with telencephalin and the amyloid precursor protein predicts a ring structure for presenilins. Neuron. 10.1016/S0896-6273(01)00512-8.

287. Serneels, L., Dejaegere, T., Craessaerts, K., Horré, K., Jorissen, E., Tousseyn, T., Hébert, S., Coolen, M., Martens, G., Zwijsen, A., et al. (2005). Differential contribution of the three Aph1 genes to γ-secretase activity in vivo. Proc. Natl. Acad. Sci. U. S. A.

10.1073/pnas.0408901102.

288. Serneels, L., Bammens, L., Zwijsen, A., Tolia, A., Chávez-Gutiérrez, L., and Strooper, B. De (2023). Functional and topological analysis of PSENEN, the fourth subunit of the γ-secretase complex. bioRxiv, 2023.07.28.550932. 10.1101/2023.07.28.550932.

289. Mercken, M., Takahashi, H., Honda, T., Sato, K., Murayama, M., Nakazato, Y., Noguchi, K., Imahori, K., and Takashima, A. (1996). Characterization of human presenilin 1 using N-terminal specific monoclonal antibodies: Evidence that Alzheimer mutations affect proteolytic processing. FEBS Lett. 10.1016/0014-5793(96)00608-4.

290. Acx, H., Serneels, L., Radaelli, E., Muyldermans, S., Vincke, C., Pepermans, E., Müller, U., Chávez-Gutiérrez, L., and De Strooper, B. (2017). Inactivation of γ-secretases leads to accumulation of substrates and non-Alzheimer neurodegeneration. EMBO Mol. Med. 10.15252/emmm.201707561.

291. Friedman, B.A., Srinivasan, K., Ayalon, G., Meilandt, W.J., Lin, H., Huntley, M.A., Cao, Y., Lee, S.H., Haddick, P.C.G., Ngu, H., et al. (2018). Diverse Brain Myeloid Expression Profiles Reveal Distinct Microglial Activation States and Aspects of Alzheimer's Disease Not Evident in Mouse Models. Cell Rep. 10.1016/j.celrep.2017.12.066.

292. Saito, T., Matsuba, Y., Mihira, N., Takano, J., Nilsson, P., Itohara, S., Iwata, N., and Saido, T.C. (2014). Single App knock-in mouse models of Alzheimer's disease. Nat. Neurosci. 10.1038/nn.3697.

293. Parkhurst, C.N., Yang, G., Ninan, I., Savas, J.N., Yates, J.R., Lafaille, J.J., Hempstead, B.L., Littman, D.R., and Gan, W.B. (2013). Microglia promote learning-dependent synapse formation through brain-derived neurotrophic factor. Cell. 10.1016/j.cell.2013.11.030.

294. Hao, Y., Hao, S., Andersen-Nissen, E., Mauck, W.M., Zheng, S., Butler, A., Lee, M.J., Wilk, A.J., Darby, C., Zager, M., et al. (2021). Integrated analysis of multimodal single-cell data. Cell. 10.1016/j.cell.2021.04.048.

295. van Wilgenburg, B., Browne, C., Vowles, J., and Cowley, S.A. (2013). Efficient, Long Term Production of Monocyte-Derived Macrophages from Human Pluripotent Stem Cells under Partly-Defined and Fully-Defined Conditions. PLoS One. 10.1371/journal.pone.0071098.

296. Bohlen, C.J., Bennett, F.C., Tucker, A.F., Collins, H.Y., Mulinyawe, S.B., and Barres, B.A. (2017). Diverse Requirements for Microglial Survival, Specification, and Function Revealed by Defined-Medium Cultures. Neuron. 10.1016/j.neuron.2017.04.043.

297. Yona, S., Kim, K.W., Wolf, Y., Mildner, A., Varol, D., Breker, M., Strauss-Ayali, D., Viukov, S., Guilliams, M., Misharin, A., et al. (2013). Fate mapping reveals origins and dynamics of monocytes and tissue macrophages under homeostasis [Immunity 38 (2013) 79-91]. Immunity. 10.1016/j.immuni.2013.05.008.

298. De Rop, F. V., Ismail, J.N., González-Blas, C.B., Hulselmans, G.J., Flerin, C.C., Janssens, J., Theunis, K., Christiaens, V.M., Wouters, J., Marcassa, G., et al. (2022). HyDrop enables droplet based single-cell ATAC-seq and single-cell RNA-seq using dissolvable hydrogel beads. Elife. 10.7554/ELIFE.73971.

299. Tran, J.C., and Doucette, A.A. (2008). Gel-eluted liquid fraction entrapment electrophoresis: An electrophoretic method for broad molecular weight range proteome separation. Anal. Chem. 10.1021/ac702197w.

300. Witkowski, C., and Harkins, J. (2010). Using the GELFREE 8100 Fractionation System for molecular weight-based fractionation with liquid phase recovery. J. Vis. Exp.

10.3791/1842.

301. Willnow, T.E., Moehring, J.M., Inocencio, N.M., Moehring, T.J., and Herz, J. (1996). The low-density-lipoprotein receptor-related protein (LRP) is processed by furin in vivo and in vitro. Biochem. J. 10.1042/bj3130071.

302. Bateman, A., Martin, M.J., Orchard, S., Magrane, M., Agivetova, R., Ahmad, S., Alpi, E., Bowler-Barnett, E.H., Britto, R., Bursteinas, B., et al. (2021). UniProt: the universal protein knowledgebase in 2021. Nucleic Acids Res. 10.1093/nar/gkaa1100.

303. Zhou, X., Wahane, S., Friedl, M.S., Kluge, M., Friedel, C.C., Avrampou, K., Zachariou, V., Guo, L., Zhang, B., He, X., et al. (2020). Microglia and macrophages promote corralling, wound compaction and recovery after spinal cord injury via Plexin-B2. Nat. Neurosci. 10.1038/s41593-020-0597-7.

304. Linnartz, B., and Neumann, H. (2013). Microglial activatory (immunoreceptor tyrosine-based activation motif)- and inhibitory (immunoreceptor tyrosine-based inhibition motif)-signaling receptors for recognition of the neuronal glycocalyx. Glia. 10.1002/glia.22359.

305. Neumann, H., Linnartz, B., and Wang, Y. (2010). Microglial immunoreceptor tyrosine-based activation and inhibition motif signaling in neuroinflammation. Int. J. Alzheimers. Dis. 10.4061/2010/587463.

306. Park, B.S., and Lee, J.O. (2013). Recognition of lipopolysaccharide pattern by TLR4 complexes. Exp. Mol. Med. 10.1038/emm.2013.97.

307. Sousa, C., Golebiewska, A., Poovathingal, S.K., Kaoma, T., Pires-Afonso, Y., Martina, S., Coowar, D., Azuaje, F., Skupin, A., Balling, R., et al. (2018). Single-cell transcriptomics reveals distinct inflammation-induced microglia signatures. EMBO Rep. *19*, 1–17. 10.15252/embr.201846171.

308. Weber, S., and Saftig, P. (2012). Ectodomain shedding and ADAMs in development. Dev. 10.1242/dev.076398.

309. Wakabayashi, T., Craessaerts, K., Bammens, L., Bentahir, M., Borgions, F., Herdewijn, P., Staes, A., Timmerman, E., Vandekerckhove, J., Rubinstein, E., et al. (2009). Analysis of the γ-secretase interactome and validation of its association with tetraspanin-enriched microdomains. Nat. Cell Biol. 10.1038/ncb1978.

310. Hur, J.Y., Frost, G.R., Wu, X., Crump, C., Pan, S.J., Wong, E., Barros, M., Li, T., Nie, P., Zhai, Y., et al. (2020). The innate immunity protein IFITM3 modulates γ-secretase in Alzheimer's disease. Nature. 10.1038/s41586-020-2681-2.

311. Myers, D.R., Zikherman, J., and Roose, J.P. (2017). Tonic Signals: Why Do Lymphocytes Bother? Trends Immunol. 10.1016/j.it.2017.06.010.

312. Roose, J.P., Diehn, M., Tomlinson, M.G., Lin, J., Alizadeh, A.A., Botstein, D., Brown, P.O., and Weiss, A. (2003). T cell receptor-independent basal signaling via Erk and Abl kinases suppresses RAG gene expression. PLoS Biol. 10.1371/journal.pbio.0000053.

313. Tan, Y.X., Zikherman, J., and Weiss, A. (2013). Novel tools to dissect the dynamic regulation of TCR signaling by the kinase Csk and the phosphatase CD45. Cold Spring Harb. Symp. Quant. Biol. 10.1101/sqb.2013.78.020347.

314. Gosselin, D., Skola, D., Coufal, N.G., Holtman, I.R., Schlachetzki, J.C.M., Sajti, E., Jaeger, B.N., O'Connor, C., Fitzpatrick, C., Pasillas, M.P., et al. (2017). An environment-dependent transcriptional network specifies human microglia identity. Science (80-.). 10.1126/science.aal3222.

315. Lloyd, A.F., Martinez-Muriana, A., Hou, P., Davis, E., Mancuso, R., Brenes, A.J., Geric, I., Snellinx, A., Craessaerts, K., Theys, T., et al. (2022). Deep proteomic analysis of human microglia and model systems reveal fundamental biological differences of in vitro and ex vivo cells. bioRxiv, 1–30.

316. Deczkowska, A., Keren-Shaul, H., Weiner, A., Colonna, M., Schwartz, M., and Amit, I. (2018). Disease-Associated Microglia: A Universal Immune Sensor of Neurodegeneration. Cell. 10.1016/j.cell.2018.05.003.

317. Avci, D., and Lemberg, M.K. (2015). Clipping or Extracting: Two Ways to Membrane Protein Degradation. Trends Cell Biol. 10.1016/j.tcb.2015.07.003.

318. Lichtenthaler, S.F., Lemberg, M.K., and Fluhrer, R. (2018). Proteolytic ectodomain shedding of membrane proteins in mammals—hardware, concepts, and recent developments. EMBO J. 10.15252/embj.201899456.

319. Lauritzen, I., Pardossi-Piquard, R., Bourgeois, A., Pagnotta, S., Biferi, M.G., Barkats, M., Lacor, P., Klein, W., Bauer, C., and Checler, F. (2016). Intraneuronal aggregation of the β-CTF fragment of APP (C99) induces Aβ-independent lysosomal-autophagic pathology. Acta Neuropathol. 10.1007/s00401-016-1577-6.

320. Alzheimer, A. (1907). Uber eine eigenartige Erkrankung der Hirnrinde. Allg Zeitschr f Psychiatr. u Psych-Gerichtl Med.

321. Artavanis-Tsakonas, S., Rand, M.D., and Lake, R.J. (1999). Notch signaling: Cell fate control and signal integration in development. Science (80-.). 10.1126/science.284.5415.770.

322. Ryan, N.S., Nicholas, J.M., Weston, P.S.J., Liang, Y., Lashley, T., Guerreiro, R., Adamson, G., Kenny, J., Beck, J., Chavez-Gutierrez, L., et al. (2016). Clinical phenotype and genetic associations in autosomal dominant familial Alzheimer's disease: a case series. Lancet Neurol. 10.1016/S1474-4422(16)30193-4.

323. Bergmans, B.A., and De Strooper, B. (2010). γ-secretases: from cell biology to therapeutic strategies. Lancet Neurol. 10.1016/S1474-4422(09)70332-1.

324. Luo, J.E., and Li, Y.M. (2022). Turning the tide on Alzheimer's disease: modulation of γ-secretase. Cell Biosci. 10.1186/s13578-021-00738-7.

325. Lott, D., Portron, A., Alam, M., Cantrill, C., Croney, R., Alcaraz, F., Sarmiento, R.M.R., Lindemann, L., Mueller, L., Mueggler, T., et al. (2023). RG6289, A NEW Γ-SECRETASE MODULATOR FOR THE TREATMENT OF ALZHEIMER'S DISEASE: DOSE SELECTION FOR A PHASE II TRIAL BASED ON POPULATION PK/PD MODELING. Alzheimer's Dis. CTAD-2023. https://medically.gene.com/global/en/unrestricted/neuroscience/CTAD-2023/ctad-2023-poster-portron-rg6289-a-new--secretase-modul.html.

326. Hou, P., Zielonka, M., Serneels, L., Martinez-Muriana, A., Fattorelli, N., Wolfs, L., Poovathingal, S., T'Syen, D., Balusu, S., Theys, T., et al. (2023). The γ-secretase substrate proteome and its role in cell signaling regulation. Mol. Cell *83*, 4106-4122.e10. 10.1016/j.molcel.2023.10.029.

Curriculum Vitae

Personal Information

Name: Pengfei Hou

Date and place of Birth: Nov. 2nd, 1992, Weihai City, Shandong Province, China

Working place: Laboratory for the Research of Neurodegenerative Diseases, VIB & KU Leuven Center for Brain and Disease Research, Herestraat 49, box 602, 3000 Leuven, Belgium

Email: Pengfei.hou@kuleuven.be

Phone number: +32 16194405

Education

2018.10 – present
PhD in Biomedical Sciences
Katholieke Universiteit Leuven, Belgium

2015.09 – 2018.06
Master in Preventive Veterinary Medicine
Jilin University, China

2011.09 – 2015.06
Bachelor in Science of Animal Quarantine
Shandong Agricultural University, China

Research Experience

2018.10 – present
Doctoral thesis
The γ-secretase substrate proteome and its role in cell signaling regulation.
VIB & KU Leuven Center for Brain and Disease Research, Leuven, Belgium
Promotor: Bart De Strooper
Co-promotors: Lutgarde Serneels and Renzo Mancuso

2015.09 – 2018.06
Master thesis
Study of the relationship between Bif-1 protein and rabies virus replication.
College of Veterinary Medicine, Jilin University, China
Promotor: Songtao Yang

2011.09 – 2015.06
Bachelor thesis
Evaluation of AoF therapeutic effects on *H1N1* infected mouse models.
College of Animal Science and Veterinary Medicine, Shandong Agricultural University, China
Promotor: Lin Wang

Technical Skills

Western Blot; RT-qPCR; MSD-ELISA; Stem cell culture and microglia differentiation; Immunofluorescence; Confocal microscopy; Flow Cytometry; Handling of experimental animals; Molecular cloning; Viral transduction; Programming language (R basic level); Image analysis (ImageJ, Nikon NIS-Elements); Utility of GraphPad Prism, Inkscape, GIMP, etc.

Conferences & Meetings

Poster presentation, The γ-secretase substrate proteome and its role in cell signaling regulation, Sept 21st - 23rd, 2023, 3rd HEFEI international summit on Alzheimer's disease (Aging and brain forum), Hefei City, China

Oral presentation, The γ-Secretase Substrate Proteome and Its Role in Microglial Cell State Regulation, March 28th - April 1st, 2023, AD/PD™ 2023 International Conference on Alzheimer's and Parkinson's Diseases and related neurological disorders, Gothenburg, Sweden

Oral presentation, The γ-secretase substrate proteome reveals the role of regulated intramembrane proteolysis in cell state of microglia, Sept 11th - 14th, 2022, 3rd International Symposium of the CRC877 "Protease World in Health & Disease", Kiel, Germany

Poster presentation, Identification of γ-secretase substrates expressing in microglia, May 4th - 6th, 2022, 2nd International Meeting of the FOR2290 'Protein Recognition and Processing in the Membrane', Munich, Germany

Awards

Outstanding Poster Prize, amount: CNY3000, theme: Aging and brain forum, awarding body: Scientific Committee of 3rd HEFEI international summit on Alzheimer's disease, Sept 23rd, 2023, Hefei City, China.

Junior Faculty Award, amount: €1000, theme: Advances in science and therapy, awarding body: Scientific Committee of AD/PD™ 2023 International Conference on Alzheimer's and Parkinson's Diseases and related neurological disorders, March 28th, 2023, Gothenburg, Sweden

PhD fellowship, amount: €1,350 monthly for 48 months, China Scholarship Council (CSC), Oct 2nd, 2018 to Oct 1st, 2022

Publications

1) **Pengfei Hou**#, Magdalena Zielonka#, Lutgarde Serneels, Anna Martinez-Muriana, Nicola Fattorelli, Leen Wolfs, Suresh Poovathingal, Dries T'Syen, Sriram Balusu, Tom Theys, Mark Fiers, Renzo Mancuso, Andrew J.M. Howden, Bart De Strooper, The γ-secretase substrate proteome and its role in cell signaling regulation, Molecular Cell, Volume 83, Issue 22, 2023, Pages 4106-4122.e10, ISSN 1097-2765, Peer reviewed. # Co-first authorship.

2) Amy F Lloyd, Anna Martinez-Muriana, **Pengfei Hou**, Emma Davis, Renzo Mancuso, Alejandro J Brenes, Ivana Geric, An Snellinx, Katleen Craessaerts, Tom Theys, Mark Fiers, Bart De Strooper, Andrew JM Howden, Deep proteomic analysis of human microglia and model systems reveal fundamental biological differences of in vitro and ex vivo cells, bioRxiv, 2022.07.07.498804; doi: https://doi.org/10.1101/2022.07.07.498804, Preprint.

Other scientific output & impact

Scientific impact:

News and comments covered by Alzforum: At the Core of Microglial Signaling: γ-Secretase

(Link: https://www.alzforum.org/news/research-news/core-microglial-signaling-g-secretase)

Societal outputs:

Volunteer teacher, The fifth edition of "A Window to the World" (online English course for primary school students from the rural area of Guizhou, China), Online, every Saturday, from September to November, 2021

Teaching assistant, KU Leuven Kinderuniversiteit (Neuroscience Workshop for primary school students), October 19th, 2019, Leuven, Belgium

Personal Acknowledgement

Looking back to the journey being completed, scenes from the past five and half years flood into my mind. While I won't deny the difficulties, I find joy in the resilience gained from overcoming each challenge whatever from my study or my life.

Bart, thank you Sir! The opportunity that you granted me to be a PhD student in the lab initiated my scientific adventure on exploring the fascinating "γ-secretase" and opened an important chapter in my life. I really enjoyed the time in BDS lab. Not only do your remarkable scientific achievements pave a solid path for those who follow, but the research environment you have cultivated, with the inclusion of many brilliant minds, consistently nurtures innovative solutions for a wide range of challenges. I am not a chatty person. But I somehow feel that I always have endless discussion with you (for all kinds of reasons). There are so many impressive moments that I probably will never forget: slide by slide, in the late night you advised me how to prepare the slides for a conference presentation; when our bi-weekly update meeting was overtime and your schedule was full in the whole week, you took time off your weekends to discuss the results with me; when my father was having a severe healthy issue, you comforted me and allowed me to return back to my country to stay at his side for months; also you went through with me the 28 versions of the manuscripts before it finally got published (I had seen this as a nightmare but then realized I learned a lot from the process when I started conceiving the new project)… Yes, it is my another great pleasure that I could do more exciting science with you!

Lutgarde, thank you for being my academic mom for the many years. I had never imagined that I could one day have a supervisor who is a senior scientist but teaches me doing experiments really hand by hand, but you did. You are a great listener that always allow me to pour out any trouble I ever had and give me your helpful suggestions. People in the lab were jealous to me and saying that I have the most reachable supervisor-I can find you almost at any minute of the day and always get immediate help from you. Thank you for thinking of even very small details for my experiment (you even dedicated your kitchen blender to help me make the drug-mixed diet for my experimental mice).

Renzo, thanks for bringing me to the microglia team which allowed me to study the classical "hardcore" target in the spotlighted microglia models, and it turned out that

we revealed very unexpected and exciting findings. You never shied away from giving praises and encouragements after each of my presentation, although sometimes I knew how much left to be desired that I did. Your cheerful and optimistic attitude for life and work is the thing that I should always learn. The skills you taught me in animal experiments were very useful, and now I could use them to teach or help other people. The notebook I used for refreshing my statistic knowledge-the homework that you assigned to me, was really a precious present from you.

I feel so lucky to daily work with a group of kind and talented people in the office. Nico, you are the person, besides my (co-)supervisors, to whom I have ever given my bi-weekly updates. Thank you for "pushing" me to read the literatures of single-cell transcriptomics, guided me to learn some basic bioinformatics and gave me suggestions, (and added me to Evgenia's blacklist). Pranav, you have been so helpful to me as you always patiently explain any of my confusions due to my language issue. And, you are right, it is the same for me to feel it like a blessing to have you guys to start our PhD adventures together! Katleen and Katrien, having you as the officemates, I never worried I would use a wrong protocol as I could ask to the experiment masters just next to me whenever I have experiment-related questions.

The microglia team members, thank you for the kind help and encouragement all the time. Leen, you know I wouldn't have completed my PhD without your help. As all of us said, you are the person that can save our days from any difficult situations. I very much appreciate having your help on those long days for single-cell experiments. Anna, do you remember that you saved one of my most important experiments by bringing Bart into the TC room, when I misunderstood Bart's meaning? How luckily it was that you met with Bart in the corridor just before I started it! Ivana, your optimistic energy can influence everyone in the lab. I am sure you also bring it to Muna. Please don't stop taking "cocaine"! (I should clarify it was a joke she previously made during a lunch.)

Big thanks to the bioinformatics team. Mark, thank you for your logical thinking and the many discussions we had. Magda, it was a great pleasure to work with you. I know the time spent on my project was more than we initially expected, but the countless discussions and many times of midnight work paid off! Ashely, Nicky and Yannick, while all of you have left the lab, your kindness and warm help in the beginning of my PhD were impressive.

Sriram, thank you for passing on a lot of your knowledge and sharing your valuable experience to me. Dries, you are not only a scientist but also the artist in the lab. You always amazed me by your talent and creativity. Danae, thank you for volunteering to organize the many activities for the lab. Imma, Sarah, Annerieke, Giulia, An, Nora, Veerle, Luuk, Angele, Daan, I feel always good to have the warm conversations with you. Xu and Di, the joining of you two to the lab made me feeling at home in Belgium. We should have more after-work gathering! Véronique, Jonas, Amber, I can imagine how much mouse work you have done for me, especially in the many urgent cases! I felt so grateful each time I entered spf9 and saw all the cages you have prepared for me.

Eliane, you had impressed me even before I arrived in Belgium. Without your help on preparing the paperwork, I wouldn't have gone through the complex administrative steps for my PhD fellowship application. Your kind help through my whole PhD journey made it pretty much smoother than what I can expect. Sulieman, it has been a pleasure to work with you. You helped me fix out the all kinds of practical issues throughout my experiments, at the meantime always injecting humor into the process. (With your advices in mind, I so far haven't been chased by red cows in Belgium). Also many thanks to Suresh, Tineke, Tanja, Raymond, Lisbeth and many others in CBD who made my PhD life easier.

感谢这些年在鲁汶认识的小伙伴们：文婷师姐，广海师兄，孙亮师兄，建敏师兄，岚娇师姐，韩旭师兄，许莹，张欣，曹新宇，钟昇平，丹丹，蒲廷，吴一凡, 晨风… 在异国他乡遇到你们是莫大的缘分，偶尔的小聚更是舒缓紧张工作的良药。

最后，我要衷心感谢我的家人们一直以来对我的支持。感谢父母的养育之恩。特别感谢舅舅对我从小到大的鼓励与引导，让我开拓眼界，敢于拼搏。由衷的感谢十多年来妻子的陪伴、鼓励和支持，让我一直能够坚定地朝着目标迈进。

侯朋飞

Pengfei Hou

2024 年 2 月于 Leuven